UNIVERSIDADE DE SÃO PAULO
Instituto de Física

Estudo da matriz-S do espalhamento entre íons pesados

Rubens Lichtenthäler Filho

Tese de livre-docência apresentada ao Instituto de Física da Universidade de São Paulo.

SÃO PAULO
1996

Índice

Resumo

Neste trabalho, o problema do espalhamento entre íons leves-pesados é abordado principalmente do ponto de vista da matriz-S. Desenvolvemos um método que permite a obtenção dos elementos da matriz-S do espalhamento elástico e seus respectivos erros diretamente a partir de distribuições angulares. Analisamos dados experimentais dos sistemas $^{12}C+^{16}O$ e $^{12}C+^{24}Mg$ em baixas energias.

Investigamos uma possível extensão analítica da matriz-S para o plano complexo com base na Teoria Algébrica do Espalhamento dentro da simetria $SO(3,1)$. O problema de canais acoplados tambem é abordado nesta teoria.

Capítulo 1

Introdução

O espalhamento elástico entre núcleos pesados em energias próximas à barreira coulombiana é o processo dominante em termos de secção de choque o que faz com que este seja uma abundante fonte de informação a respeito do mecanismo de reação. Por outro lado, na colisão entre íons pesados, mesmo em baixas energias, há um número razoável de canais de reação abertos fazendo com que o mecanismo envolvido nestas colisões esteja longe de ser simples. A possibilidade de se descrever semi–classicamente certos aspectos da colisão entre íons pesados é bastante atraente e deu origem a muitos modelos teóricos bem sucedidos em situações em que o comprimento de onda de De Broglie é pequeno comparado às dimensões do sistema. Isso ocorre para íons de massa da camada f-p em energias perto do barreira coulombiana, ou mesmo na camada s-d em energias bem mais altas, em torno de algumas dezenas de MeV por nucleon. No entanto, no espalhamento entre íons da camada s-d em energias próximas à barreira coulombiana, os efeitos quânticos são demasiadamente importantes e inviabilizam interpretações semi–clássicas. Efeitos do tipo ressonante e o acoplamento entre canais, fazem com que o potencial de interação seja não local, apresentando uma forte dependência com a energia.

Um a abordagem alternativa à descrição em termos de um potencial de interação, pode ser obtida a partir da matriz-S que contém toda a informação a respeito do processo de espalhamento. O estudo da matriz-S em função do momento angular e da energia possibilita a identificação de polos de Regge e ressonâncias de uma maneira transparente. Além disso, uma vez determinada a matriz-S, facilmente constroe-se a função de deflexão que exibe mecanismos do tipo arco–íris e efeito glória nucleares. O seu conhecimento é o ponto de partida para a obtenção do potencial de interação, seja por processos de inversão, seja a partir de teorias mais fundamentais.

Neste trabalho descrevemos um projeto de pesquisa que vem se desenvolvendo nos ultimos anos e que trata basicamente do estudo do mecanismo de reação entre íons leves-pesados e pesados em energias em torno da barreira coulombiana. A unidade deste trabalho se realiza na sua abordagem em termos da matriz-S para a descrição do processo de espalhamento.

No capítulo 2 apresentamos um método para a obtenção dos elementos da matriz-S do espalhamento elástico diretamente a partir de distribuições angulares experimentais. No

capítulo 3 analisamos dados dos sistemas $^{12}C+^{16}O$ e $^{12}C+^{24}Mg$ utilizando este método. No capítulo 4 descrevemos a Teoria Algébrica do Espalhamento que é uma teoria baseada na matriz-S na qual o problema de mais de um canal de reação pode ser tratado. No capítulo 5 traçamos as principais conclusões. No final do trabalho anexamos cópias de alguns do nossos artigos aos quais nos referimos no decorrer do texto.

Capítulo 2

Um método para a obtenção da matriz-S a partir de dados experimentais.

2.1 Introdução

Duas propriedades importantes são impostas à matriz-S, analiticidade e unitariedade. A unitariedade vem da conservação do fluxo total e no caso de apenas um canal de reação implica em $|S_\ell(k)| = 1$. A analiticidade implica em certas propriedades da matriz-S quando é feita a extensão analítica para o plano complexo das variáveis ℓ e k. Uma conseqüência disto é que os polos da matriz-S para energia negativa são os estados ligados do potencial. No entanto, apenas estas duas propriedades não são suficientes para determinar a forma funcional da matriz-S.

A idéia deste projeto foi inspirada na necessidade de se desenvolver um método que permitisse a obtenção da matriz-S do espalhamento elástico diretamente a partir de distribuições angulares experimentais. Como a interação nuclear forte é de curto alcance, apenas algumas ondas parciais são espalhadas e a matriz-S nuclear é igual a unidade para momentos angulares acima de um certo valor. No caso de sistemas leves-pesados ($24 \leq A_{proj.} + A_{alvo} \leq 60$) em energias próximas à barreira coulombiana o momento angular máximo pode ser variar entre $L_{max} \approx 5 - 30$ dependendo obviamente da energia e do raio do sistema. Desta forma, o numero de parametros (elementos de matriz) a serem determinados é de $2(L_{max} + 2)$ e está entre 12 e 62.

A obtenção da matriz-S à partir de distribuições angulares tem sido feita utilizando-se métodos [1, 2, 3] de procura nos quais variam-se as defasagens e minimiza-se a função chi-quadrado. Devido ao fato da relação entre secção de choque e as defasagens nucleares ser altamente não linear, estes métodos se baseiam em uma procura local, ou seja, a solução é determinada unicamente pelo gradiente local da função chi-quadrado no espaço de $(2L_{max}+2)$ parametros. Desta forma, eventuais mínimos locais da função chi-quadrado podem ser tomados como solução. Além disso, a condição de unitariedade da matriz-S não é observada o que faz com que algumas soluções devam ser descartadas por violar o

vínculo unitário $|S_\ell(k)| \leq 1$.

O método de análise em defasagens que desenvolvemos [4, 5] (anexo 1) se baseia na observação de que o chi-quadrado é uma função de quarto grau dos elementos da matriz-S e a procura é feita diretamente nestes elementos, em vez das defasagens nucleares, o que lhe confere certas características globais como mostraremos a seguir.

2.2 Descrição do Método de quarto grau.

A amplitude de espalhamento é escrita como:

$$f(\theta) = f_c(\theta) + f_n(\theta),$$

onde

$$f_c(\theta) = -\eta \exp(2i\sigma_0) \frac{\exp[-i\eta \log \sin^2(\frac{\theta}{2})]}{2k \sin^2(\frac{\theta}{2})}$$

é a amplitude coulombiana e

$$f_n(\theta) = \frac{1}{2ik} \sum_{\ell=0}^{\infty} (2\ell+1) S_\ell^c (S_\ell^n - 1) P_\ell(\cos\theta) \tag{2.1}$$

é a parte nuclear da amplitude que contém os elementos da matriz-S S_ℓ^n a serem determinados. O procedimento consiste em minimizar o chi-quadrado dado por:

$$\chi^2 = \sum_{j=1}^{N} \frac{[\sigma(\theta_j) - \sigma^e(\theta_j)]^2}{\Delta^2(\theta_j)}, \tag{2.2}$$

onde $\sigma^e(\theta_j)$ é a secção de choque experimental e $\Delta(\theta_j)$ são os erros. A secção de choque é escrita como:

$$\sigma(\theta_j) = |f(\theta_j)|^2. \tag{2.3}$$

A direção na qual os elementos da matriz-S são variados é determinada pelo gradiente da função chi-quadrado cujas componentes podem ser calculadas analiticamente:

$$u_\ell = \frac{\partial \chi^2}{\partial x_\ell} = \frac{2(2\ell+1)}{k} \sum_{j=1}^{N} \frac{\sigma(\theta_j) - \sigma^e(\theta_j)}{\Delta^2(\theta_j)} P_\ell(\cos\theta_j) \Im[f^*(\theta_j) S_\ell^c],$$

$$v_\ell = \frac{\partial \chi^2}{\partial y_\ell} = \frac{2(2\ell+1)}{k} \sum_{j=1}^{N} \frac{\sigma(\theta_j) - \sigma^e(\theta_j)}{\Delta^2(\theta_j)} P_\ell(\cos\theta_j) \Re[f^*(\theta_j) S_\ell^{(c)}].$$

A matriz-S pode ser escrita como:

$$S_\ell^n = S_\ell^{0n} + \alpha(u_\ell + i v_\ell) \tag{2.4}$$

onde S_ℓ^{0n} é a matriz-S anterior e α um fator de escala que representa o deslocamento na direção do gradiente. Observa-se que α, até agora, não depende do momento angular. Mais adiante mostraremos que a imposição do vínculo unitário pode introduzir uma dependência do momento angular.

O primeiro passo da análise consiste na escolha da matriz-S de partida S_ℓ^{0n}. Em geral procura-se partir de uma matriz-S de um cálculo de modelo otico e que reproduza as características principais do espalhamento como o momento angular razante e difusividade. No entanto, como mostraremos a seguir, as soluções encontradas pelo método não parecem depender do ponto de partida.

Substituindo-se as expressões (3) e (4) em (2) pode-se escrever:

$$\chi^2 = A\alpha^4 + B\alpha^3 + C\alpha^2 + D\alpha + \chi_0^2, \tag{2.5}$$

onde os coeficientes A, B, C e D são calculados analiticamente. Maiores detalhes sobre as formulas para estes coeficientes podem ser obtidos na referência [4] (anexo 1). A função chi–quadrado apresenta pontos de máximo ou mínimo nas raizes da equação cúbica:

$$4A\alpha^3 + 3B\alpha^2 + 2C\alpha + D = 0. \tag{2.6}$$

Como A e D são sempre positivos, esta equação tem ao menos uma raiz real negativa e que corresponde a um mínimo local pois está no sentido contrário ao do gradiente e é portanto o sentido do deslocamento que diminue o chi–quadrado. Entretanto, a equação pode ter tambem três raízes reais indicando a existência de dois mínimos e um máximo. Na figura 2.1 mostramos o chi–quadrado em função da parte real do elemento $S_{\ell=4}$ para uma matriz-S e distribuição angular sintéticas geradas por um cálculo de modelo otico. Observa-se a presença dos dois mínimos, o negativo correspondendo à solução local, enquanto que o verdadeiro mínimo se encontra à direita. Um processo baseado apenas no gradiente do chi–quadrado pode portanto, dependendo do ponto de partida, ser dirigido ao falso mínimo. O método aqui descrito detecta a presenços dois mínimos e escolhe o de menor chi–quadrado sendo portanto um método global em uma dimensão.

Antes de fazer a escolha do mínimo é necessário impor-se a condição de unitariedade dada por:

$$\mid S_\ell^{0n} + \alpha(u_\ell + iv_\ell) \mid = 1 \tag{2.7}$$

e que pode ser escrita como:

$$\alpha^2(u_\ell^2 + v_\ell^2) + 2\gamma_\ell\alpha - (1 - \mid S_\ell'^n \mid^2) = 0 \tag{2.8}$$

com $\gamma_\ell = u_\ell x'_\ell + v_\ell y'_\ell$. Esta equação tem, para cada ℓ, duas raizes α_1 e α_2 que correspondem aos pontos onde o vetor gradiente cruza o círculo unitário como mostra a figura 2.2.

O vínculo unitário é imposto tomando-se $\alpha = \alpha_1$ se $\alpha \leq \alpha_1$, $\alpha = \alpha_2$ se $\alpha \geq \alpha_2$ e a própria solução α se $\alpha_1 \leq \alpha \leq \alpha_2$. Este processo consiste em trazer de volta para o círculo unitário as soluções que porventura caiam fora deste círculo o que corresponde às duas primeiras condições. A terceira condição corresponde a uma solução dentro do círculo e é portanto aceitável. Observa-se que a condição de vínculo deve ser imposta para cada onda parcial o que pode introduzir uma dependencia do momento angular em α.

O processo de procura consiste em se calcular o vetor gradiente, determinar o mínimo na sua direção, recalcular a matriz-S impondo o vínculo unitário e repetir este procedimento até que um mínimo global seja encontrado. Este processo é bastante estável, no

sentido de que o chi–quadrado sempre diminue, e fornece sempre uma solução unitária. No entanto, quando se está suficientemente próximo do mínimo, é possível uma linearização do método. Nesta situação o chi–quadrado passa a ser uma função do segundo grau em α o que corresponde aos dois primeiros termos da eq.2.5 serem desprezíveis e a procura pode ser feita simultaneamente em todas as direções determinando-se os erros nos elementos da matriz-S.

2.3 Aproximação Quadrática

Tomando-se o intervalo de variação da matriz-S na faixa $[l_{min}, l_{max}]$, podemos definir novos indices i e m que variam entre 1 e nl onde $nl = l_{max} - l_{min} + 1$ é o numero ondas parciais ajustados. Definindo-se $a_i = x_{i+\ell_1}$ e $a_{i+\ell_2} = y_{i+\ell_1}$ escrevemos:

$$\chi^2 = \chi_0^2 + \sum_i B_i \Delta a_i + \frac{1}{2} \sum_{im} A_{im} \Delta a_i \Delta a_m.$$

com

$$\begin{aligned} B_i &= \frac{\partial \chi^2}{\partial a_i} \\ A_{im} &= \frac{\partial^2 \chi^2}{\partial a_i \partial a_m} \end{aligned}$$

Os novos elementos da matriz-S são dados por: $a_i^n = a_i + \Delta a_i$ onde:

$$\Delta a_i = -\sum_m (A_{im} + \lambda \delta_{im})^{-1} B_m,$$

e λ é o parametro de regularização [6].

Nesta aproximação, a procura é realizada simultaneamente em todas as direções e uma vez que o mínimo é encontrado, os erros nos elementos da matriz-S e os coeficiente de correlação são dados por:

$$\begin{aligned} \delta a_i &= \sqrt{A_{ii}^{-1}}, \\ \rho_{im} &= \frac{A_{im}^{-1}}{\delta a_i \delta a_m}. \end{aligned}$$

Expressões algébricas para os elementos de matriz $A_{i,m}$ e B foram deduzidos e são fornecidos na referência [4] anexa.

Nos próximos capítulos descreveremos aplicações deste método para dados experimentais dos sistemas $^{12}C+^{16}O$ e $^{12}C+^{24}Mg$.

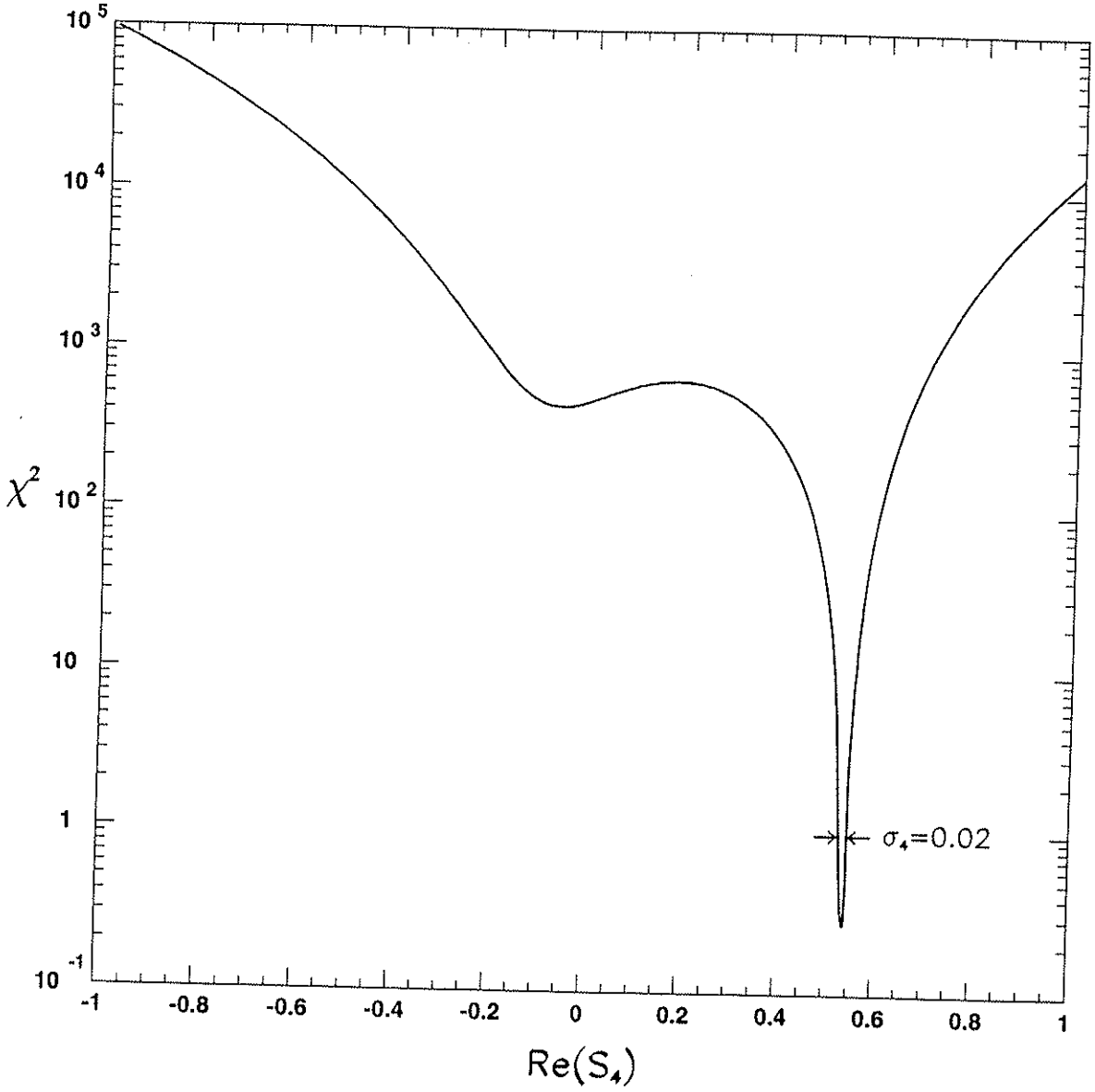

Figura 2.1: O χ^2 como função de $\Re(S_4)$ para um caso simulado.

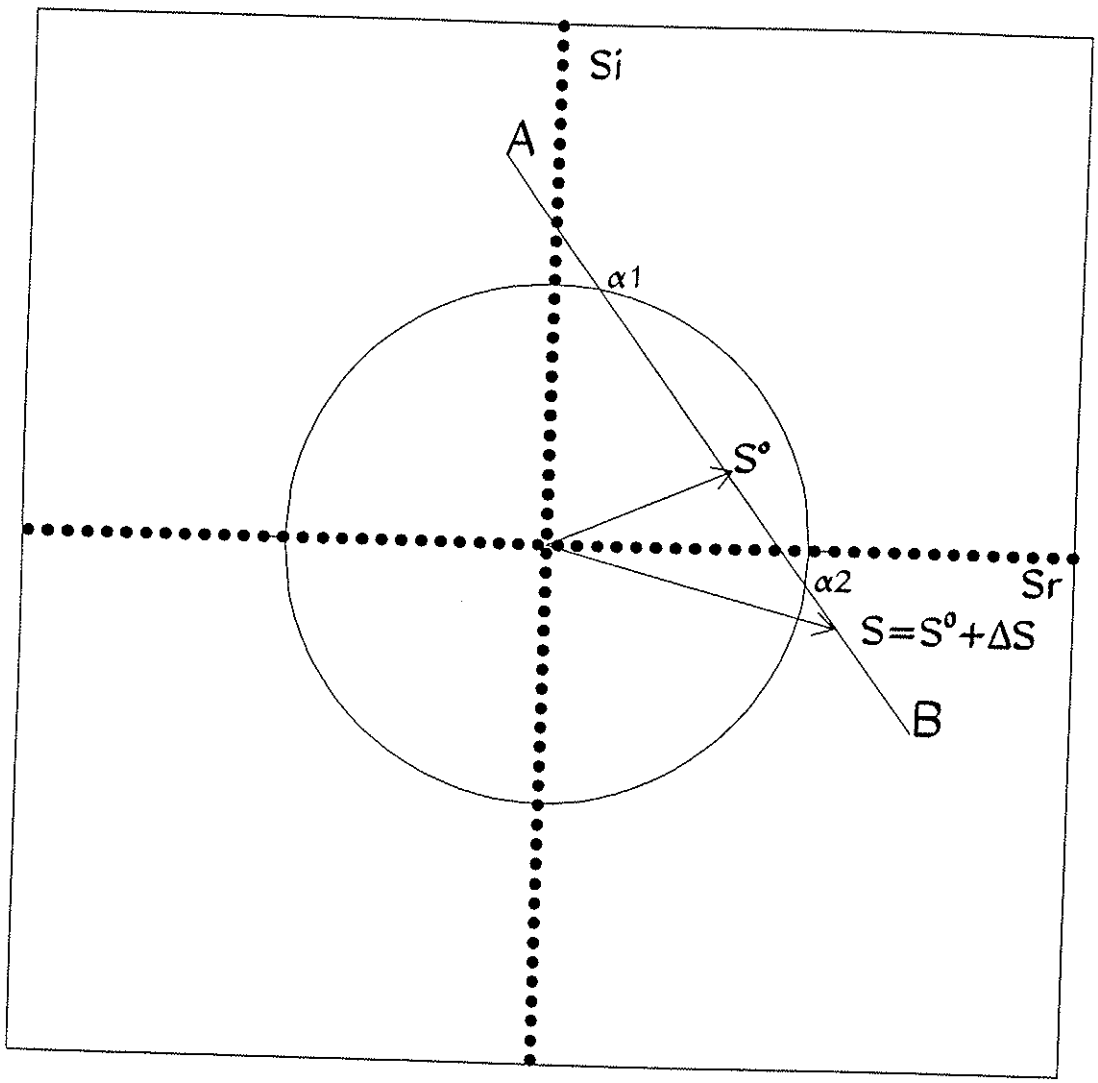

Figura 2.2: Representação pictórica da condição de unitariedade. A reta AB representa a direção do gradiente.

Capítulo 3

Aplicações do método a dados experimentais.

3.1 O sistema $^{12}C+^{16}O$

O método foi aplicado à 16 distribuições angulares do sistema $^{12}C+^{16}O$ medidas em energias de 8.55MeV até 26.74MeV no centro de massa sendo a barreira coulombiana para este sistema em torno de 8.5MeV. Estes dados foram obtidos em parte no Pelletron por A. C. C. Villari [2], por Frölich [7] e por P. Charles [8] e consistem em distribuições angulares completas medidas com passos em energia que variam entre 1 e 2 MeV no sistema de centro de massa.

Na figura 3.1 a seguir mostramos os resultados dos ajustes para 6 energias representativas.

Na tabela I estão as energias ajustadas, o maximo valor de momento angular, o numero de pontos experimentais, numero de graus de liberdade e o chi-quadrado reduzido obtido.

Na figura 3.2 exibimos o modulo das matrizes-S obtidas com os respectivos erros nas mesmas energias. Observa-se que nos casos em que os erros são grandes, as distribuições angulares são incompletas ou tem erros experimentais tambem grandes. Ficou evidente desta análise que são necessárias medidas completas de distribuições angulares a fim de se obter matrizes-S precisas.

Em todos os casos analisados o método se mostrou bastante estável obtendo sempre uma solução unitária e praticamente sem interferência do operador. Este é um aspecto importante pois nos programas de análise em defasagens disponíveis até então muitas vezes era exigida a intervenção do operador limitando o número de ondas parciais ajustadas e repetindo a procura de vários pontos de partida diferentes a fim de obter uma solução unitária para a matriz-S.

3.1.1 Mecanismos de reação e as matrizes-S obtidas

Nas figura 3.3 mostramos diagramas de Argand em função do momento angular obtidos para as energias 21.86MeV e 23.14MeV .

$E_{C.M.}(MeV)$	ℓ_{max}	N_0	N	χ^2
8.549	9	42	22	20
9.064	9	43	23	13
10.010	12	43	17	14
11.040	13	43	15	12
11.980	13	44	16	16
13.013	14	41	11	13
14.042	15	45	13	14
14.984	16	44	10	41
17.280	19	87	47	50
19.400	19	68	28	5.8
20.790	20	87	45	34
21.860	21	88	44	19
23.140	23	103	55	5.5
24.490	24	84	34	3.5
25.500	24	88	38	10
26.740	25	87	35	4.9

Tabela 3.1: Um sumário das dezeseis energias analisadas.

ℓ_0	$\Gamma/2$	Δ
13.50	2.25	3.00
6.50	0.93	1.51
2.70	1.00	1.50
0.00	0.75	1.20

Tabela 3.2: Parametros dos quatro polos de Regge observados em 23.14 MeV.

Observa-se nestes diagramas a ocorrencia "laços" no sentido anti-horário na medida em que o momento angular diminue o que é uma assinatura da presença de polos de Regge [9, 10]. Em particular na energia de 23.14MeV observam-se 4 voltas completas. Foi feito um ajuste parametrizando-se a matriz-S em termos de polos de Regge a partir da expressão:

$$S_\ell = \prod_1^4 \frac{\ell - \ell_0 + i(D - \Gamma/2)}{\ell - \ell_0 - i\Gamma/2}. \tag{3.1}$$

onde Γ é a largura total da ressonância no espaço de momento angular e D a largura parcial. A condição de unitariedade impõe que $D \leq \Gamma$. Quando o zero está abaixo do eixo real ($\Gamma/2 \leq D \leq \Gamma$), o "laço" contorna a origem do diagrama de Argand e diz-se que a ressonância está fortemente acoplada ao canal elástico. Se $D \leq \Gamma/2$ o "laço" não contorna a origem e a ressonância está fracamente acoplada ao canal elástico.

As larguras e posições dos polos obtidos estão na tabela 3.2.

Outro aspecto interessante, e que está presente na matriz-S obtida na energia de 26.74MeV, é a depenência da paridade que pode ser observada claramente no seu módulo

em função do momento angular. A existência de um termo dependente da paridade na matriz-S pode ser devida à contribuição de um processo onde há a troca de indentidade entre alvo e projétil contribuindo para o espalhamento elástico. No caso do espalhamento $^{12}C+^{16}O$ a transferência de uma partícula-α leva de volta ao canal elástico e pode portanto ser a responsável por esse comportamento. Podemos escrever a matriz-S como sendo composta pela soma de um termo "direto" S_ℓ^0 e um termo de Majorana (S_ℓ^m) onde a dependência da paridade é explicitada:

$$S_\ell = S_\ell^0 + (-1)^\ell S_\ell^m. \tag{3.2}$$

Os dois termos da equação acima podem ser estimados interpolando-se separadamente a matriz-S para momentos angulares pares (S_{par}) e impares (S_{impar}). Obtemos então:

$$S_\ell^0 = \frac{S_{par} + S_{impar}}{2} \tag{3.3}$$

e

$$S_\ell^m = S_{par} - S_\ell^0. \tag{3.4}$$

Na figura 3.4 mostramos diagramas de Argand obtidos para os termos diretos e de Majorana. A interpolação foi feita com splines lineares.

Observa-se novamente presença de polos de Regge em ambos os termos. Ressaltamos o fato de que este comportamento não é observado no diagrama de Argand para a matriz-S total S_ℓ^0 onde a trajetória do diagrama é aparentemente caótica.

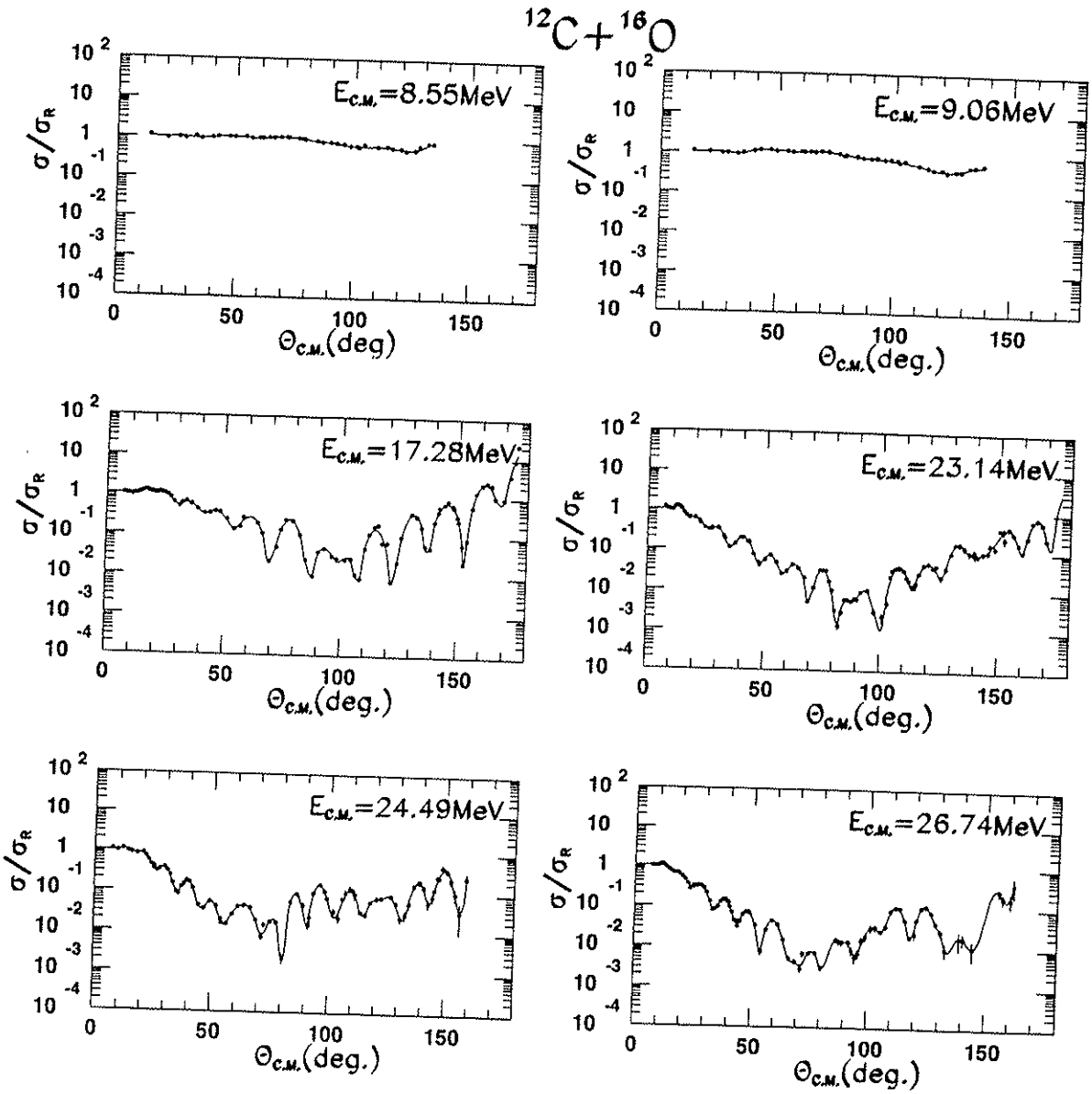

Figura 3.1: Ajuste das distribuições angulares experimentais.

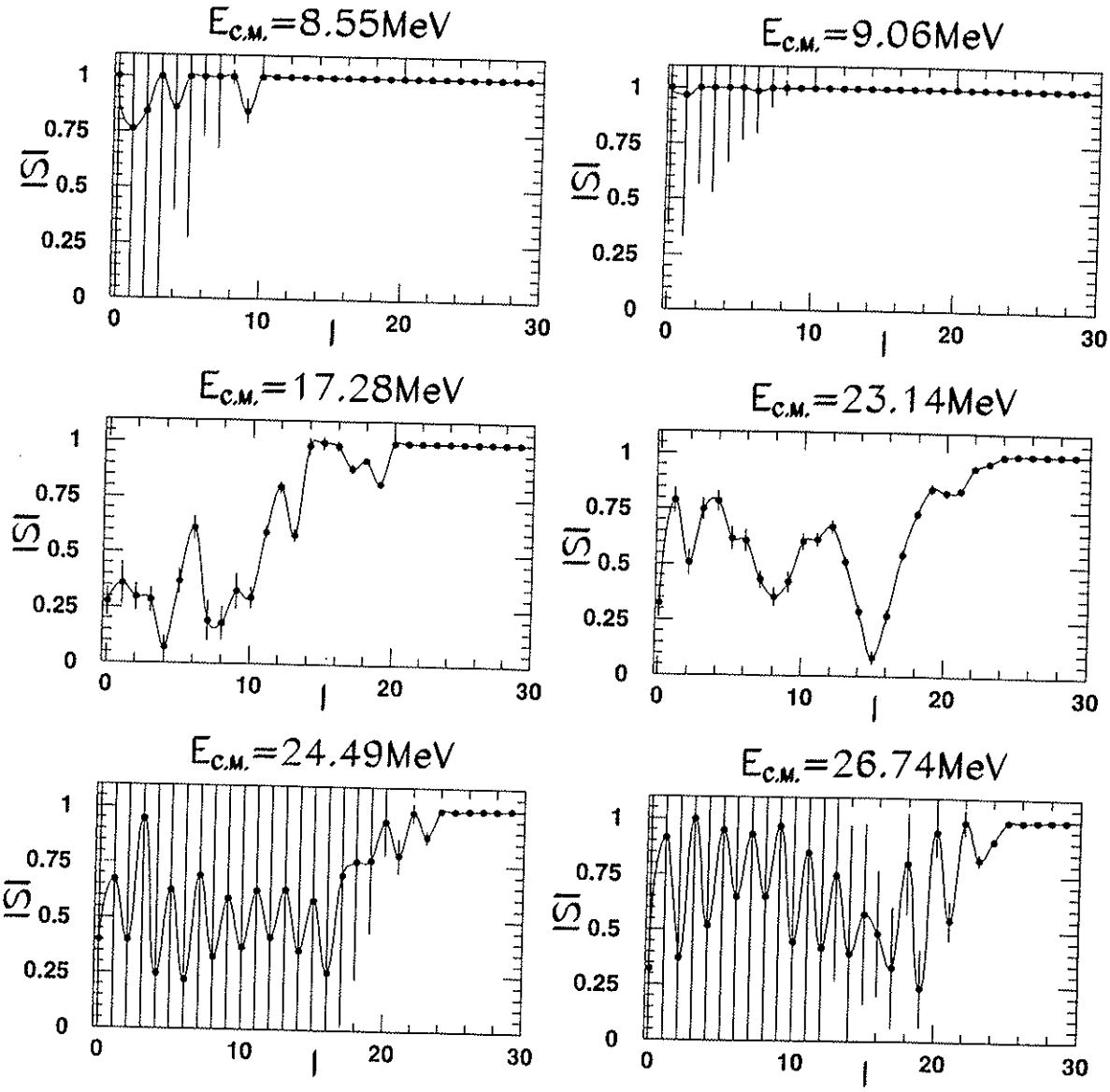

Figura 3.2: Modulos da matrizes-S obtidas correspondente aos ajustes da figura 3.1.

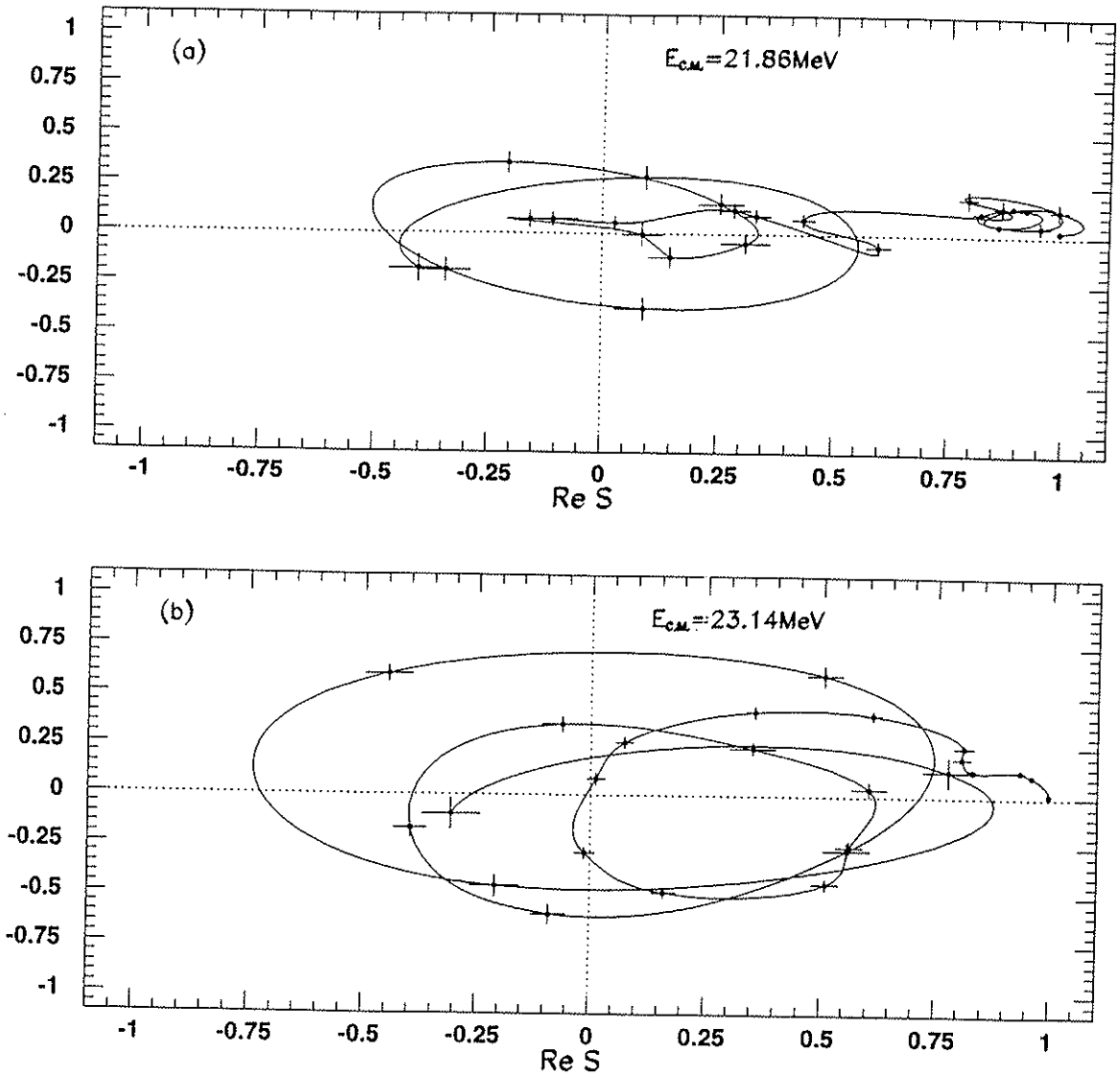

Figura 3.3: Diagramas de Argand em função do momento angular.

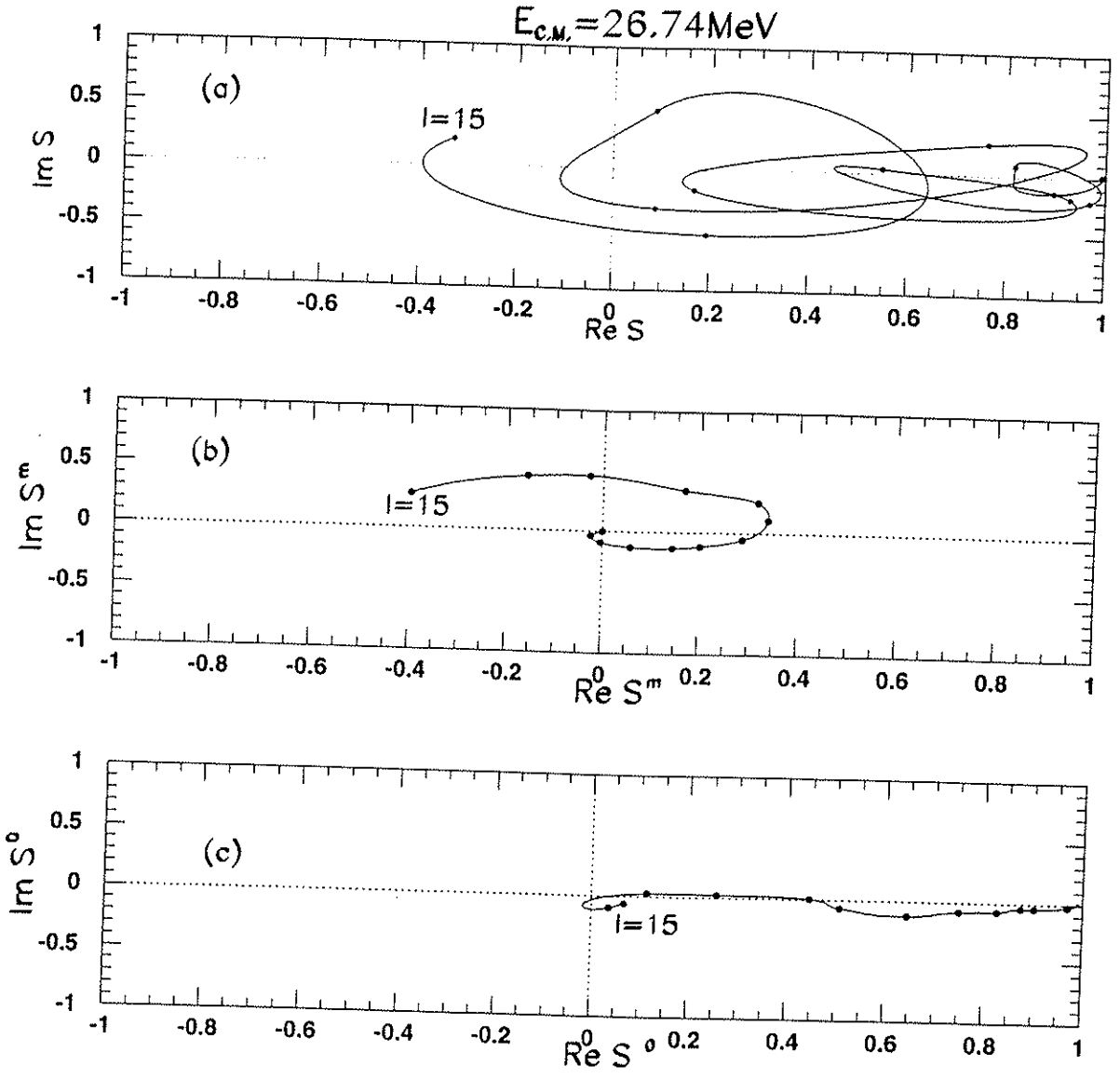

Figura 3.4: Diagramas de Argand par os termos direto e de Majorana em E_{cm} = 26.74MeV.

3.2 O sistema $^{12}C+^{24}Mg$

O sistema $^{12}C+^{24}Mg$ é um dos sistemas n-α mais estudados por nosso grupo [11, 12, 13, 14]. Em energias em torno de 2 a 3 vezes a barreira coulombiana ($E_b^{lab} \approx 16MeV$) este sistema apresenta o fenômeno denominado "Anomalous Large Angle Scattering" com distribuições angulares oscilatórias e subida da secção de choque em angulos traseiros tanto no canal elástico como nos canais inelásticos e em reações de transferência alfa. Este comportamento não é previsto pelo modelo de absorção forte [15] que em certo momento foi considerado válido para sistemas nesta região de massa e energia. O fato de que as secções de choque de reações de transferência alfa são bastante elevadas em sistemas n-α, deu origem a interpretação destes fenômenos como provenientes do acoplamento com estes canais de transferência. No entanto, mesmo em energias mais baixas, onde os canais de transferência são muito pouco populados, já havia sido observado o comportamento oscilatório das distribuições angulares elásticas neste mesmo sistema [14](anexo 2). Nosso grupo decidiu realizar medidas completas de distribuições angulares e funções de excitação para este sistema em energias próximas à da barreira coulombiana. Foram medidas distribuições angulares do espalhamento elástico $^{12}C+^{24}Mg$ em energias de 16MeV a 24MeV no sistema de laboratório com passos de 0.5MeV [13] e funções de excitação em $\Theta_{cm} = 90^o$ e $\Theta_{cm} = 180^o$ com resolução em torno de 30KeV [16](anexo 3). As distribuições angulares foram analisadas por W. Sciani e A. Lépine [13] por cálculos de modelo otico e foi obtido um potencial dependente da energia que reproduz as oscilações observadas e que apresenta como característica principal uma forte transparência mesmo no interior dos nucleos. Este comportamento não havia sido observado em sistemas pesados em baixas energias e contraria frontalmente as previsões do modelo de absorção forte.

A seguir apresentaremos os resultados da análise da matriz-S das mesmas distribuições angulares e as medidas das funções de excitação.

3.2.1 Análise da Matriz-S

A análise das 15 distribuições angulares medidas foi feita utilizando-se basicamente a aproximação linear do método desenvolvido. Devido ao fato de que as medidas foram feitas em energias próximas à barreira coulombiana, a interação nuclear é pouco intensa e o método linear se mostrou estável. O ponto de partida para a análise foi sempre a matriz-S coulombiana, ou seja, $S_\ell^n = 1.0$ para todos os valores de momento angular e a solução foi sempre encontrada após 2000 interações aproximadamente. Como na matriz-S de partida não havia nenhuma suposição a respeito do raio nuclear foi possível se minimizar o chi-quadrado reduzido, variando-se o numero máximo de ondas parciais consideradas no cálculo (L_{max}). Na figura 3.5 mostramos o chi-quadrado reduzido obtido após 1000 interações em função de L_{max} na energia de 24MeV. Observamos que o chi-quadrado apresenta um mínimo em torno de $L_{max} = 10$ e aumenta rapidamente para valores inferiores. Para valores maiores o chi-quadrado aumenta lentamente mostrando que as ondas parciais mais altas participam pouco do espalhamento nuclear. O valor de L_{max} foi sempre escolhido no mínimo imediatamente após à subida evitando deste modo

a superabundância de parametros ajustados.

Nas figuras 3.6, 3.7, 3.8 mostramos as 15 distribuições angulares ajustadas. Os valores de chi-quadrado reduzido estiveram sempre em torno de 1. Nas figuras 3.9, 3.10, 3.11 estão os modulos da matrizes-S obtidas em função do momento angular e os respectivos erros.

Em algumas energias como 17 MeV, 19 MeV e 22 MeV observamos que os erros são grandes para ondas parciais de baixo momento angular mostrando que nada pode se afirmar sobre a matriz-S. Para as outras energias os erros são menores e observa-se que a matrizes em geral apresentam estruturas em função do momento angular e transparência para momentos angulares proximos de $l = 0$. Nas energias 16 MeV e 23 MeV os erros são bastante pequenos e observam-se fortes oscilações no modulo da matriz-S com uma transparência acentuada. Na energia mais alta 24 MeV, o modulo da matriz-S já é bastante pequeno em momentos angulares baixos indicando que a partir desta energia há um aumento na secção de choque de reação. Nas energias mais baixas apenas a fusão e espalhamento inelástico contribuem significativamente para a absorção. O fato dos erros serem grandes para algumas energias é devido à qualidade e principalmente à completeza das distribuições angulares experimentais. Em particular, as energias onde os erros são maiores são as que tem menos pontos medidos como pode ser observado nas figuras 3.6, 3.7, 3.8.

A análise apenas do modulo da matriz-S não é suficiente para uma compreensão mais profunda do mecanismo de reação. É importante o estudo do comportamento da fase nuclear como função do momento angular e da energia. Nas figuras 3.12, 3.13, 3.14 estão mostrados os diagramas de Argand ($S_r \times S_i$) com os erros, em função do momento angular para todas as energias analisadas.

Nota-se que na maioria das energias os diagramas apresentam polos de Regge. Em alguns casos como em 23 MeV, observam-se 4 polos dos quais dois contornam a origem do diagrama o que significa que a largura parcial é maior do que a metade da largura total dos polos o que caracteriza um acoplamento forte com o canal elástico. Há casos como em 16 MeV onde os polos não contornam a origem indicando acoplamento fraco com o canal elástico. Devido ao fato dos erros serem grandes, fica difícil se definir de maneira inequívoca o comportamento dos polos individualmente como função da energia.

Nas figuras 3.15, 3.16 mostra-se o comportamento da defasagem nuclear em função da energia para vários valores de momento angular juntamente com os erros.

No eixo vertical está graficada a defasagem nuclear real dividida por π e um aumento de 1 unidade nesta grandeza corresponderia a uma ressonância. Em nenhum dos casos são observadas ressonâncias fortemente acopladas ao canal elástico. Em geral as defasagens nucleares são pequenas estando compreendidas no intervalo $[-\pi/2, \pi/2]$. Apenas para $l = 1$ e $l = 5$ em 23MeV há uma variação que poderia ser maior ou igual a 1 dentro dos erros. Entretanto,ressonâncias fracas não estão descartadas e correspondem a comportamentos do tipo observado por exemplo para $l = 2$, $l = 3$ e $l = 5$ em 19.5MeV onde a fase decresce para valores negativos e volta a crescer. Isto corresponde a uma volta no diagrama de Argand em torno de um ponto fora da origem. Todavia, devido aos erros, não se pode ser conclusivo a respeito da existência ou não destas ressonâncias. Observa-se tambem

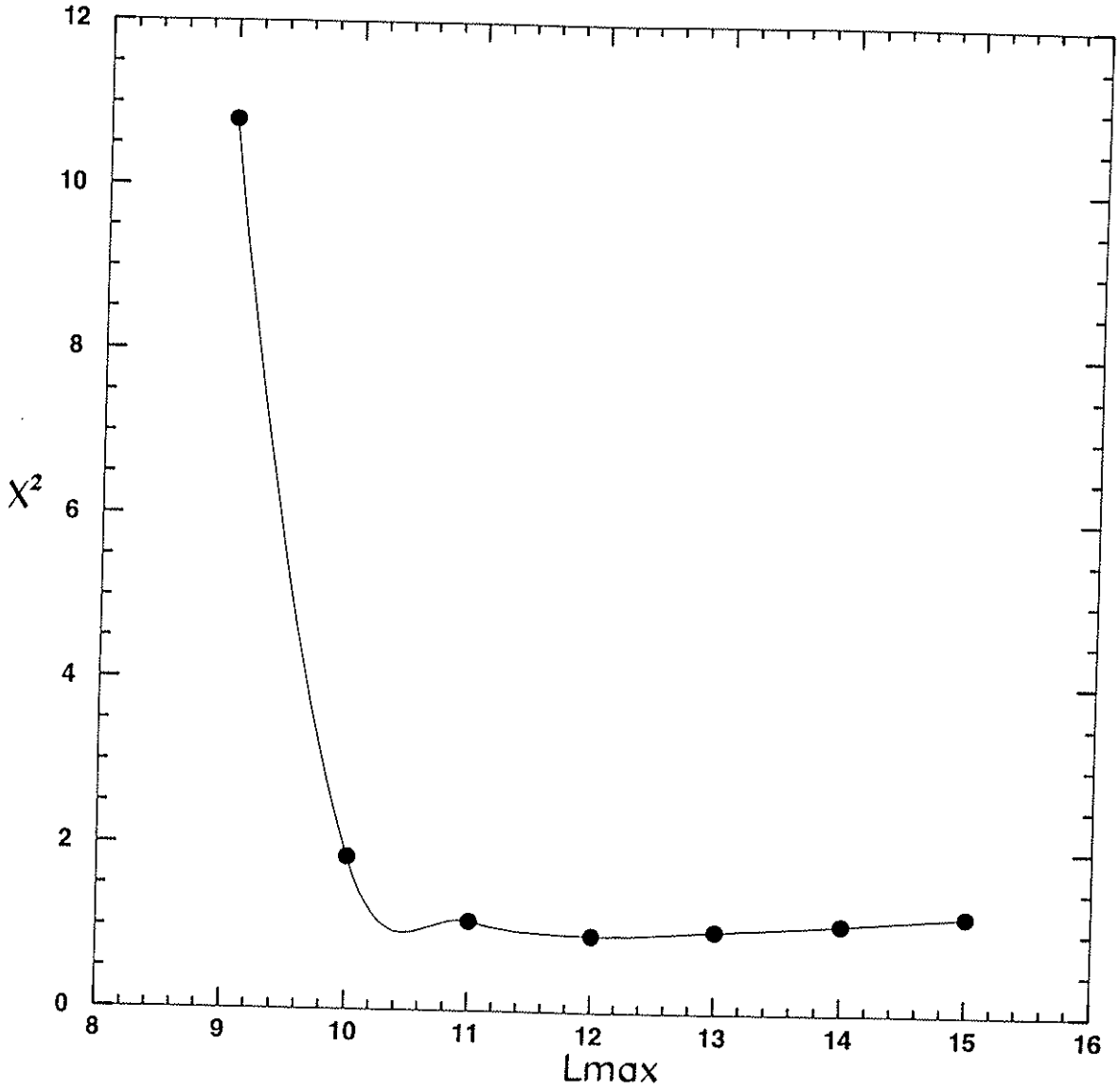

Figura 3.5: Chi-quadrado como função de L_{max}.

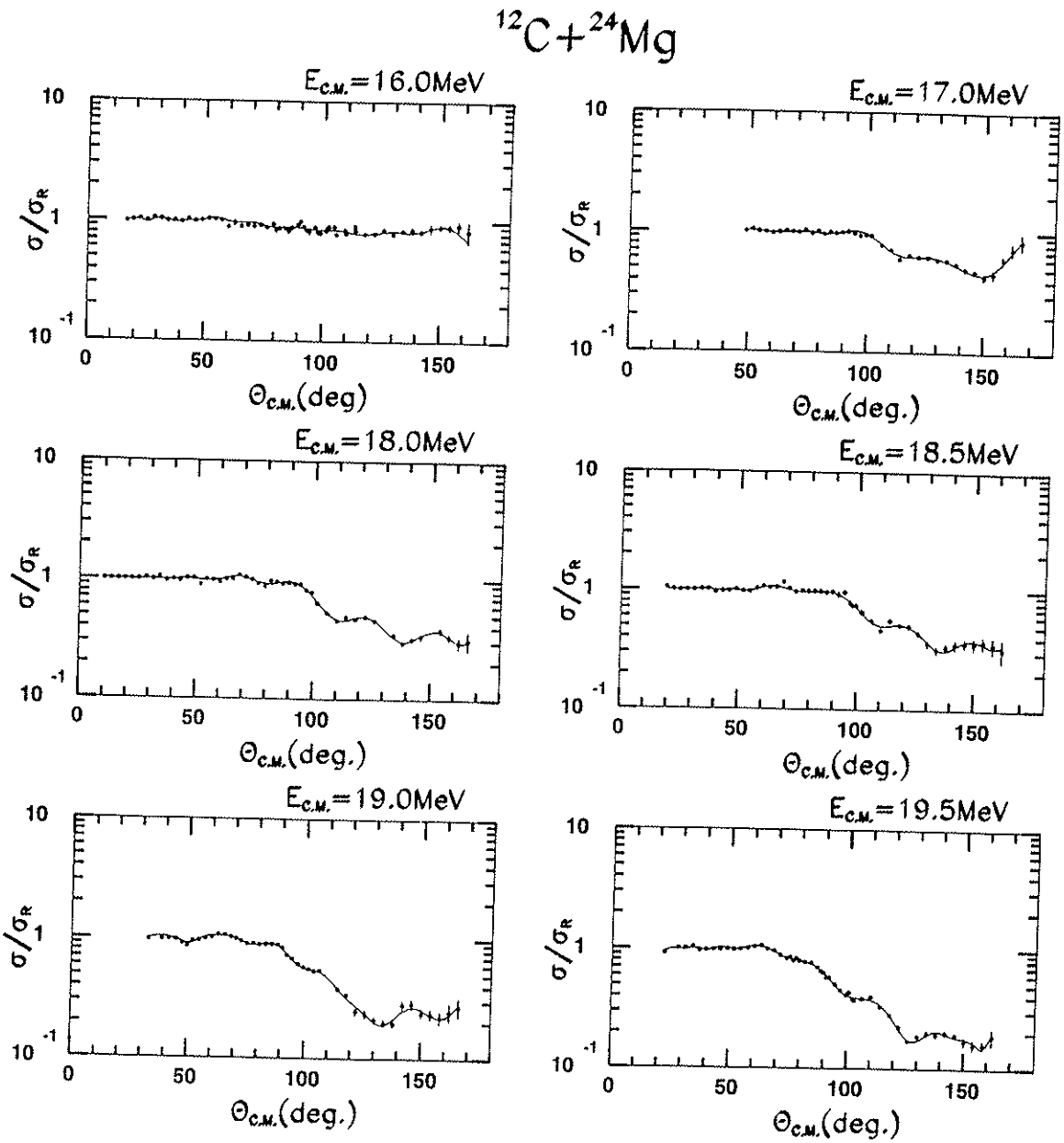

Figura 3.6: Distribuições angulares $^{12}C+^{24}Mg$.

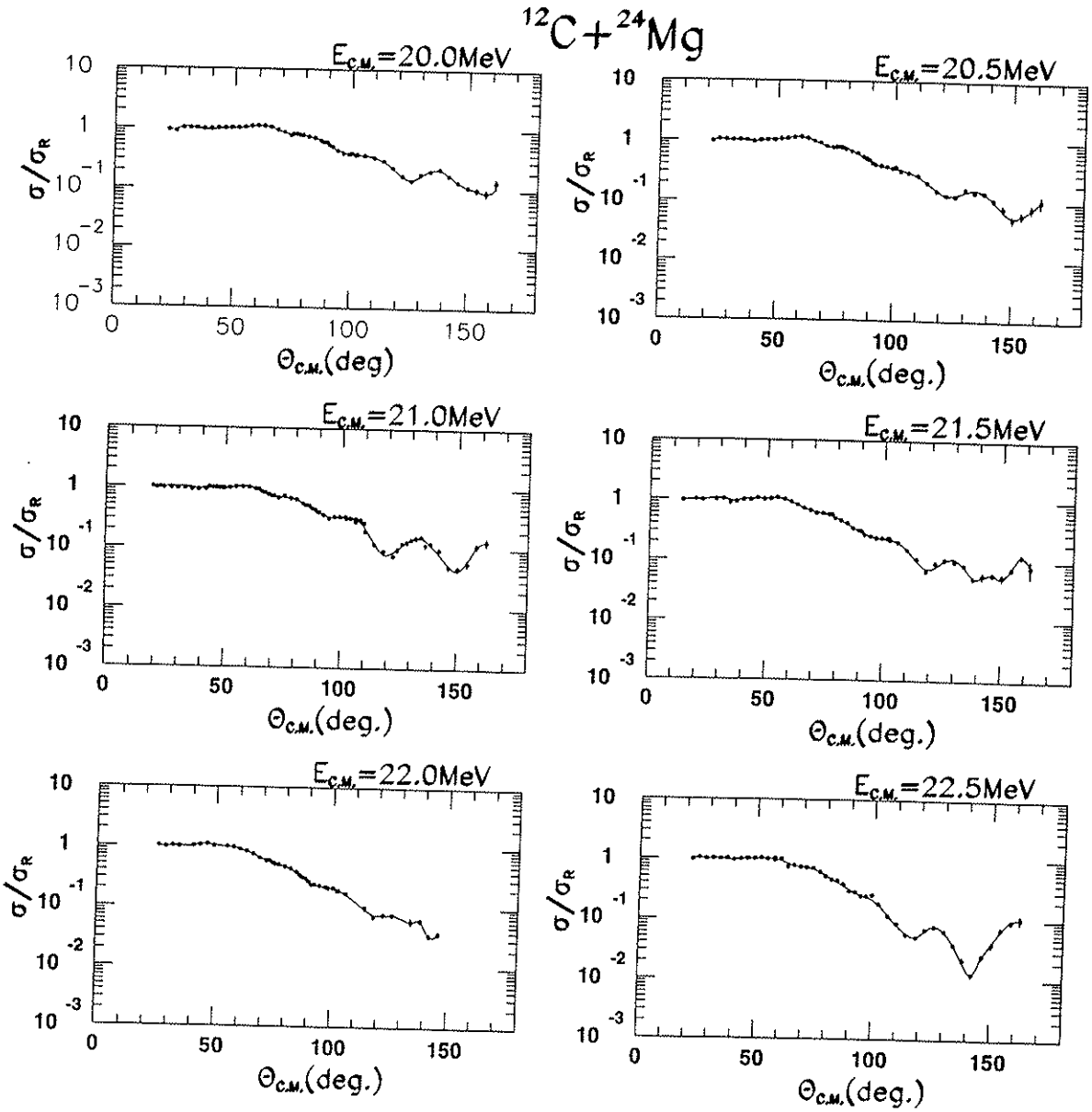

Figura 3.7: Distribuições angulares $^{12}C+^{24}Mg$.

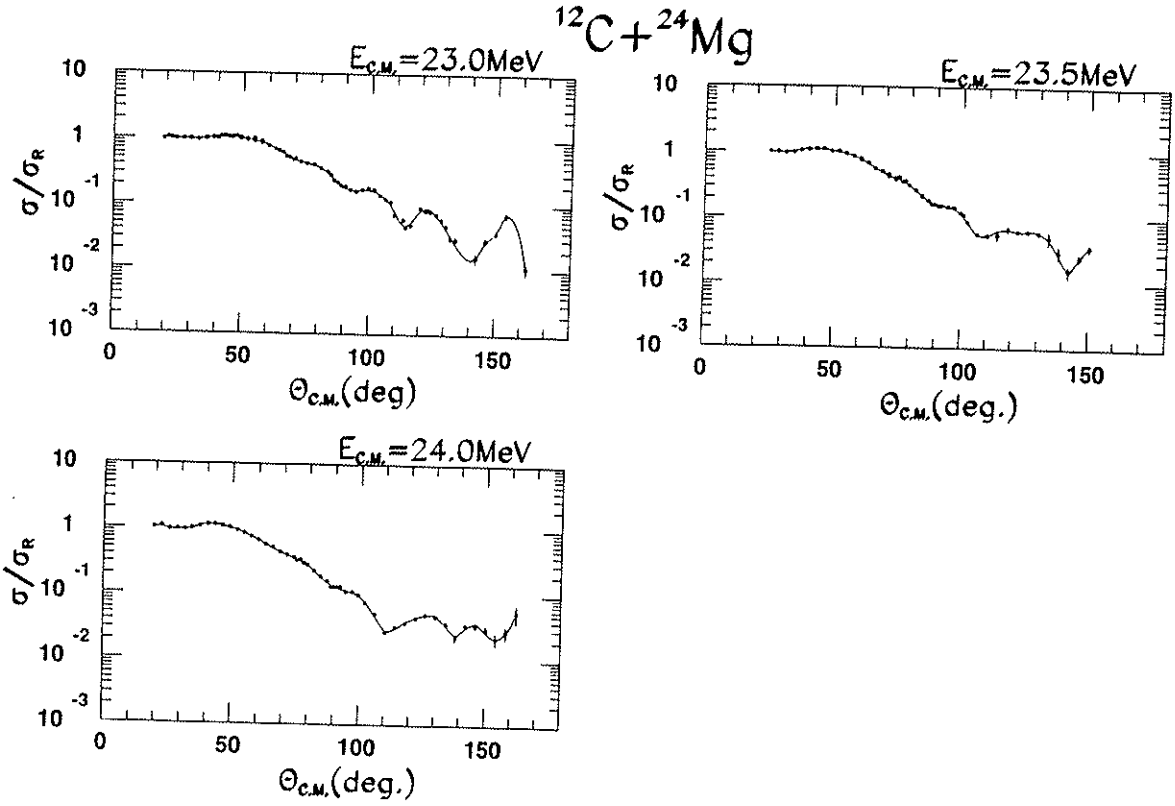

Figura 3.8: Distribuições angulares $^{12}C+^{24}Mg$.

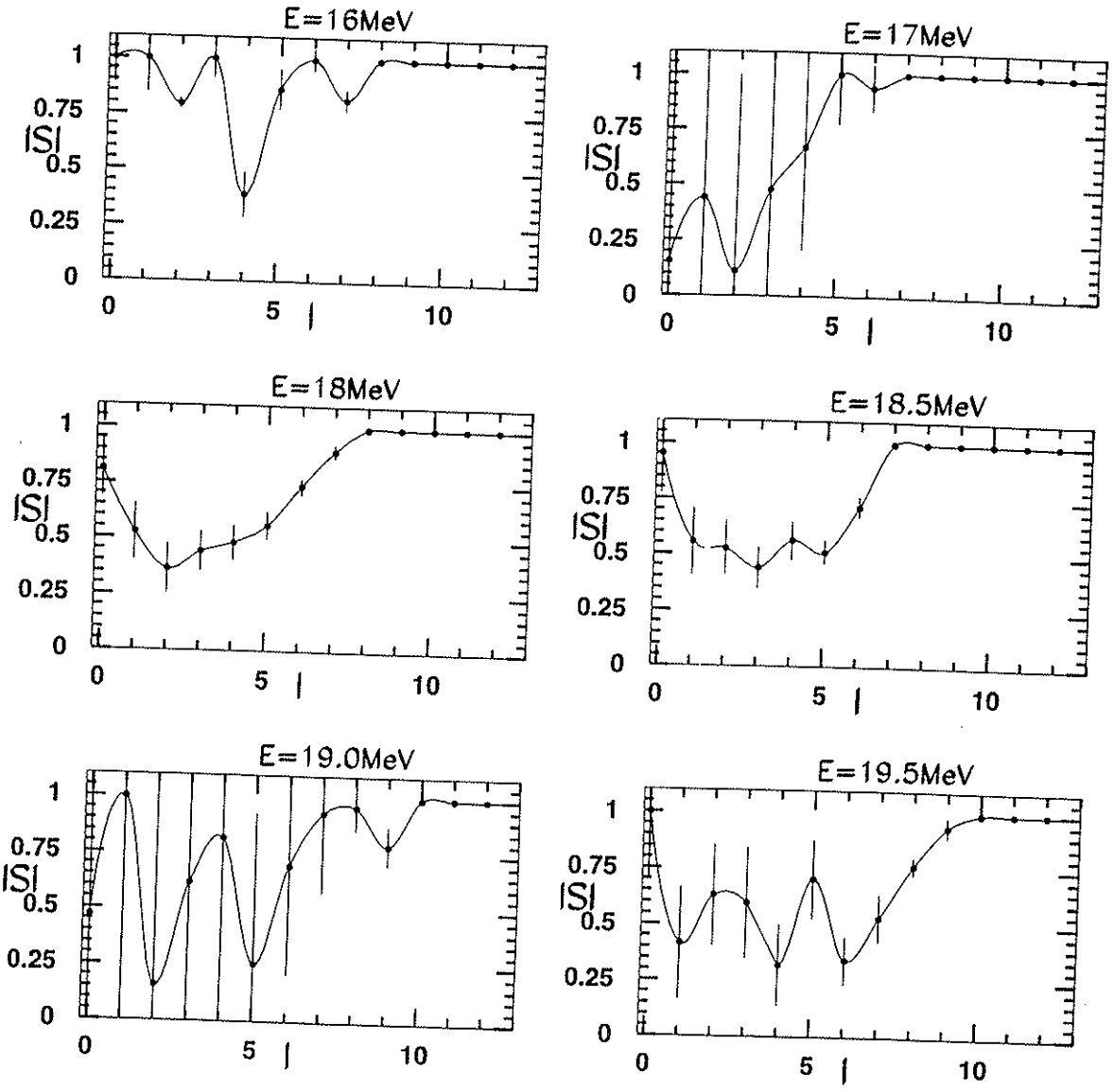

Figura 3.9: Módulo das matrizes-S obtidas.

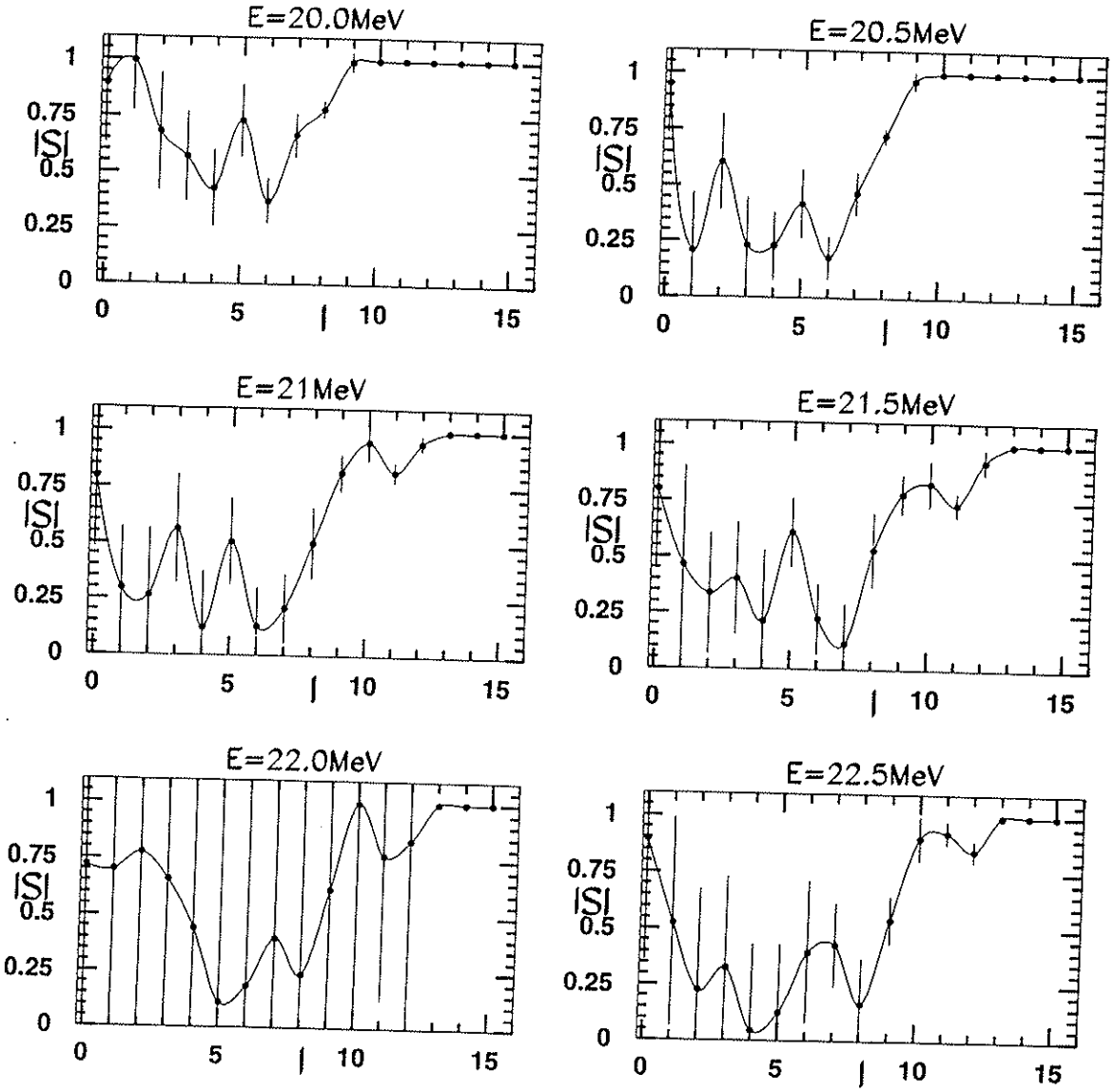

Figura 3.10: Módulo das matrizes-S obtidas.

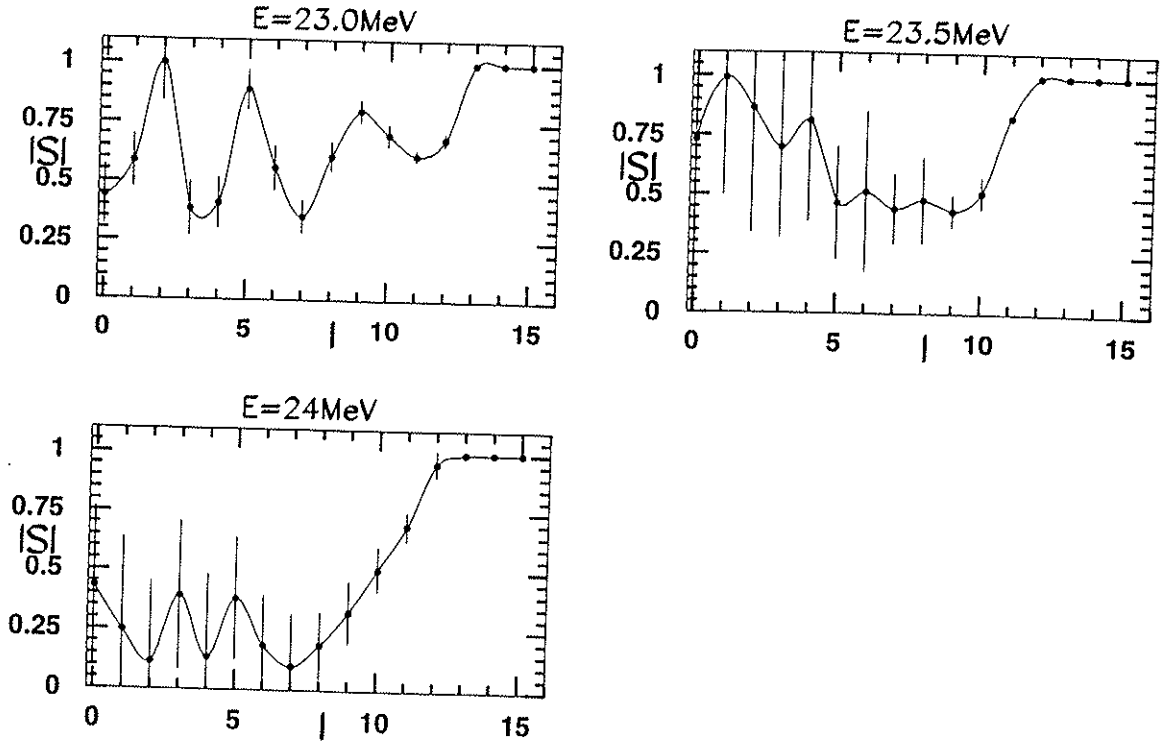

Figura 3.11: Módulo das matrizes-S obtidas.

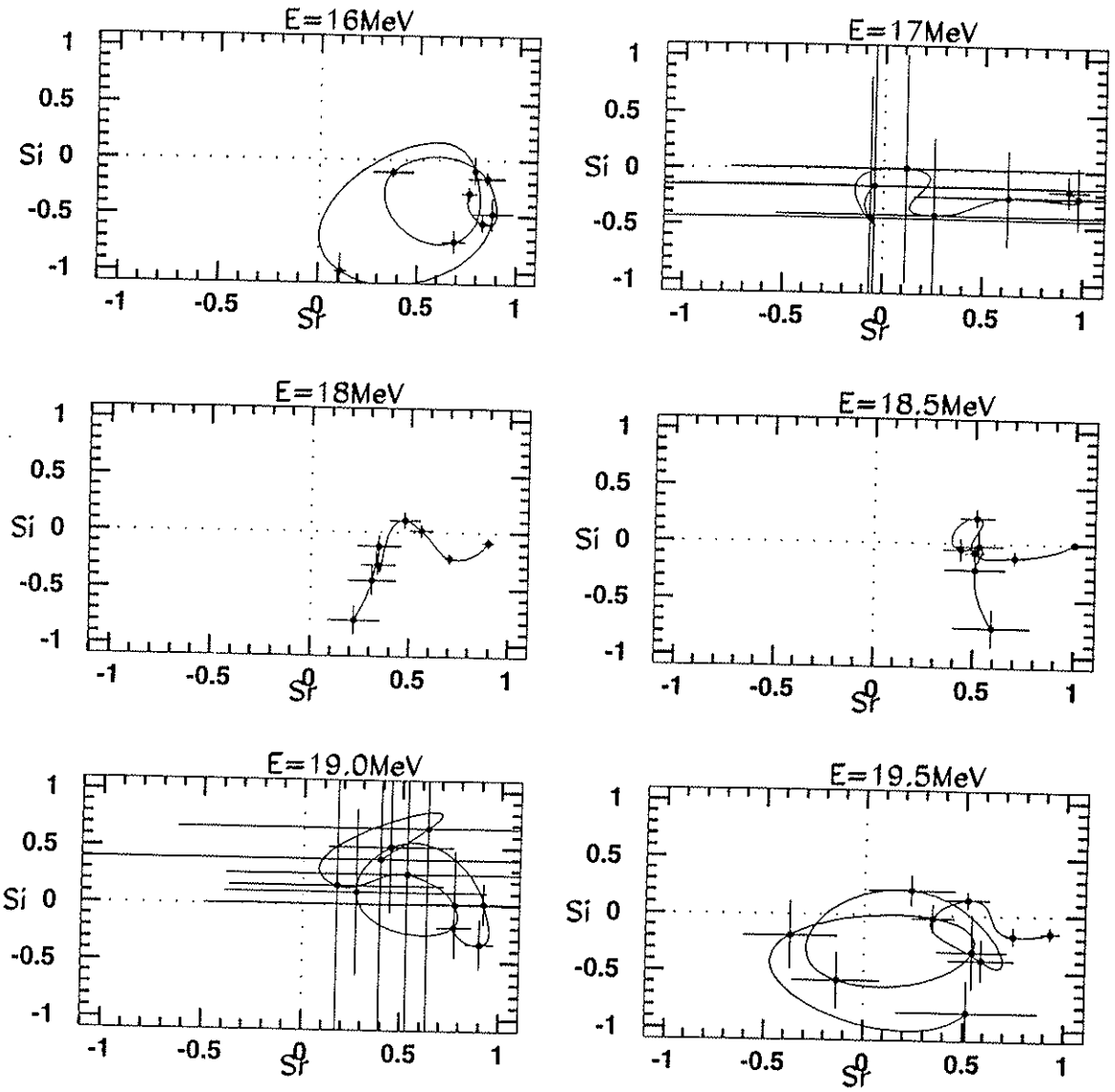

Figura 3.12: Diagramas de argand em função do momento angular.

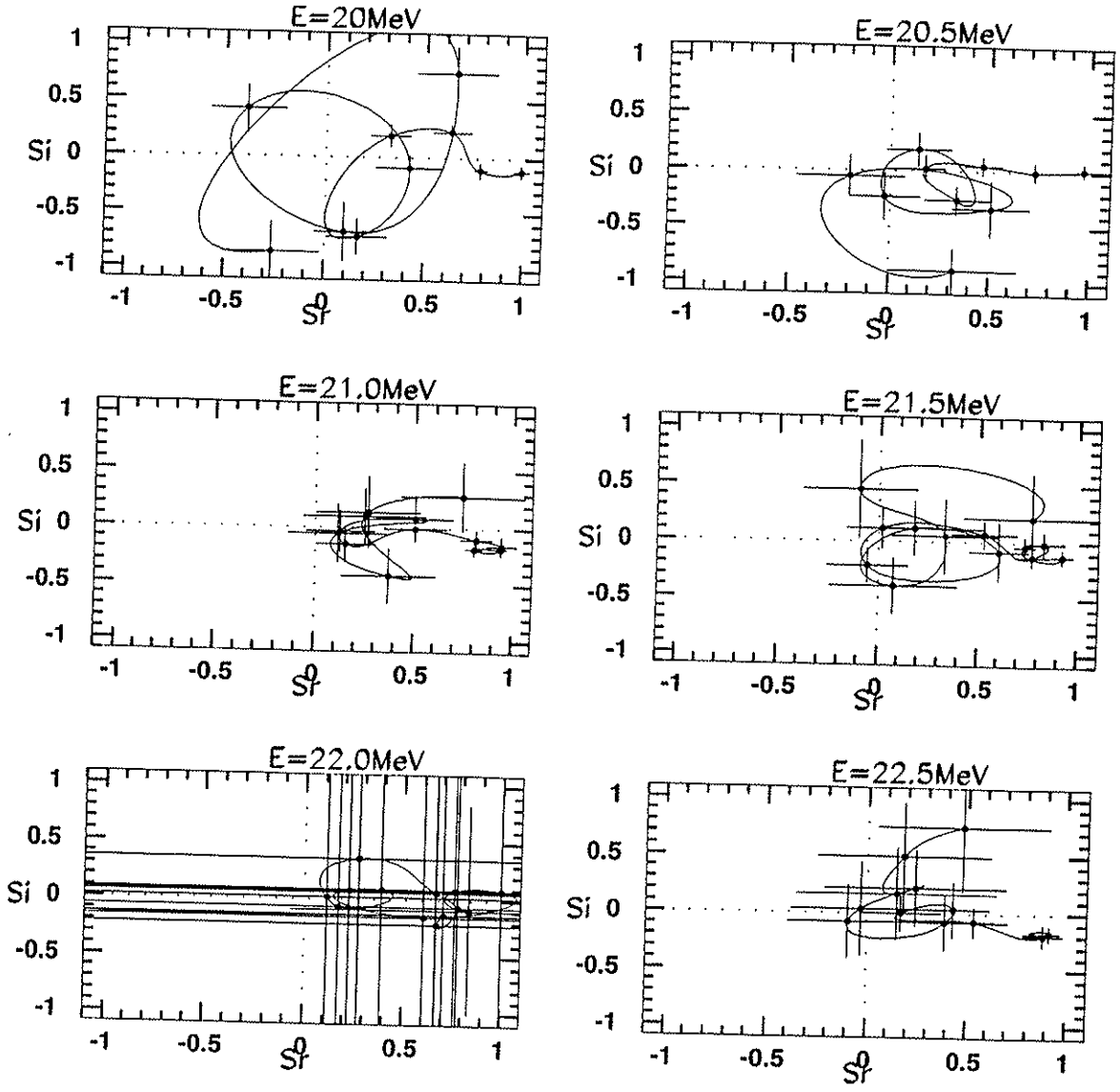

Figura 3.13: Diagramas de argand em função do momento angular.

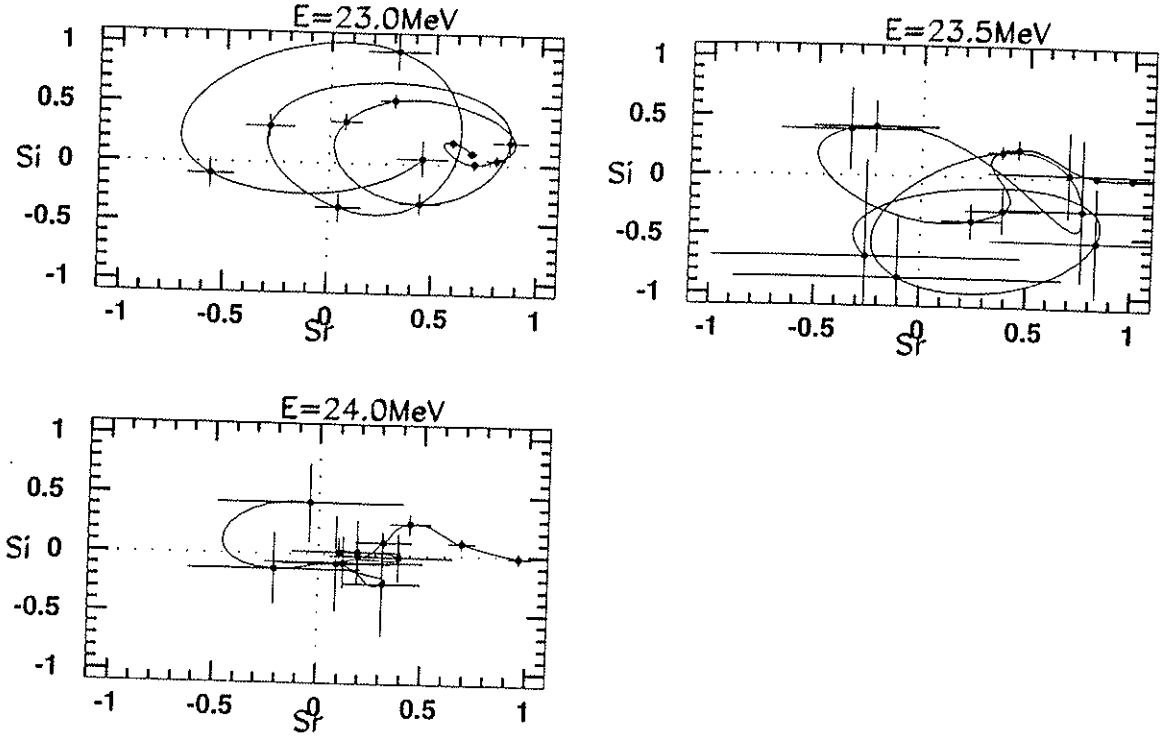

Figura 3.14: Diagramas de argand em função do momento angular.

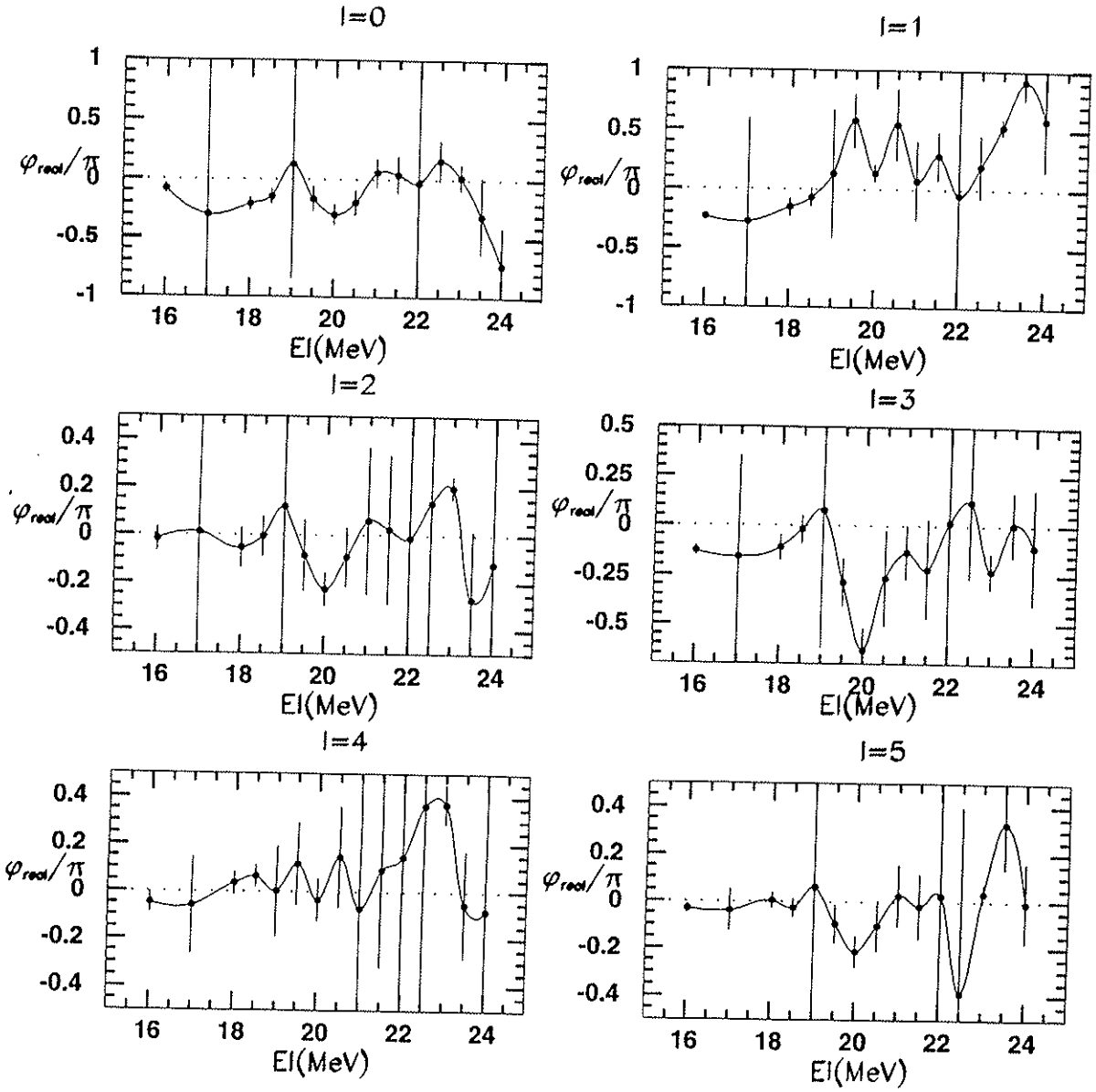

Figura 3.15: Fase nuclear real em unidades de π em função da energia.

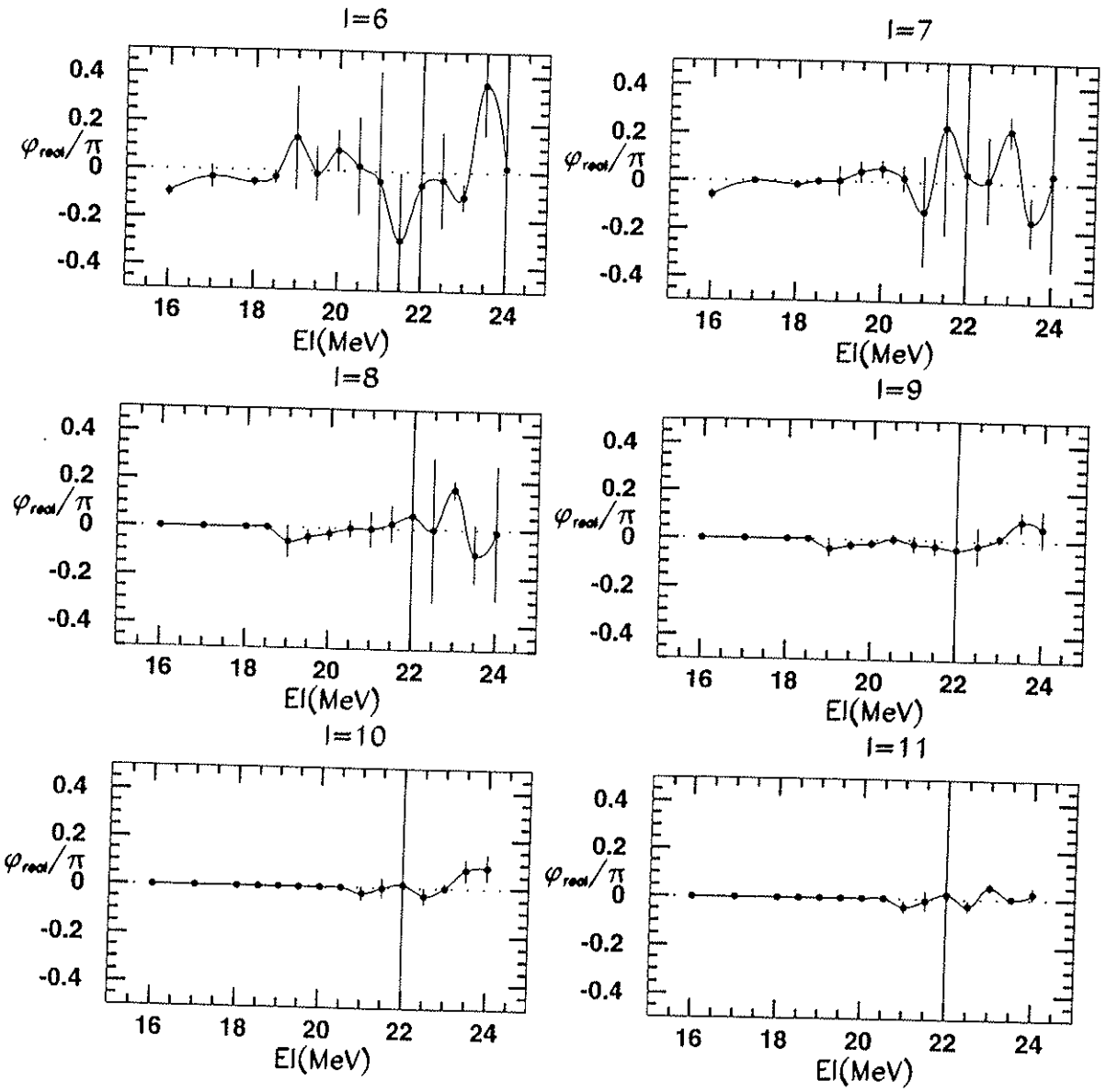

Figura 3.16: Fase nuclear real em unidades de π em função da energia.

que o passo em energia destes dados é de 500 KeV no sistema de laboratório ou 300 KeV no centro de massa e que a existência de ressonâncias de larguras menores não seria detectada nesta análise.

3.2.2 Funções de Excitação do sistema $^{12}C+^{24}Mg$

Foram medidas funções de excitação [16] para o espalhamento elástico$^{12}C+^{24}Mg$ em $\Theta_{cm} = 90^o$ e $\Theta_{cm} = 140^o$ com passos de 50KeV no sistema de laboratório o que fornece 30KeV no sistema de centro de massa. Na figura 3.17 estão mostrados os dados obtidos. (Anexo 3)

Observa-se que não estão presentes estruturas fortes com a energia o que é consistente com a análise das fases em função da energia feita anteriormente na qual nenhuma ressonância fortemente acoplada ao canal elástico foi observada. Na figura 3.17 mostramos o resultado de uma análise de autocorrelação das funções de excitação. Uma largura de coerência de 110KeV foi detectada em $\Theta_{cm} = 90^o$ e corresponde a largura esperada das flutuações devido processo de formação de nucleo composto [17]. Esta análise permitiu a estimativa da secção de choque media de flutuação devido a formação do nucleo composto e decaimento no canal elástico que é de 0.048mb o que corresponde a aproximadamente 0.3 % da secção de choque elástica média. Este resultado é importante pois mostra que a contribuição do processo de fusão e decaimento no canal elástico é muito pequena. Este processo contribui incoerentemente na secção de choque elástica e, quando está presente, deve ser subtraido da secção de choque medida.

Com o objetivo de se ressaltar a presença de estruturas de pequena amplitude, na figura 3.18 exibimos a quantidade $(\sigma/\langle\sigma\rangle_\Delta - 1)$ com $\Delta = 2$ MeV em função da energia para $\Theta_{cm} = 90^o$ e $\Theta_{cm} = 140^o$ e comparamos com uma função de excitação medida por Mermaz em $\Theta_{cm} = 180^o$. Observamos a presença de estruturas correlacionadas nos 3 angulos. Fizemos uma atribuição de spins para estas estruturas coerente com o fato de que em $\Theta_{cm} = 90^o$ apenas ondas pares contribuem enquanto que nos outros angulos todas as ondas estão presentes. Os valores estão indicados na figura e parecem seguir uma banda rotacional.

3.3 Relação com o Modelo Otico.

É interessante se estudar em que circunstâncias os fenômenos observados na matriz-S como polos de Regge podem ser produzidos num modelo tradicional como o modelo otico se utilizamos potenciais locais parametrizados na forma de Woods-Saxon. Nas figuras 3.20, 3.21, 3.22 mostramos diagramas de Argand em função do momento angular das matrizes-S obtidas a partir de um cálculo de modelo otico para o sistema $^{12}C+^{24}Mg$ utilizando o potencial determinado por A. Lépine e W. Sciani [13].

Devido ao fato de que a parte imaginária deste potencial é bastante pequena $W/V \approx 0.02$, polos são trazidos para perto do eixo real o que provoca o aparecimento dos "laços" observados nos diagramas de Argand. Cada "laço" corresponde a presença de um par

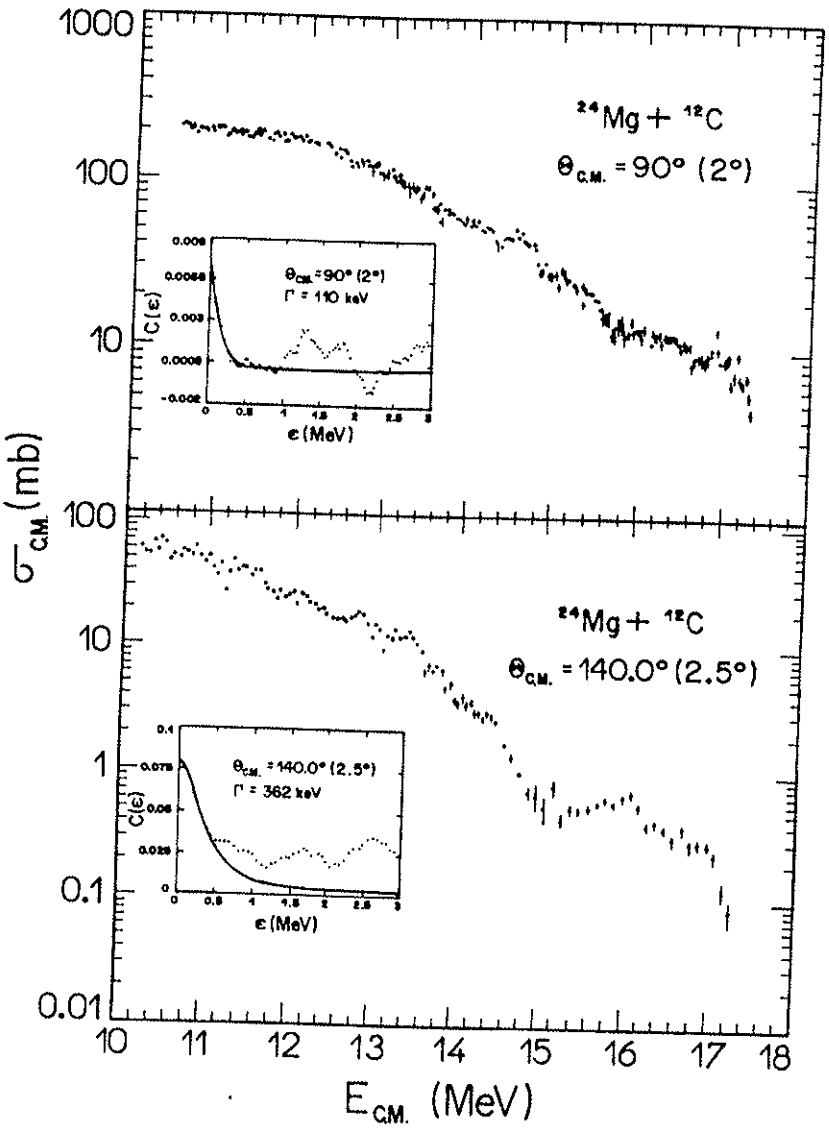

Figura 3.17: Funções de excitação medidas em $\Theta_{cm} = 90^0$ e 140^o e as correspondentes funções de autocorrelação.

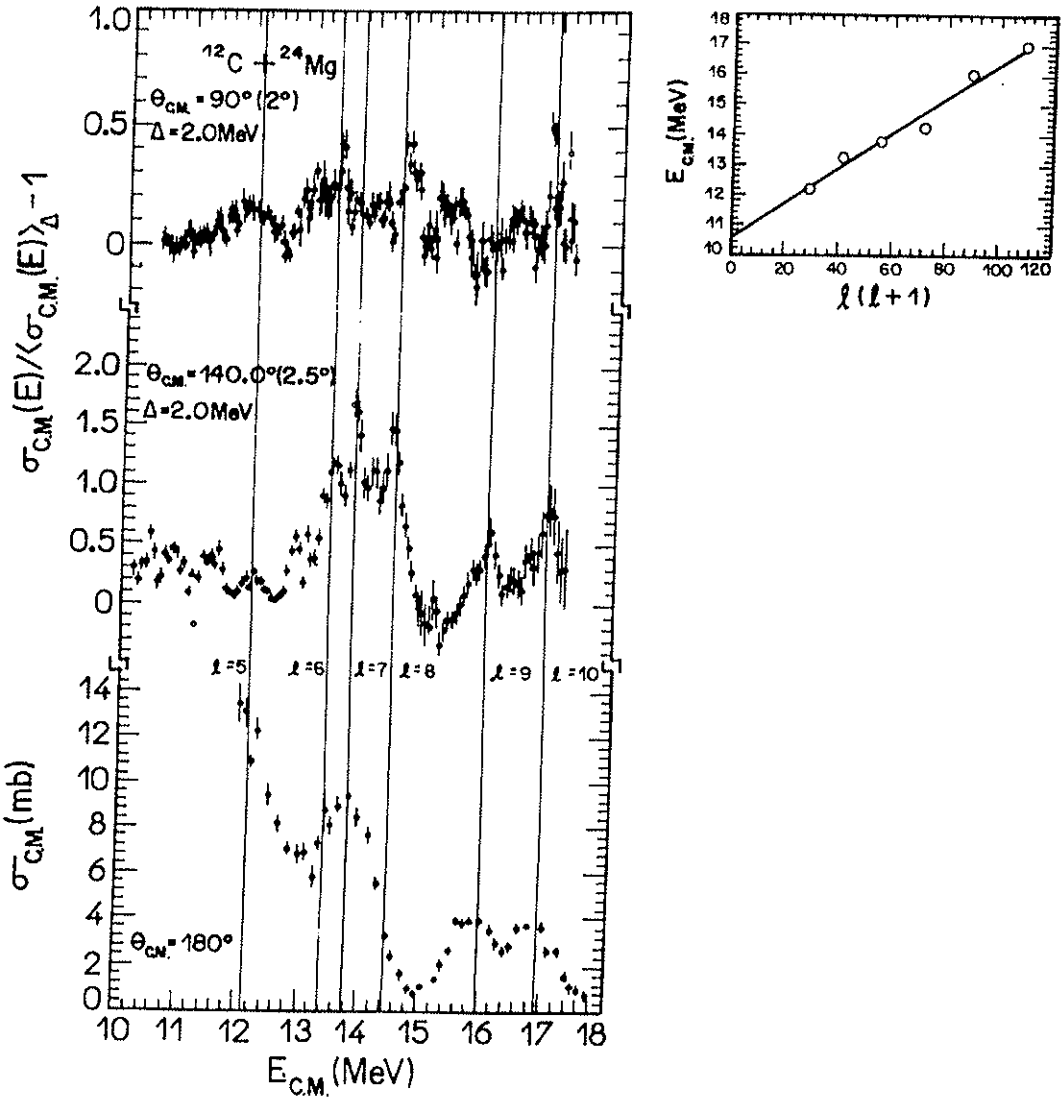

Figura 3.18: Funções de excitação em $\Theta_{cm} = 90°$, $140°$ e $180°$.

polo–zero dado pela expressão:

$$S_\ell = \prod_1^4 \frac{\ell - \ell_0 + i(D - \Gamma/2)}{\ell - \ell_0 - i\Gamma/2}. \tag{3.5}$$

Observamos que em energias baixas, os polos estão fracamente acoplados ao canal elástico $D \leq \Gamma/2$ e a medida em que a energia aumenta os polos tendem a envolver a origem $D \geq \Gamma/2$ ao passo que novos polos surgem em momentos angulares altos. Este comportamento pode ser entendido qualitativamente na figura 3.19 onde está mostrado o potencial efetivo para vários momentos angulares. Note que a escala no eixo vertical na figura foi transformada de modo a poder ser comparada diretamente com a energia de laboratório incidente.

Observamos que o potencial apresenta uma "bolsa" atrativa para todos os valores de momento angular que participam do espalhamento nestas energias. Como a parte imaginária do potencial é bastante pequena, isto permite a formação de estados tipo estacionários na bolsa atrativa sempre que um numero inteiro de semi– comprimentos de onda couber extamente na bolsa para um dado valor de momento angular. Neste caso este, momento angular ressoará. Na região de baixas energias pode-se observar que a partícula não tem energia para superar a barreira centrífuga e o estado ressonante se forma apenas por efeito tunel resultando em um polo fracamente acoplado. Na medida em que a energia aumenta a partícula pode vencer a barreira centrífuga e coulombiana e eventualmente formam-se estados ressonantes para certos valores de momento angular que estão fortemente acoplados ao canal elástico. Observamos que a partir de 20 MeV estes casos passam a ocorrer segundo este modelo. Em 24 MeV observa-se claramente a presença de 3 polos fortes e 1 fracamente acoplado. Observa-se destes diagramas de Argand que o modulo da matriz-S vem diminuindo conforme a energia aumenta enquanto que a fase nuclear real é sempre pequena para energias até 20 MeV e está no primeiro e quarto quadrantes. Pode-se dizer que há uma concordância qualitativa entre as matrizes-S obtidas pela análise dos dados e as do modelo otico favorecendo a imagem de que há de fato a formação destes estados ressonantes no potencial íon–íon.

3.4 Algumas considerações Teóricas

Estes dois exemplos ilustram o tipo de física que pode ser explicitada a partir da matriz-S sem nenhuma suposição a respeito do mecanismo de reação. A presença de polos de Regge é o que podemos esperar observar numa análise da matriz-S em função do momento angular em um sistema quântico que apresenta ressonâncias. Evidentemente o próximo passo deveria ser o desenvolvimento de modelos teóricos a partir dos quais possamos obter os fenômenos observados na matriz-S. Como um primeiro passo, a inclusão do canal de transferência–α acoplado ao elástico direto parece ser essencial no sistema $^{12}C+^{16}O$. A esse respeito há um intenso trabalho teórico e experimental em sistemas da camada s–d [15, 18, 19, 20, 21, 22, 23] onde mostra-se que este acoplamento pode introduzir na matriz-S uma "janela" em momento angular na região em torno do momento

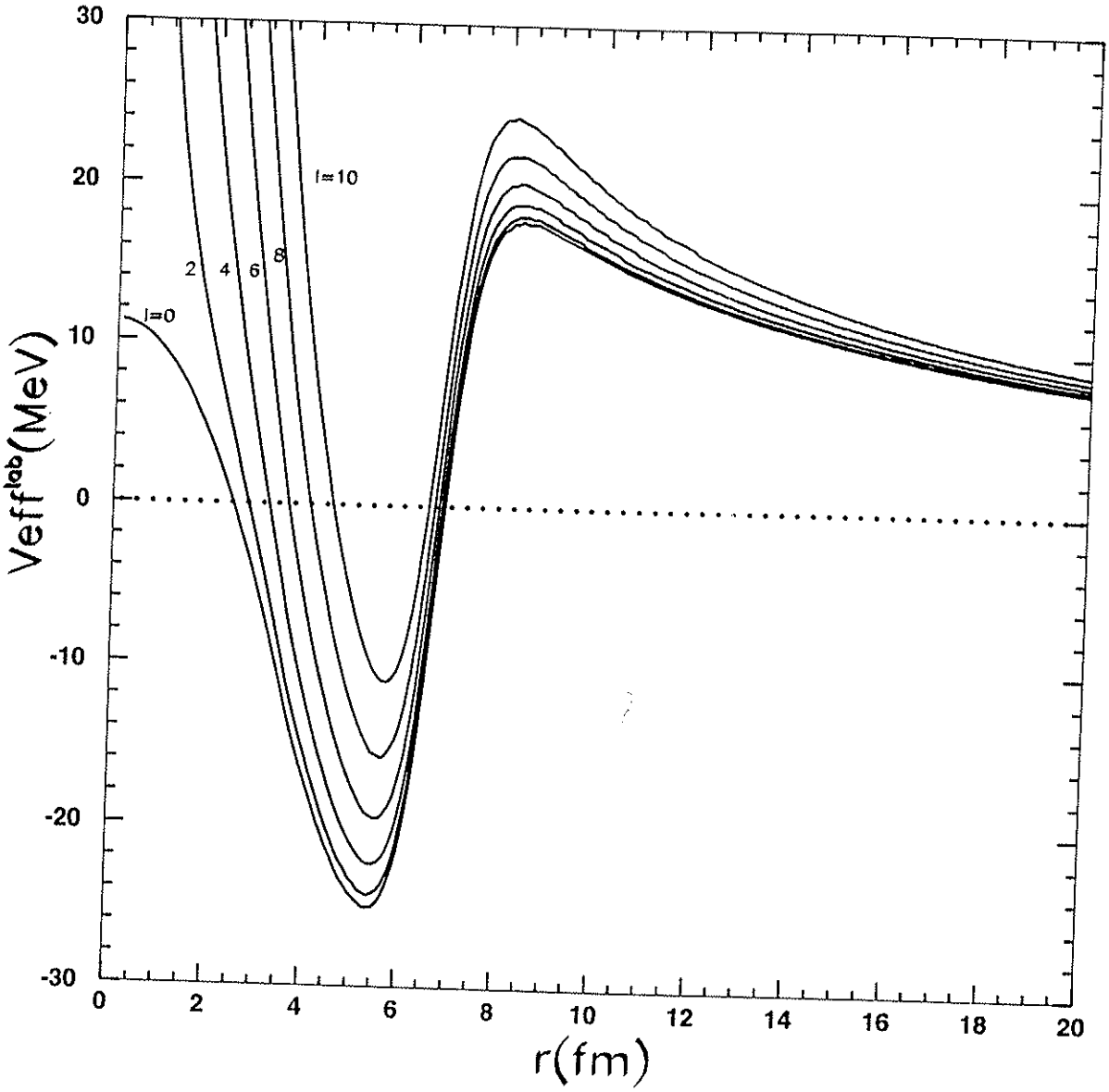

Figura 3.19: Potencial efetivo em $E_l = 21.0\text{MeV}$.

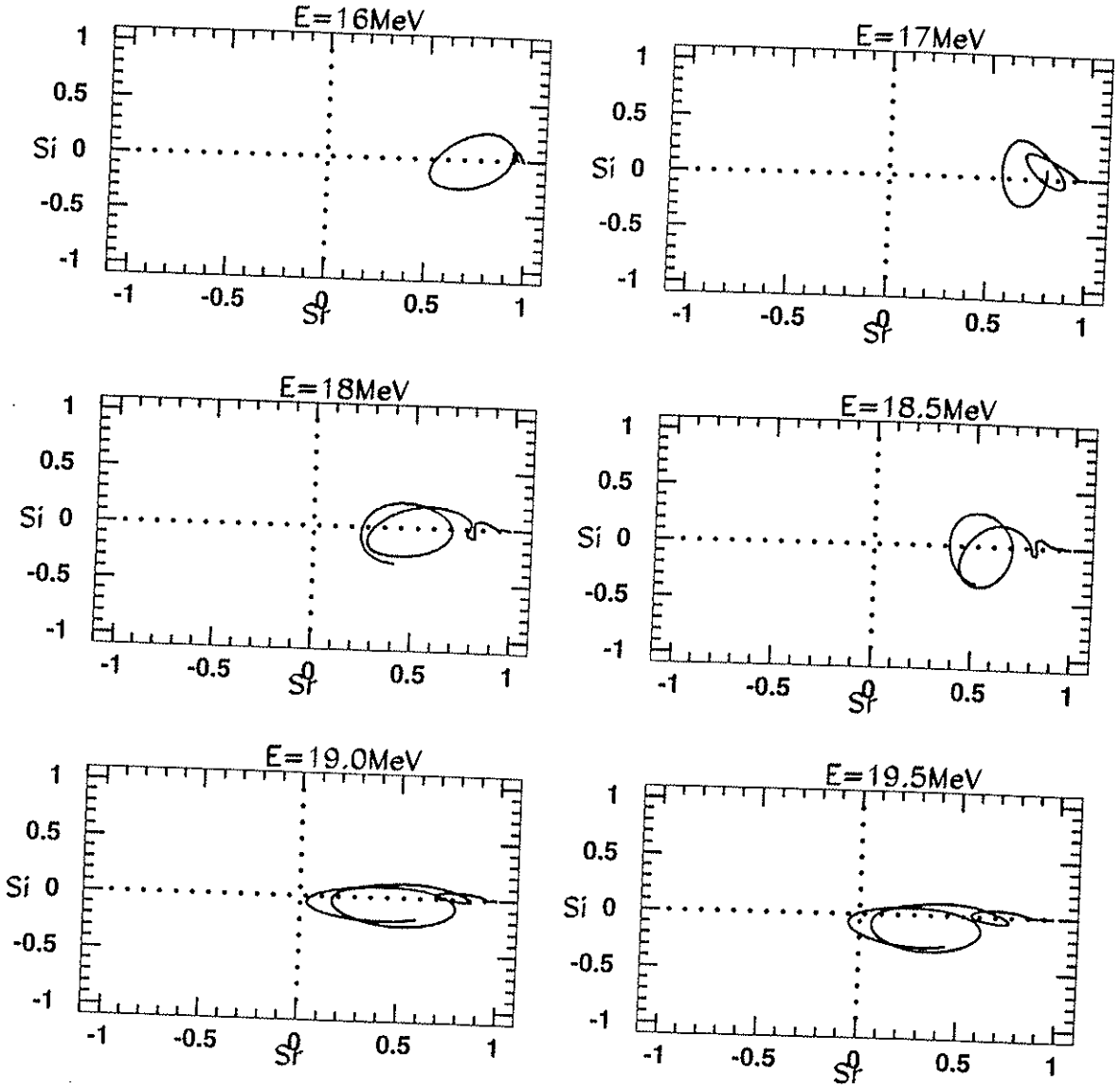

Figura 3.20: Diagramas de Argand em função do momento angular de um potencial otico.

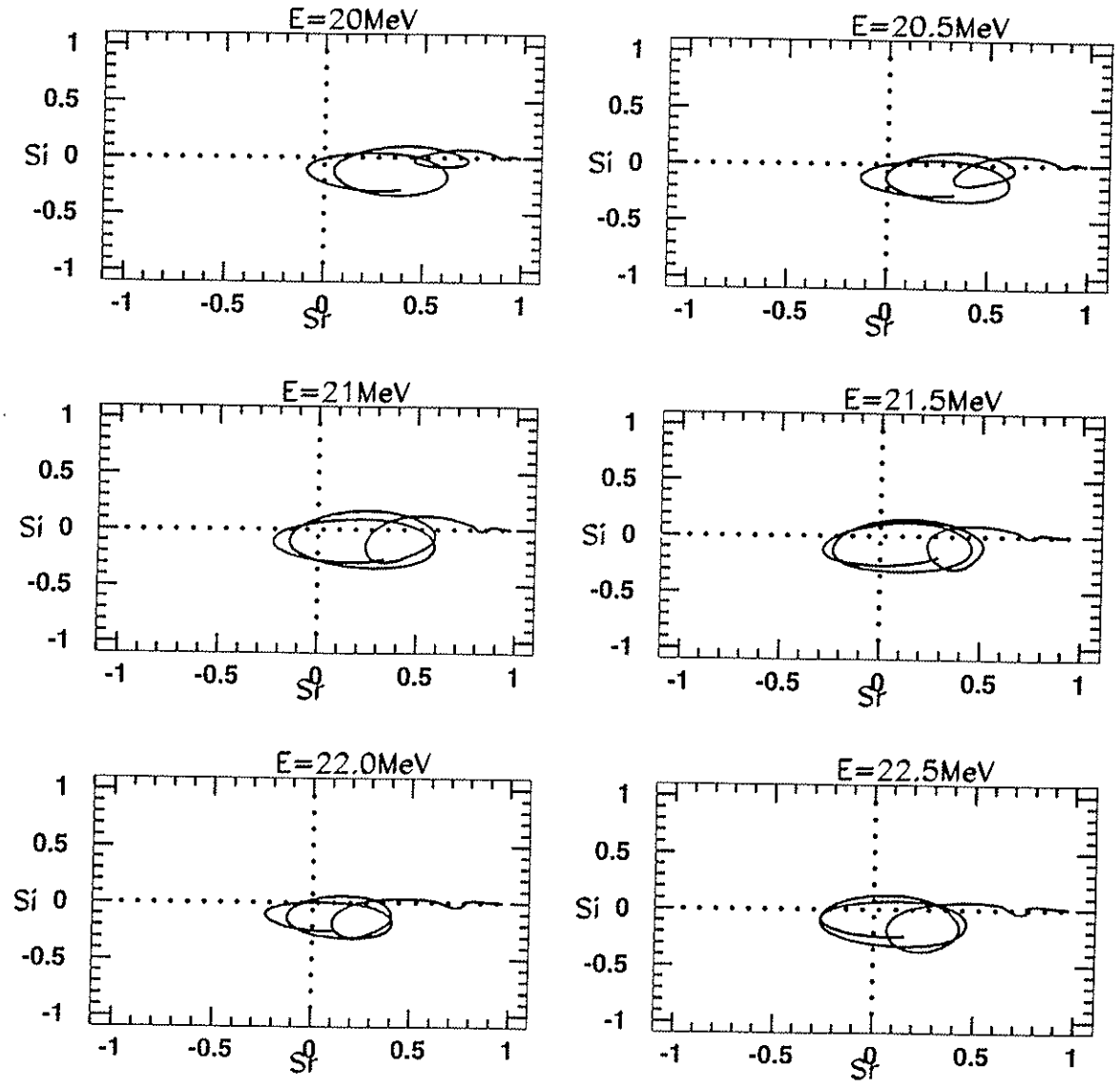

Figura 3.21: Diagramas de Argand em função do momento angular de um potencial otico

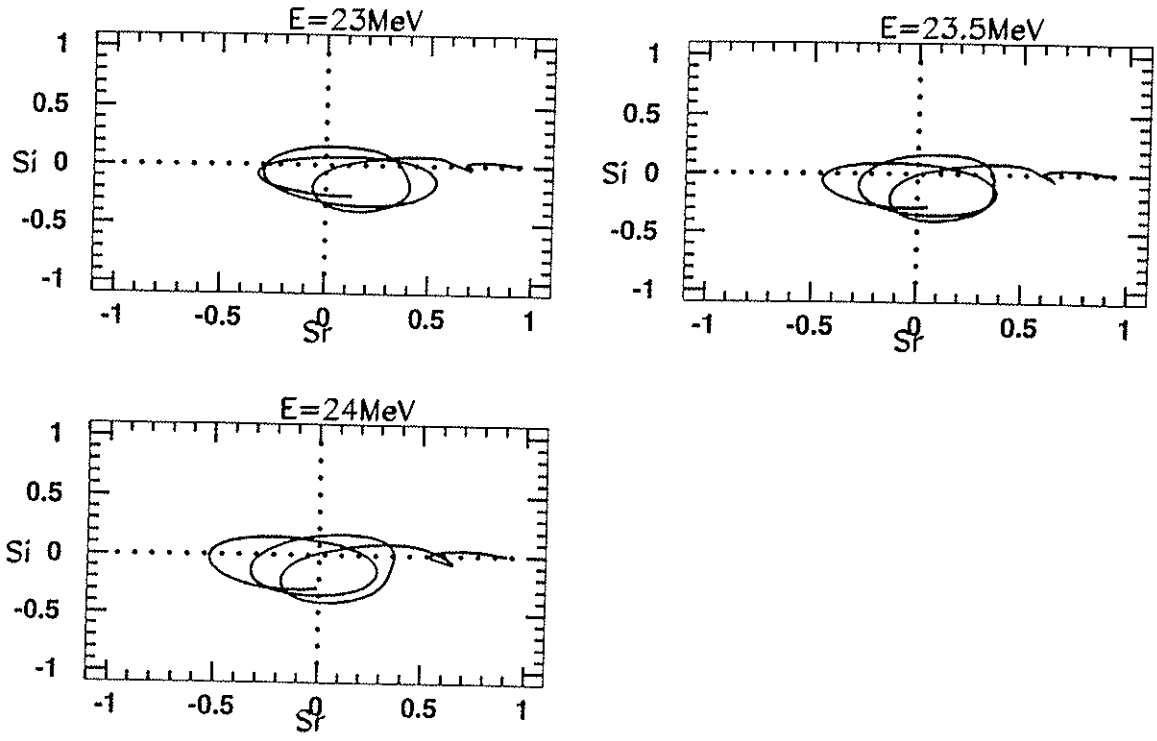

Figura 3.22: Diagramas de Argand em função do momento angular de um potencial otico.

angular razante. Este tipo de efeito pode ser simulado tambem por polos de Regge o que poderia explicar em parte os polos observados. Além disso no caso do sistema $^{12}C+^{16}O$ é evidente que o acoplamento com uma reação de transferência alfa naturalmente leva a uma dependência da paridade. Um segundo caminho a ser seguido seria a investigação sobre a formação de estados ressonantes na colisão entre os íons ^{12}C e ^{16}O. Este tipo de fenômeno foi primeiramente observado na década de 60 pelo grupo de Bromley [24, 25] em funções de excitação do sistema $^{12}C+^{12}C$ em energias em torno da barreira coulombiana. Nestes dados foram observadas fortes estruturas no espalhamento elástico com larguras em torno de $100-200$keV correlacionadas em angulo e entre diferentes canais. Mais tarde foram tambem observadas estruturas intermediárias com larguras em torno de 300keV nas funções de excitação nos sistema $^{12}C+^{16}O$ e $^{16}O+^{16}O$ [26, 27, 28]embora a correlação entre diferentes canais não fosse tão evidente o que colocou alguma dúvida sobre a interpretação em termos de ressonâncias. Observou-se em energias acima da barreira coulombiana a presença de estruturas finas no $^{12}C+^{12}C$ em 90^{o} [29] que foram interpretadas como flutuações de Ericson. A pequena diferença entre as larguras observadas nos processo ressonantes (estruturas intermediárias) e nas flutuaçõs estatísticas dificulta a separação entre estes dois processos em termos experimentais. Cálculos de Hauser–Feschbach [2] para a secção de choque de decaimento do sistema composto ^{28}Si no canal elástico para o sistema $^{12}C+^{16}O$ nas energias analisadas no presente trabalho mostram que a contribuição deste processo deve ser desprezível exceto talvez em torno de 90^{o} onde uma pequena contribuição pode ser esperada. Deve-se ressaltar que estes cálculos dependem fortemente da densidade de níveis do sistema composto na energia de excitação considerada e portanto não podem ser considerados como definitivos.

Uma análise das defasagens como função da energia pode fornecer a resposta para estas questões. No caso em que ressonâncias estão presentes, deve haver um comportamento em função da energia crescente similar ao observado em função do momento angular no caso dos polos de Regge, isto é, a defasagem nuclear deve variar de π sempre que passar por uma ressonância. Todavia, para se observar este tipo de comportamento são absolutamente essenciais medidas com passos em energia menores do que as larguras parciais das ressonâncias. No caso do sistema $^{12}C+^{16}O$ se esperam larguras em torno de 300keV [30] e como o passo em energia das distribuições angulares medidas é de 1MeV não foi possível a observação de ressonâncias. No caso do $^{12}C+^{24}Mg$ observamos a presença de estruturas correlacionadas em angulo e cujas larguras podem ser tambem da ordem de 300KeV. Novamente a medida de distribuições angulares completas e com passos de energia pequenos da ordem de 100KeV é essencial para se determinar a presença de ressonâncias.

O método de análise dos dados a partir da determinação da matriz-S, permite que se realizem simulações com dados sintéticos com o objetivo de se mapear a região angular na qual devem ser feitas medidas de modo a se obter matrizes-S com precisão suficiente para uma análise sem ambiguidades. Este fato abre uma nova perspectiva em termos experimentais e muito esforço deve ainda ser desprendido até que se obtenha uma resposta definitiva sobre o mecanismo de reação envolvido no espalhamento entre íons leves-pesados na região da barreira coulombiana.

Capítulo 4

A Teoria Algébrica do Espalhamento.

4.1 Introdução

Teorias de grupo tem uma larga aplicação em física e em particular em física nuclear. As aplicações mais bem sucedidas estão na à obtenção dos espectros de estados ligados tanto em núcleos como em moleculas[31, 32, 33]. No caso do espalhamento, o problema consiste em se saber se metodos de teoria de grupo são capazes de fornecer a forma da matriz-S. Isso mostrou-se possível em alguns casos como os potenciais de Morse, Pöschl-Teller [34] e no caso do potencial coulombiano[35] onde uma solução exata e puramente algébrica é obtida. Y. Alhassid e F. Iachello, baseados no sucesso dos métodos de teoria de grupo para o caso coulombiano, desenvolveram a Teoria Algébrica do Espalhamento [36] para íons pesados. Nesta teoria, o problema de canais acoplados é bastante simplificado o que permite a sua utilização em situações em que um grande número de canais de reação está aberto. A Teoria algébrica se mostrou bem sucedida na análise de dados experimentais do espalhamento entre íons pesados em energias próximas à barreira coulombiana [37, 38]. A seguir apresentaremos os aspectos fundamentais desta teoria e alguns desenvolvimentos recentes.

4.2 A matriz-S $SO(3,1)$ e o espalhamento elástico.

A versão da Teoria Algébrica que descreveremos neste trabalho se baseia na suposição de que a Hamiltoniana para o espalhamento entre íons pesados segue aproximadamente uma simetria $SO(3,1)$. Neste caso a matriz-S pode ser escrita como uma razão de duas funções gama:

$$S_\ell = \frac{\Gamma(\ell + 1 + iv)}{\Gamma(\ell + 1 - iv)}, \tag{4.1}$$

onde v, que é chamado potencial algébrico, é igual ao parâmetro de Sommerfeld $\eta = \mu Z_1 Z_2 e^2/\hbar^2 k$ no caso de espalhamento coulombiano puro quando a simetria $SO(3,1)$ é

exata [36]. A partir de ums abordagem totalmente diferente, esta forma para a matriz-S foi obtida tambem por Müller e Schilcher [39] para o caso em que o potencial é uma superposição de Yukawas. Como a função gama não tem zeros e seus polos estão localizados nos valores inteiros negativos do seu argumento [40], todos os polos da matriz-S $SO(3,1)$ coulombiana são dados pela condição:

$$\ell + 1 + i\eta = -n \tag{4.2}$$

onde $n = 0, 1, 2, 3....$ Substituindo-se o valor de η na expressão acima obtemos: $E = -\frac{-\mu(Z_1 Z_2 e^2)^2}{2\hbar^2 \nu^2}$ com $\nu = n + \ell + 1$ o que fornece exatamente os estados ligados no potencial coulombiano conforme a suposição de analiticidade.

Se a interação nuclear forte está presente o potencial algébrico é generalizado e passa a depender tambem do momento angular.

$$v_\ell(k) = \eta + v_\ell^s(k). \tag{4.3}$$

O segundo termo do lado direito da equação acima é em geral bem menor do que o parâmetro de Sommerfeld (em torno de 1% a 2%) no caso de íons pesados em baixas energias o que significa a dominâcia da interação coulombiana e justifica a adoção da simetria $SO(3,1)$.

A absorção pode ser introduzida na teoria pela parte imaginária do potencial algébrico de maneira análoga ao potencial otico. Para que o vínculo unitário $|S_\ell| \leq 1$ seja respeitado é necessário que $Im(v_\ell^s(k)) \geq 0$.

A fim de se aplicar a teoria à dados, é necessário um modelo que descreva a dependência de $v_\ell^s(k)$ em função do momento angular. A teoria não fornece esta dependência e a primeira parametrização proposta por Alhassid e Iachello [36] adotou uma forma tipo Woods-Saxon caracterizada por uma intensidade, o momento angular "rasante" ($\ell 0$) que é definido pelo raio e energia do sistema e uma difusividade (Δ), todos dependentes da energia. Esta forma de 6 parâmetros (3 para a parte real e 3 para a imaginária) foi utilizada em várias aplicações com bons resultados. No entanto, devido a simplicidade que problema de inversão *matriz-S* $\rightarrow$ *potencial algébrico* assume para a matriz-S $SO(3,1)$, é possível se obter numericamente o potencial algébrico que reproduz exatamente uma dada matriz-S [41](anexo 4). Isto é feito expandindo-se em Taylor a matriz-S em torno de um certo v^0 como:

$$v(l,k) = v^0 + \frac{-ilog(S/S^0)}{\psi(l+1+i\eta+iv^0) + \psi(l+1-i\eta-iv^0)}, \tag{4.4}$$

onde ψ é a função digama. O problema é resolvido iterativamente e verifica-se que o processo é rapidamente convergente e independente do ponto de partida. Utilizando-se esta ferramenta, foi possível se propor uma parametrização para o potencial algébrico mostrando-se que tanto o momento angular "rasante" como a difusividade que definem o potencial algébrico no espaço ℓ tem uma dependência simples com a energia restando apenas a determinação da intensidade [41](anexo 4).

Um estudo da relação entre o modelo otico Wood-Saxon no espaço r e o potencial algébrico através do processo de inversão foi feito para o sistema $^{16}O+^{63}Cu$ [42] (anexo 5) mostrando a necessidade da inclusão de termos de segunda ordem no potencial algébrico. No caso de absorção forte, a parte real do potencial algébrico pode se tornar negativa para baixos momentos angulares devido à contribuição de reflexões no poço imaginário (figura 4.1) e este fato não era levado em conta nas parametrizações propostas até então. Com a introdução deste efeito foi possível uma análise bastante precisa de distribuições angulares do sistema $^{16}O+^{63}Cu$ em energias em torno da barreira coulombiana. Extraindo-se a dependência com a energia da intensidade do potencial algébrico desta análise, observou-se um comportamento semelhante à anomalia de limiar (figuras 4.2 e 4.3) [46].

Uma vez que a simetria $SO(3,1)$ fornece a forma funcional da matriz-S que depende por sua vez do potencial algébrico, a extensão para o plano complexo da matriz-S passa pela extensão do potencial algébrico. Isto impõe certas propriedades à forma funcional adotada para modelar o potencial algébrico. Em particular formas baseadas em expressões tipo Woods-Saxon no espaço ℓ possuem polos no plano complexo em $\ell = \ell 0 + i\pi\Delta$ e estes polos no argumento da função gama produzem singularidades essenciais na matriz-S. Para evitar esse comportamento sugerimos [44] (anexo 6) uma expressão para o potencial algébrico baseada na função gama incompleta que é uma função inteira [40]. Além de não conter polos, a forma geral proposta para o potencial algébrico (Eq.4.4) preserva os polos originais da matriz-S coulombiana uma vez que a função digama se anula para argumentos inteiros negativos. Apesar da função gama incompleta ser compatível com as propriedades analíticas da matriz-S, no que diz respeito a sua utilização prática na análise de dados, os resultados obtidos são muito semelhantes aos que se obtem quando se utiliza formas baseadas na função de Woods-Saxon. Isto se deve provavelmente ao fato de que os polos da função de Woods-Saxon estejam suficientemente longe do eixo real para valores razoáveis da difusividade Δ. Vale a pena comentar que em muitas análises de dados baseadas em parametrizações tipo Woods-Saxon da matriz-S verificou-se a necessidade de utilizar valores pequenos da difusividade Δ a fim de reproduzir oscilações na distribuição angular. Isso corresponde a trazer um polo da função Woods-Saxon para perto do eixo real e com isso se simula, sem muito controle, a presença de um polo de Regge na matriz-S. Com a forma proposta, pode-se controlar totalmente a posição e largura de cada polo de Regge introduzido na matriz-S uma vez que isto é feito diretamente sobre um potencial algébrico que por si só não contém polos.

4.3 O problema de canais acoplados na Teoria Algébrica

Quando mais de um canal de reação está presente, a matriz-S $SO(3,1)$ assume a forma matricial:

$$S = \frac{\Gamma(L+1+iv)}{\Gamma(L+1-iv)}, \tag{4.5}$$

onde v agora é a matriz do potencial algébrico que contém a dinâmica do espalhamento nos diferentes canais considerados. No caso de partículas sem spin a matriz v tem dimensão

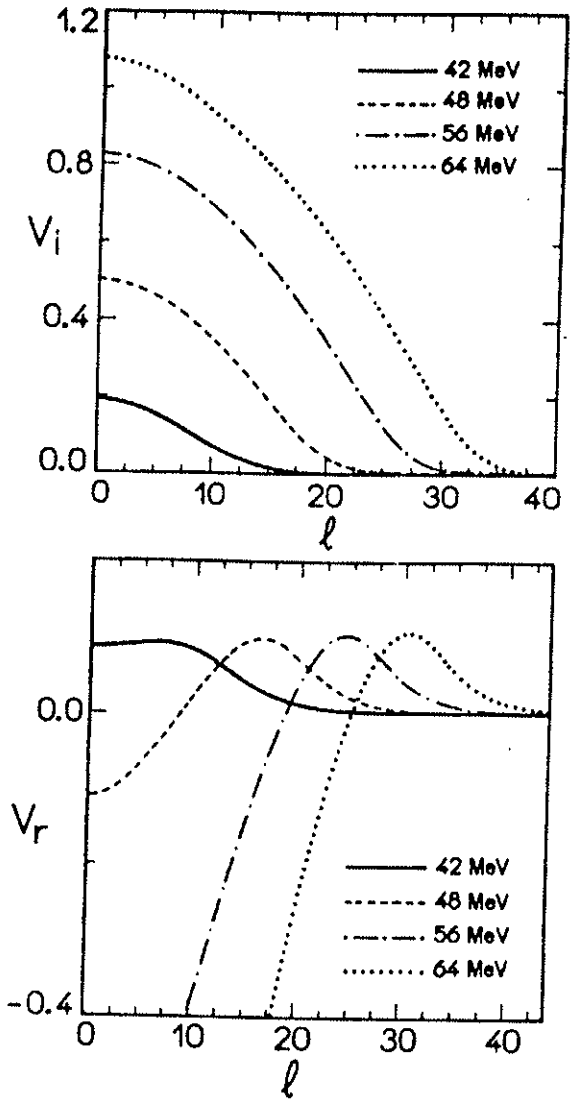

Figura 4.1: Os potenciais algébricos real e imaginário como função do momento angular.

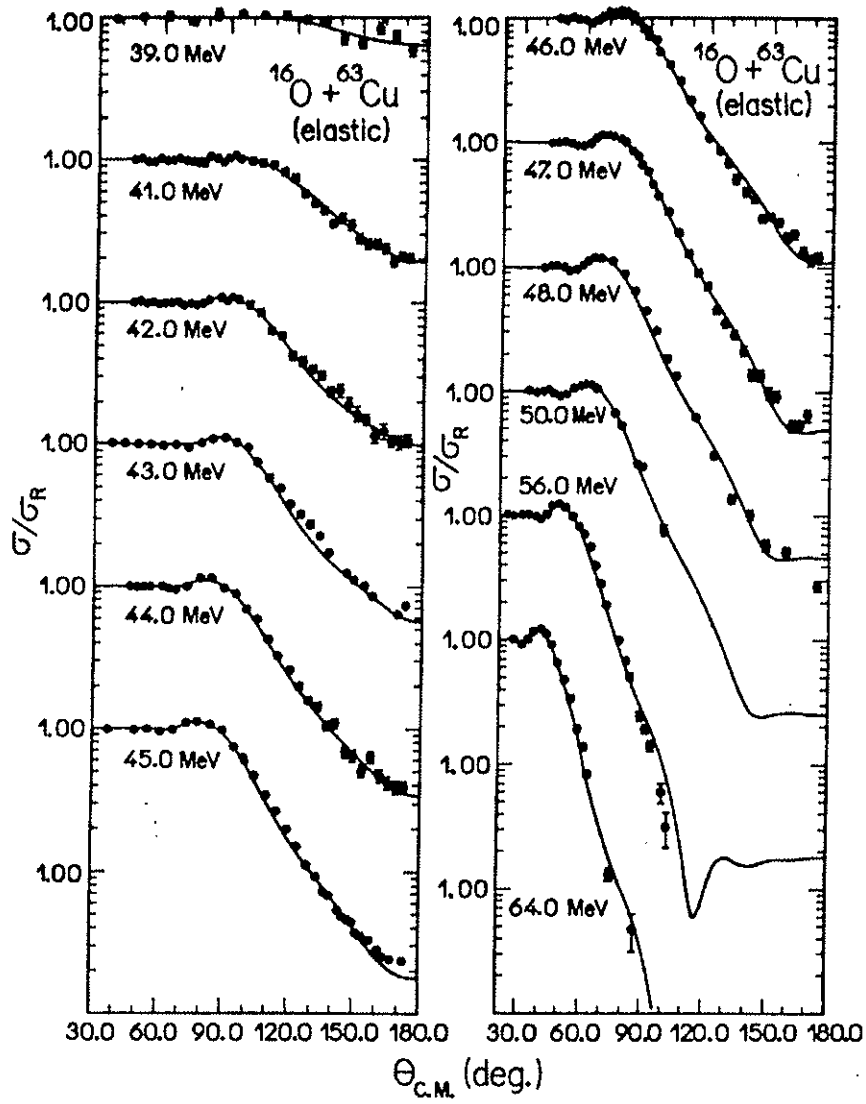

Figura 4.2: Distribuições angulares $^{16}O+^{63}Cu$. A linha sólida são cálculos com a Teoria Algébrica.

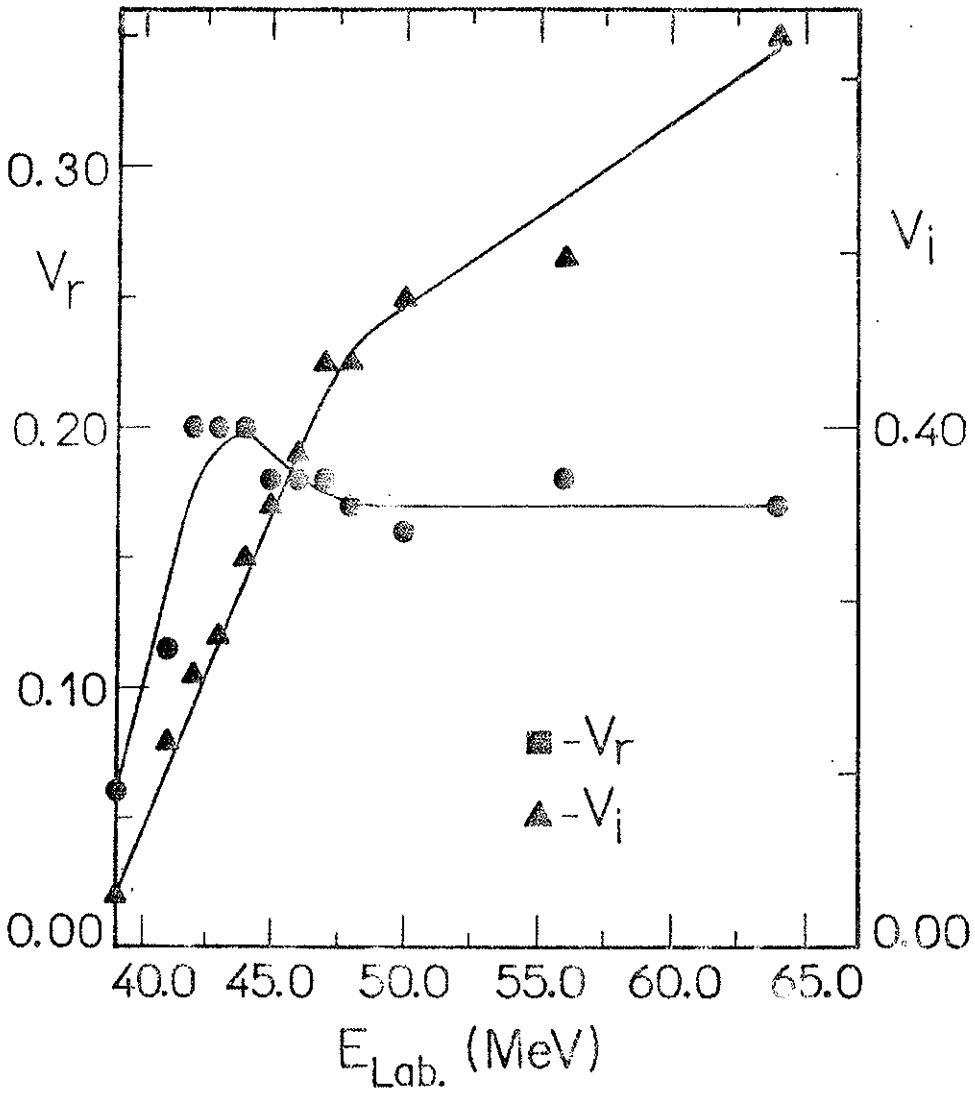

Figura 4.3: Potencial algébrico em função da energia.

igual ao numero de canais considerados. Neste caso, L é uma matriz multipla da matriz unidade 1 e portanto comuta com v de modo que o problema pode ser resolvido pelo algoritmo:

- diagonalisar v;
- escrever a matriz-S numa representação em que S e v são diagonais,

$$S_{\alpha\alpha} = \frac{\Gamma(L+1+iv_{\alpha\alpha})}{\Gamma(L+1-iv_{\alpha\alpha})}, \tag{4.6}$$

onde $v_{\alpha\alpha}$ é o α-ésimo autovalor de v;

- voltar a representação original pela transformação:$S = ZS_{diag}Z^{-1}$, onde Z é a matriz que diagonalisa v.

A introdução do spin na Teoria Algébrica não é trivial uma vez que os diferentes valores de momento angular nos diferentes canais fazem com que L não seja mais multipla da matriz unidade e não comute com v o que faz com que não se possa diagonalisar simultaneamente o potencial algébrico e a matriz-S. Neste caso, introduz-se o numero quântico J que é o momento angular total e que se conserva durante a colisão. A matriz-S fica então:

$$S = \frac{\Gamma(J+1+iv)}{\Gamma(J+1-iv)} \tag{4.7}$$

onde J e v comutam de modo que podemos resolver o problema pelo mesmo algoritmo utilizado no caso de spin zero [45] (anexo 7). É importante notar que a matriz do potencial algébrico agora tem uma dimensão dada por $\sum_1^N(2S_i+1)$ onde N é o numero de canais considerados e S_i o spin de cada canal, de forma que, a dinâmica do acoplamento entre os diferentes possíveis subestados de momento angular é levado em conta explicitamente. Em [45] (anexo 7) fazemos uma aplicação deste método para dados experimentais do sistema ^{16}O+^{65}Cu espalhamento elástico e os 5 primeiros estados excitados do ^{63}Cu. Verificou-se que o efeito do spin nas distribuições angulares é de basicamente reduzir a amplitude das oscilações. Os elementos de matriz do potencial algébrico que descrevem as transições entre os diferentes canais (α,α') são escritos como [46]:

$$\begin{aligned} V_{\alpha L\alpha' L'} &= (4\pi)^{-1/2}\sum_{\lambda}(-1)^{J-S_\alpha} i^{L'-L-\lambda}\hat{L}\hat{L}'\hat{S}_{\alpha'}(LL'00 \mid \lambda 0) \\ &\quad \times W(L,L',S_\alpha,S_{\alpha'} \mid \lambda,J)V^{\lambda}_{\alpha\alpha'}(l)(S_{\alpha'} \mid\mid V \mid\mid S_\alpha), \end{aligned} \tag{4.8}$$

onde L e L' são os possíveis valores dos momentos angulares nos canais inicial e final e S_α representa os spins dos canais. $V^{\lambda}_{\alpha\alpha'}$ são os fatores de forma dependentes do momento angular e que incluem a excitação coulombiana e nuclear e $(S_{\alpha'} \mid\mid V \mid\mid S_\alpha)$ os elementos de matriz reduzidos que contém a informação da estrutura nuclear. Os elementos de matriz reduzidos podem ser tratados como parâmetros livres ou obtidos de modelos nucleares como o modelo rotacional, vibracional, Interacting Boson Model (IBM) ou Interacting

Boson Fermion Model (IBMF) com a possibilidade de se descrever tanto a parte de espalhamento como a estrutura nuclear em termos de modelos algébricos. O papel de modelos nucleares neste caso será o de fornecer as intensidades relativas entre os diferentes elementos de matriz de acoplamento e deste modo reduzir o número de parâmetros envolvidos no cálculo.

Uma aplicação destas ideias à dados experimentais pode ser encontrada em [47](anexo 8), onde analisamos dados do espalhamento $^{16}O+^{63}Cu$ elástico e os primeiros 5 estados excitados do ^{63}Cu em 9 energias em torno da barreira coulombiana. Neste cálculo, os elementos de matriz reduzidos que fazem as transições para os estados excitados foram determinados no modelo IBMF.

No momento, o principal problema na Teoria Algébrica do Espalhamento consiste na determinação de potenciais algébricos realistas para o cálculo dos elementos de matriz de transição entre canais de reação principalmente na excitação nuclear inelástica e em reações de transferência. Este trabalho tem sido feito com base no processo de inversão *matriz-S* $\rightarrow$ *potencial algébrico* partindo-se de matrizes-S obtidas de modelos tradicional como cálculos de modelo otico e canais acoplados estabelecendo-se assim uma relação entre esses modelos e a Teoria Algébrica. A extensão do método de inversão para mais de um canal de reação é possível e deve ser feita de modo a se investigar mais profundamente as propriedades dos potenciais algébricos em outros canais além do elástico.

Capítulo 5

Conclusões

Este trabalho consiste em uma sistematização dos trabalhos desenvolvidos desde 1988 que focalizam principalmente a matriz-S de espalhamento, sua determinação a partir de dados experimentais e de modelos teóricos, e a física que pode ser obtida através do seu conhecimento.

Desenvolvemos um método para a obtenção da matriz-S diretamente a partir de dados experimentais no caso de apenas 1 canal de reação. Apresentamos uma análise de distribuições angulares elásticas dos sistemas $^{12}C+^{16}O$ e $^{12}C+^{24}Mg$ em várias energias. As matrizes-S obtidas mostram a presença de polos de Regge com uma evidência que até então não havia sido observada. Podemos afirmar com base nestas análises que a inclusão destes polos é essencial em qualquer descrição do espalhamento elástico em sistemas de nucleos das camadas p e s–d. Uma análise de modelo otico com potenciais transparentes prevê a presença de polos de Regge na matriz-S qualitativamente em acordo com as matrizes-S obtidas diretamente dos dados. A dependência com a energia dos elementos da matriz-S elástica já não é tão evidente. Os passos em energia e a precisão e completeza dos dados experimentais não permitem ainda a determinação das defasagens nucleares sem que haja ambiguidades. No entanto, no caso do sistema $^{12}C+^{24}Mg$ e nas energias estudadas, não há qualquer evidência da existência de ressonâncias isoladas fortemente acopladas ao canal elástico. A existência de ressonâncias fracas não está descartada.

A Teoria Algébrica do Espalhamento parece ser um caminho possível para uma descrição da matriz-S quando mais de um canal de reação está envolvido. Todavia, é importante a determinação de potencias algébricos que descrevam os elementos de matriz de acoplamento entre canais. Podemos afirmar que o potencial algébrico no canal elástico é bem conhecido e fornece uma descrição precisa das distribuições angulares experimentais de sistemas pesados. Tambem o potencial responsável pela excitação coulombiana é razoavelmente bem conhecido. Entretanto, a excitação nuclear e os processos de transferência ainda necessitam de estudos mais profundos.

A descrição do processo de espalhamento em termos de matriz-S pode fornecer resultados muito precisos tanto no caso de íons leves pesados onde processos tipo ressonante estão presentes como em sistemas mais pesados e fortemente absorventes. O desenvolvimento de um método para obtenção da matriz-S diretamente a partir dos dados experimentais

evidenciou o fato de que medidas precisas e completas de distribuições angulares com passos pequenos de energia são essenciais para a uma descrição sem ambiguidades do processo de espalhamento. O fato de se poder obter a matriz-S e sua incerteza a partir de simulações com dados sintéticos abre uma nova perspectiva no planejamento de futuras experiências.

Bibliografia

[1] H. J. Krappe and H. H. Rossner, Z. Phys. A **314**, 149 (1983).

[2] A. C. C. Villari, Tese de Doutoramento IFUSP-1987

[3] A. C. C. Villari, A. Lépine-Szily, R. Lichtenthäler Filho, O. Portesan Filho, M. M. Obuti, J. M. Oliveira Jr. and N. Added, Nucl. Phys. **A501**, 605 (1989).

[4] V. Chisté, R. Lichtenthäler, A. C. C. Villari, L. C. Gomes, submetido a Phys. Rev. **C**

[5] V. Chisté, Tese de Mestrado, IFUSP-1995

[6] W. H. Press, S. A. Teukolsky, W. T. Vettering and B. P. Flannery, Numerical Recipes in C, Cambridge University Press (1992).

[7] H. Fröhlich, P. Dück, W. Trev and H. Voit, Phys. Rev. **C27**, 578 (1983).

[8] P. Charles, Thesis number 2378, Orsay, France (1981).

[9] V. de Alfaro and T. Regge, Potential Scattering, North-Holland Publ. Co., Amsterdam (1965)

[10] K. M. McVoy, Phys. Rev. **C3**, 1104 (1971).

[11] R. Lichtenthäler Jr., A. Lépine-Szily, A. C. C. Villari, W. Mittig, V. J. G. Porto, C. V. Acquadro, Phys. Rev. **C26**, 2487 (1982)

[12] A. Lépine-Szily, M. M. Obuti, R. Lichtenthäler, J. M. Oliveira Jr., A. C. C. Villari, Phys. Lett. **B243**, 23 (1990)

[13] W. Sciani, Tese de Doutoramento, IFUSP (1996)

[14] A. Lépine-Szily, W. Sciani, Y. K. Watari, W. Mittig, R. Lichtenthäler, M. M. Obuti, J. M. Oliveira Jr., A. C. C. Villari, Phys. Lett. **B304**, 45 (1993)

[15] W. E. Frahn and M. S. Hussein, Nucl. Phys. **A346**, 237 (1980).

[16] P. Fachini, Tese de Mestrado ,IFUSP (1995)

[17] T. Ericson, Annals of Physics, **23**, 390 (1963)

[18] R. Lichtenthäler, A. Lépine-Szily, A. C. C. Villari and A. Portezan Filho, Phys. Rev. **C39**, 884 (1989).

[19] A. Lépine-Szily, R. Lichtenthaler, M. M. Obuti, J. M. Oliveira Jr., O. Portezan Filho, W. Sciani and A. C. C. Villari, Phys. Rev. **C40**, 681 (1989).

[20] R. Lichtenthaler, A. Lépine-Szily, A. C. C. Villari, W. Mittig, V. J. G. Porto and C. V. Acquadro, Phys. Rev. **C26**, 2487 (1982).

[21] L. F. Canto, R. Donangelo, M. S. Hussein and A. Lépine-Szily, Phys. Rev. Lett., **51**, 95 (1983).

[22] M. S. Hussein, A. N. Aleixo, L. F. Canto, P. Carrilho, R. Donangelo and L. S. Paula, J. Phys. **C13**, 967 (1987).

[23] A. Lépine-Szily, M. M. Obuti, R. Lichtenthaler, J. M. Oliveira Jr. and A. C. C. Villari, Phys Lett. **B243**, 23 (1990).

[24] E. Almqvist, D. A. Bromley and F. A. Kuehner, Phys. Rev. Lett. **4**, 365 (1960).

[25] D. A. Bromley, F. A. Kuehner and E. Almqvist, Phys. Rev. Lett. **4**, 515 (1960).

[26] M. L. Halbert, C. B. Fulmer, S. Raman, M. J. Saltmarsh, A. H. Snell, P. H. Stelson, Phys. Lett. **51b** 341(1974)

[27] J. V. Maher, M. W. Sachs, R. H. Siemssen, A. Weidingen, D. A. Bromley, Phys. Rev. **188**1665(1969)

[28] P. Braun-Munzinger and J. Barrete, Phys. Rep. **87** (1982)

[29] D. Shapira, R. G. Stokstad, D. A. Bromley, Phys. Rev. **C10** 1063(1974)

[30] H. W. Wilschut, P. Braun-Munzinger, G. M. Berkowitz, R. H. Freifelder, J. S. Karp and T. R. Renner, Phys. Lett. **38**, 944 (1977).

[31] A. Arima, F. Iachello, Ann. Phys. (N.Y.) **99**, 253 (1976), e **111**, 201(1978), e **123**, 468(1979).

[32] F. Iachello, Chem. Phys. lett. **78**, 581(1981) e F. Iachello, R. D. Levine, J. Chem. Phys. **77**, 3046(1982).

[33] F. Iachello and P. Van Isacker, *The Interacting Boson-Fermion Model* (Cambridge University Press, 1991).

[34] Y. Alhassid, F. Gürsey and F. Iachello, Annals of Physics **167**, 181(1976).

[35] M. J. Engelfield, *Group Theory and the Coulomb Problem*, Wiley, New York (1972).

[36] Y. Alhassid and F. Iachello, Nucl. Phys. **A501**, 585 (1989).

[37] A. Lépine-Szily, M. M. Obuti, R. Lichtenthäler Filho, J. M. Oliveira Jr., A. C. C. Villari, Phys. Lett. **B243**, 23(1990).

[38] A. Lépine-Szily, J. M. Oliveira Jr., P. Fachini, R. Lichtenthäler Filho, M. M. Obuti, W. Sciani, M. K. Steinmayer, A. C. C. Villari, Nucl. Phys. **A539**,687(1992).

[39] H. J. Müller and K. Schilcher, J. Math. Phys. **9**, 255(1968)

[40] *Handbook of mathematical Tables*, edited by M. Abramowitz and I. A. Segun (Dover Publicatíons, New York, 1964).

[41] R. Lichtenthäler Filho, A. C. C. Villari, L. C. Gomes, P. Carrilho Soares, Phys. Lett. **B269**, 49(1991)

[42] R. Lichtenthäler, D. Pereira, L. C. Chamon, L. C. Gomes, A. Ventura and L. Zuffi, Phys. Rev. **C50**, 3033 (1994).

[43] G. R. Satchler, Phys. Rep. **199**, 147(1991)

[44] R. Lichtenthäler and L. C. Gomes, Phys. Rev. **C50**, 3163 (1994).

[45] R. Lichtenthäler Filho, A. Ventura, L. Zuffi, Phys. Rev. **C46**, 707 (1992)

[46] G. R. Satchler, *Direct Nuclear Reactions* (Clarendon, New York, 1983).

[47] R. Lichtenthäler Filho, Proceedings da *International Conference ON Perspectives For The Interacting Boson Model on the Occasion of its 20TH Anniversary* p.521 (199) Padova, Ed. World Scientific.

vai

ANEXO 1

S-matrix analysis of heavy ion elastic scattering*

V. Chisté, R. Lichtenthäler, A. C. C. Villari† and L. C. Gomes
Departamento de Física Nuclear
Laboratório do Pelletron
Instituto de Física
Universidade de São Paulo, Caixa Postal 66318,
05389-970 - São Paulo, SP, Brasil.
(March 15, 1996)

A procedure to minimize χ^2 is described which explores the fact that the χ^2 distribution is of the fourth degree in the S-matrix elements. Due to the fact that all the three roots of the scale parameter for the minimum of χ^2 in its gradient direction are algebraically determined, gives to the procedure some global features that previous methods did not contemplate. The search procedure also preserves the unitary bound constraint of the S-matrix at every step, allowing it to be taken care in an automatic fashion. When the search in the gradient direction slows down, the procedure reverts to the traditional quadratic approximation with zero order regularization. The method is applied to the elastic scattering of the $^{12}C + {}^{16}O$ reaction near the Coulomb barrier.

24.10.-i, 25.70.bc

I. INTRODUCTION

The analysis of the elastic scattering channel of heavy ion collisions near the Coulomb barrier has been extensively done with the help of the Woods-Saxon optical potential [1]. Much of what we learned came from these analysis which give a somewhat structureless behavior of the collision. Another approach to the analysis of these collisions has been proposed by Alhassid and Iachello [2], the algebraic potential based on the SO(3,1) symmetry but, in actual applications, this approach showed properties similar to the W-S potential [3,4] and, at this moment, it is not clear whether the algebraic approach has a physical content different from the W-S optical potential. However, extensive measurements and analysis of light heavy ion systems [5–9] have shown resonances that cannot be easily explained in the context of the W-S optical potential. These resonances of total widths of the order of 300 keV preclude such a simple explanation and suggest that a rich intermediate structure is present in the collisions.

An alternative way out of this scheme, at least for spinless collisions, is to use S-matrix or phase shift analysis. Even in this case, a systematic study of the intermediate structure was made difficult by the lack of a reliable automatic, stable search for the S-matrix elements for the elastic channel. It is the absence of stability that made unreliable the phase shift analysis in heavy ion collisions. Very frequently, starting the search from different initial conditions, different sets for the S-matrix were found and had different physical contents.

In this paper, we present a procedure for determining the real and imaginary parts of the S-matrix elements for spinless collisions which converges automatically to a physical solution even when 25 angular momentum channels are simultaneously searched. The procedure is based on the simple observation that the χ^2 function for the angular distribution is a fourth degree polynomial in the S-matrix elements. This is a radical departure from the procedure of Krappe and Rossner [10] that consider the highly non linear transformation $S_\ell = \exp(\eta_{\ell 1} + i\eta_{\ell 2}^2)$. Our procedure resulted stable when analyzing, without external manipulation, sixteen elastic angular distributions of the $^{12}C + {}^{16}O$ system.

II. THE PROCEDURE

We write the scattering amplitude as

$$f(\theta) = f_c(\theta) + f_n(\theta),$$

*Partial support by CNPq.

where

$$f_c(\theta) = -\eta \exp(2i\sigma_0) \frac{\exp[-i\eta \log \sin^2(\frac{\theta}{2})]}{2k \sin^2(\frac{\theta}{2})}$$

is the Coulomb amplitude and

$$f_n(\theta) = \frac{1}{2ik} \sum_{\ell=0}^{\infty} (2\ell+1) S_\ell^c (S_\ell^n - 1) P_\ell(\cos\theta) \tag{1}$$

is the nuclear part of the total amplitude. The purpose of the procedure is to search for the unknown matrix elements S_ℓ^n, from $\ell = 0$ up to $\ell = \ell_{max}$ which minimize the χ^2 defined by

$$\chi^2 = \sum_{j=1}^{N} \frac{[\sigma(\theta_j) - \sigma^e(\theta_j)]^2}{\Delta^2(\theta_j)},$$

where $\sigma^e(\theta_j)$ are the experimental cross sections and $\Delta(\theta_j)$ the experimental errors at the observed center of mass angle θ_j. The search proceeds first in the direction of the gradient in the parameter space. The choice of ℓ_{max} depends on the size of the system and the energy under consideration, and above its value de S-matrix elements are assumed to be unity. We write $S_\ell^n = x_\ell + iy_\ell$ and set

$$u_\ell = \frac{\partial \chi^2}{\partial x_\ell} = \frac{2(2\ell+1)}{k} \sum_{j=1}^{N} \frac{\sigma(\theta_j) - \sigma^e(\theta_j)}{\Delta^2(\theta_j)} P_\ell(\cos\theta_j) \Im[f^*(\theta_j) S_\ell^c],$$

$$v_\ell = \frac{\partial \chi^2}{\partial y_\ell} = \frac{2(2\ell+1)}{k} \sum_{j=1}^{N} \frac{\sigma(\theta_j) - \sigma^e(\theta_j)}{\Delta^2(\theta_j)} P_\ell(\cos\theta_j) \Re[f^*(\theta_j) S_\ell^{(c)}].$$

We write

$$S_\ell^n = S_\ell'^n + \alpha(u_\ell + iv_\ell) \tag{2}$$

where $S_\ell'^n$ is the previous and S_ℓ^n the new matrix element shifted in the direction of the gradient of χ^2.

Substituting the previous equation in the expression for χ^2 we obtain a polynomial of the fourth degree in α:

$$\chi^2 = A\alpha^4 + B\alpha^3 + C\alpha^2 + D\alpha + \chi_0^2,$$

where the coefficients A, B, C and D are easily obtained in analytical form. We set

$$\phi(\theta) = \frac{1}{2ik} \sum_{\ell \in L} (2\ell+1) S_\ell^c (u_\ell + iv_\ell) P_\ell(\cos\theta),$$

and we have

$$A = \sum_{j=1}^{N} \frac{|\phi(\theta_j)|^4}{\Delta^2(\theta_j)}, \tag{3}$$

$$B = 4 \sum_{j=1}^{N} \frac{|\phi(\theta_j)|^2}{\Delta^2(\theta_j)} \Re[f(\theta_j)\phi^*(\theta_j)], \tag{4}$$

$$C = 2 \sum_{j=1}^{N} \frac{|\phi(\theta_j)|^2}{\Delta^2(\theta_j)} (\sigma(\theta_j) - \sigma^e(\theta_j)) + 4 \sum_{j=1}^{N} \frac{[\Re(f(\theta_j)\phi^*(\theta_j))]^2}{\Delta^2(\theta_j)}, \tag{5}$$

$$D = \sum_{\ell=\ell_{min}}^{\ell_{max}} (u_\ell^2 + v_\ell^2). \tag{6}$$

The values of α for which χ^2 is an extreme are given by the roots of the cubic equation:

$$4A\alpha^3 + 3B\alpha^2 + 2C\alpha + D = 0 \tag{7}$$

The values of A and D are positive what indicates that the cubic equation always has at least one negative root which corresponds to the local minimum pointed by the negative direction of the gradient. Quite often the equation has three reals roots indicating the existence of a second minimum. Our search procedure always consider the possibility of branching to this second minimum whenever the value of χ^2 on it is smaller than the value on the local minimum. FIG. 1 exhibits the value of χ^2 as a function of $\Re(S_\ell)$ for $\ell = 4$ at a typical situation of the analysis of the $^{12}C + {}^{16}O$ angular distribution. The experimental points were actually, in this case, simulated by an optical potential. The errors in the equation for χ^2 were assumed constant and equal to 10%. One clearly observes, within the interval [-1,1] for $\Re(S_4)$, the presence of two minima for χ^2. This simple case illustrates that a search based only in the existence of the local minimum, depending on where the search starts, finds only the false minimum. In our procedure, for the case illustrated, it finds the true minimum in a single iteration. In this figure we also shown the estimated error $\sigma_4 = 0.02$ for $\Re(S_4)$ as the width of curve calculated where χ^2 is equal one unity above its minimum value.

Before making the choice at which minimum to branch to, we impose the unitary bound for each S_ℓ.

The equation $\mid S_\ell'^n + \alpha(u_\ell + iv_\ell) \mid = 1$ gives

$$\alpha^2(u_\ell^2 + v_\ell^2) + 2\gamma_\ell\alpha - (1 - \mid S_\ell'^n \mid^2) = 0. \tag{8}$$

with $\gamma_\ell = u_\ell x'_\ell + v_\ell y'_\ell$. The two roots of this equation are

$$\alpha'_\ell = -\frac{\gamma_\ell + \sqrt{\gamma_\ell^2 + (u_\ell^2 + v_\ell^2)(1 - \mid S_\ell'^n \mid^2)}}{u_\ell^2 + v_\ell^2} \leq 0,$$

$$\alpha''_\ell = -\frac{\gamma_\ell - \sqrt{\gamma_\ell^2 + (u_\ell^2 + v_\ell^2)(1 - \mid S_\ell'^n \mid^2)}}{u_\ell^2 + v_\ell^2} \geq 0.$$

The unitary bound on each S_ℓ is easily imposed by writing the new values as $S_\ell'^n + \alpha_\ell(u_\ell + iv_\ell)$ with

$$\begin{aligned} \alpha_\ell &= \alpha'_\ell \text{ for } \alpha_\ell < \alpha'_\ell \\ &= \alpha_\ell \text{ for } \alpha'_\ell \leq \alpha_\ell \leq \alpha''_\ell \\ &= \alpha''_\ell \text{ for } \alpha_\ell \geq \alpha''_\ell. \end{aligned}$$

The case when $\alpha'_\ell = \alpha''_\ell = 0$ needs consideration. This occurs whenever the S_ℓ is on the unitary circle ($\mid S'_\ell \mid = 1$) and the gradient is tangent to this circle ($\gamma_\ell = 0$). In this particular case we write $S_\ell^{(n)} = S'_\ell \exp(i\beta_\ell)$ with $\beta_\ell = \alpha_0(v_\ell x'_\ell - u_\ell y'_\ell)$, what corresponds to a displacement on the unitary circle.

The search along the gradient directions stops whenever the value of the gradient is sufficient small to guarantee that, in eq. (7), the linear approximation is valid. When this happens, the procedure reverts to a search in every direction of the parameter space by changing the above method to the standard one [11] based on the quadratic approximation for χ^2. To avoid instability due to the large number of parameters involved, the zero order regularization [12] was introduced.

III. THE QUADRATIC APPROXIMATION

We assume L to be the interval $[\ell_{min}, \ell_{max}]$ and set $\ell_1 = \ell_{min} - 1$ and $\ell_2 = \ell_{max} - \ell_{min} + 1$. Changing to the notation $a_i = x_{i+\ell_1}$ and $a_{i+\ell_2} = y_{i+\ell_1}$ we write

$$\chi^2 = \chi_0^2 + \sum_i B_i \Delta a_i + \frac{1}{2}\sum_{im} A_{im}\Delta a_i \Delta a_m.$$

with

$$B_i = \frac{\partial \chi^2}{\partial a_i}$$

$$A_{im} = \frac{\partial^2 \chi^2}{\partial a_i \partial a_m}$$

The new values of the parameters are obtained shifting the old values by the following amount

$$\Delta a_i = -\sum_m (A_{im} + \lambda\delta_{im})^{-1} B_m,$$

where λ is the regularizing parameter [12]. We set

$$\lambda = \frac{TrA}{2\ell_2},$$

and the search iterates until the variation of χ^2 between two successive iterations is less than 0.1%. At this point the errors δa_i and the correlation coefficients ρ_{im} are calculated by:

$$\delta a_i = \sqrt{A^{-1}_{ii}},$$
$$\rho_{im} = \frac{A^{-1}_{im}}{\delta a_i \delta a_m}.$$

The analytical expressions for B_i and A_{im} are the following ($1 \leq i, m \leq \ell_2$):

$$B_i = \frac{2}{k}(2(i+\ell_1)+1)\sum_j^N \frac{\sigma(\theta_j)-\sigma^e(\theta_j)}{\Delta^2(\theta_j)} P_{i+\ell_1}(\theta_j)\Im(f^*(\theta_j)S^c_{i+\ell_1})$$

$$B_{i+\ell_2} = \frac{2}{k}(2(i+\ell_1)+1)\sum_j^N \frac{\sigma(\theta_j)-\sigma^e(\theta_j)}{\Delta^2(\theta_j)} P_{i+\ell_1}(\theta_j)\Re(f^*(\theta_j)S^c_{i+\ell_1})$$

$$A_{im} = \frac{1}{2k^2}(2(i+\ell_1)+1)(2(m+\ell_1)+1)\times$$
$$\sum_j^N \Re\left(\frac{2\sigma(\theta_j)-\sigma^e(\theta_j)}{\Delta^2(\theta_j)} S^c_{i+\ell_1}S^{c*}_{m+\ell_1} - \frac{f_j^{*2}}{\Delta^2(\theta_j)} S^c_{i+\ell_1}S^c_{m+\ell_1}\right) P_{i+\ell_1}(\theta_j)P_{m+\ell_1}(\theta_j)$$

$$A_{i+\ell_2,m+\ell_2} = \frac{1}{2k^2}(2(i+\ell_1)+1)(2(m+\ell_1)+1)\times$$
$$\sum_j^N \Re\left(\frac{2\sigma(\theta_j)-\sigma^e(\theta_j)}{\Delta^2(\theta_j)} S^c_{i+\ell_1}S^{c*}_{m+\ell_1} + \frac{f_j^{*2}}{\Delta^2(\theta_j)} S^c_{i+\ell_1}S^c_{m+\ell_1}\right) P_{i+\ell_1}(\theta_j)P_{m+\ell_1}(\theta_j)$$

$$A_{i,m+\ell_2} = \frac{1}{2k^2}(2(i+\ell_1)+1)(2(m+\ell_1)+1)\times$$
$$\sum_j^N \Im\left(\frac{2\sigma(\theta_j)-\sigma^e(\theta_j)}{\Delta^2(\theta_j)} S^c_{i+\ell_1}S^{c*}_{m+\ell_1} + \frac{f_j^{*2}}{\Delta^2(\theta_j)} S^c_{i+\ell_1}S^c_{m+\ell_1}\right) P_{i+\ell_1}(\theta_j)P_{m+\ell_1}(\theta_j)$$

$$A_{i+\ell_2,m} = \frac{1}{2k^2}(2(i+\ell_1)+1)(2(m+\ell_1)+1)\times$$
$$\sum_j^N \Im\left(\frac{-2\sigma(\theta_j)+\sigma^e(\theta_j)}{\Delta^2(\theta_j)} S^c_{i+\ell_1}S^{c*}_{m+\ell_1} + \frac{f_j^{*2}}{\Delta^2(\theta_j)} S^c_{i+\ell_1}S^c_{m+\ell_1}\right) P_{i+\ell_1}(\theta_j)P_{m+\ell_1}(\theta_j)$$

IV. THE $^{12}C + {}^{16}O$ ELASTIC CHANNEL

The procedure was applied to the analysis of sixteen elastic angular distributions measured in the $^{12}C + {}^{16}O$ collision. The data were obtained by Fröhlich [8] in the range [8.549 MeV, 14.984 MeV], by Villari [13] (forward angles) and Charles [14] (backward angles) in the range [17.28 MeV, 21.86 MeV] and Villari [13] in the range [23.14 MeV, 26.74 MeV], with all energies referred to the center of mass system. For each one of the analyzed distributions we started from an S-matrix generated by the Woods-Saxon potential found by Charles [14], that describes mainly the forward diffractive part of the distributions.

Table I gives a summary of our results. The columns give the energy of the angular distribution in the center of mass system ($E_{C.M.}$), the maximum value of ℓ considered (ℓ_{max}), the number of experimental points measured (N_0), the number of degrees of freedom of the χ^2 distribution (N), and the reduced value of χ^2 after the analysis (χ^2/N). Once the initial set for the S-matrix and the value of ℓ_{max} were chosen, the search of the final solution proceeded without any intermediate manipulation. FIG. 2 presents the fits obtained for 6 angular distributions at $E_{c.m.} = 8.55; 9.06; 17.28; 23.14; 24.49$ and 26.74MeV.

We observe that even in the worst case, at $E_{c.m.} = 17.28$MeV with $\chi^2 = 50$, the fit is excellent. The apparently large value of χ^2 reflects the fact that we have included only the statistical errors ($< 1\%$), what underestimates the total errors of the measured cross sections [13]. The richness of structures in the angular distributions reflects in the patterns observed in the Argand diagrams of the S-matrix. A full discussion of all the sixteen distributions analyzed in beyond this paper but we consider here three features that were conspicuously seen.

FIG. 3 exhibits two Argand diagrams for the (a) 21.86 MeV and (b) 23.14 MeV as a function of the angular momentum, corresponding to two consecutive energies analyzed. The errors are also indicated in the figures. We observe that the errors decrease as ℓ increases as expected. FIG. 3b, in particular, exhibit a pattern of four loops around the origin which are the signature of the presence of four Regge poles [15]. The fact that the loops encircle the origin says that their partial widths are larger than half of the corresponding total widths, characterizing a strong coupling to the elastic channel [16]. The pole parameters were easily obtained from the S-matrix and table II gives the position (ℓ_0), the half total width ($\Gamma/2$) and the partial width (Δ) for each pole. Though the four poles are easily determined at 23.14 MeV, the neighboring distribution shows that at least one pole has moved drastically away from the origins of the diagrams making difficult to follow the movements of the poles. This results because the energy intervals between the neighboring distributions are too large (> 1 MeV) in comparison to the widths of possible resonances in this energy region. The rapid variation of the diagrams, from one to the next neighboring energy, indicates that the structures are of the intermediate character and not single particle or potential resonances, whose widths are expected to be larger than 1 MeV. In any case, the presence of a few poles simultaneously at quite a few analyzed energies are strong evidences of structures but of intermediate character. Such structures were already observed by Wilschut et al [7]. Measuring angular distributions at steps less than 100 keV, from 19.50 MeV to 21.00 MeV in the C.M. system, these authors identified one resonance of total width equal to 300 ± 100 keV at 19.8 ± 0.1 MeV. At lower energies, Fröhlich et al. [8] were able to identify eight resonances between 8.5 MeV and 15 MeV, all of them with widths less or equal to 320 keV.

In FIG. 4 the absolute value of S_ℓ is plotted as a function of ℓ at the same 6 energies of FIG. 2. We observe that at $E_{c.m.} = 24.49$ and 26.74MeV the errors are very large for low ℓ and nothing can be said about the interaction.(Though the errors are large, the A matrix defined in section 3 is not singular.) The zigzag pattern of the points at $E_{c.m.} = 26.74$MeV for $\ell \geq 15$ is a signature for the presence of an exchange component in the nuclear interaction, possibly due the exchange of α-particles between target and projectile. Writing

$$S_\ell = S_\ell^0 + (-1)^\ell S_\ell^m,$$

the direct (S_ℓ^0) and the Majorana (S_ℓ^m) components of the S-matrix can easily be determined. FIGS. 5b and 5c exhibit this decomposition and we observe that the direct part of the interaction is purely absorptive while the Majorana component exhibits, possibly, one Regge pole. This clearly observed pattern could not be appreciated if we had plotted the two components together as it is shown in FIG. 5a.

One question that is usually raised with respect to such searches is to what extent the set of values obtained for the S-matrix is stable. To shed some light on this question we investigated the reason why some angular distributions yield small errors for the S-matrix while others yield very large ones. Examining all this sixteen distributions we found that those resulting in large errors were precisely those that lacked experimental point for large angles ($\Theta_{c.m.} \leq 160$ deg). We conclude that the stability of the search strongly depends on the completeness of the angular distributions.

V. CONCLUSIONS

The procedure developed was able to search automatically the real and imaginary parts of the elastic S-matrix elements without violating the unitary bound. It was clearly observed that measurements of complete angular distributions are essential for the precise determination of the S-matrix elements. Regge poles and Majorana exchange components were identified. We hope that such facilities will stimulate the measurements of the elastic channels for heavy ion systems in a systematic way, specially in the region of importance for astrophysics, with small energy steps to map, all the possible mechanisms involved in a given energy resolution.

---

† Present Address: GANIL. B. P. 5027, 14021-Caen, Cedex, France.

[1] G. R. Satchler, Phys. Rep. **199**, 147 (1991).

[2] Y. Alhassid and F. Iachello, Nucl. Phys. **A501**, 585 (1989).
[3] R. Lichtethäler and L. C. Gomes, Phys. Rev. **C50**, 3163 (1994).
[4] R. Lichtenthäler, D. Pereira, L. C. Chamon, L. C. Gomes, A. Ventura and L. Zuffi, Phys. Rev. C50, 3033 (1994).
[5] E. Almqvist, D. A. Bromley and F. A. Kuehner, Phys. Rev. Lett. **4**, 365 (1960).
[6] D. A. Bromley, F. A. Kuehner and E. Almqvist, Phys. Rev. Lett. **4**, 515 (1960).
[7] H. W. Wilschut, P. Braun-Munzinger, G. M. Berkowitz, R. H. Freifelder, J. S. Karp and T. R. Renner, Phys. Lett. **38**, 944 (1977).
[8] H. Fröhlich, P. Dück, W. Trev and H. Voit, Phys. Rev. **C27**, 578 (1983).
[9] N. Cindro, Ann. Phys. Fr. **13**, 289 (1983).
[10] H. J. Krappe and H. H. Rossner, Z. Phys. A **314**, 149 (1983).
[11] P. R. Bevington, Data Reduction and Error Analysis for the Physical Sciences, McGraw-Hill Book Co. (1969).
[12] W. H. Press, S. A. Teukolsky, W. T. Vettering and B. P. Flannery, Numerical Recipes in C, Cambridge University Press (1992).
[13] A. C. C. Villari, A. Lépine-Szily, R. Lichtenthäler Filho, O. Portesan Filho, M. M. Obuti, J. M. Oliveira Jr. and N. Added, Nucl. Phys. **A501**, 605 (1989).
[14] P. Charles, Thesis number 2378, Orsay, France (1981).
[15] V. de Alfaro and T. Regge, Potential Scattering, North-Holland Publ. Co., Amsterdam (1965)
[16] K. M. McVoy, Phys. Rev. **C3**, 1104 (1971).

FIG. 1. The χ^2 as function of $\Re(S_4)$ for a simulated case. It also exhibits σ_4, the estimated error for $\Re(S_4)$

FIG. 2. The angular distribution fits for 6 analysed energies.

FIG. 3. The Argand diagrams for two consecutive analyzed energies as indicated. The solid lines are a guide to the eyes. The errors of the real and imaginary parts of the S-matrix are indicated.

FIG. 4. The absolute value of the S-matrix as function of the angular momentum for 6 energies. The errors are indicated by the vertical bars.

FIG. 5. The Argand diagrams for $15 \leq \ell \leq 30$ of (a) total S-matrix, (b) Majorana and the (c) direct components of the S-matrix for the energy indicated. The solid lines are a guide to the eyes.

$E_{C.M.}(MeV)$	ℓ_{max}	N_0	N	χ^2
8.549	9	42	22	20
9.064	9	43	23	13
10.010	12	43	17	14
11.040	13	43	15	12
11.980	13	44	16	16
13.013	14	41	11	13
14.042	15	45	13	14
14.984	16	44	10	41
17.280	19	87	47	50
19.400	19	68	28	5.8
20.790	20	87	45	34
21.860	21	88	44	19
23.140	23	103	55	5.5
24.490	24	84	34	3.5
25.500	24	88	38	10
26.740	25	87	35	4.9

TABLE I. A summary of the sixteen energies analyzed. The labels of the columns are explained in the text

ℓ_0	$\Gamma/2$	Δ
13.50	2.25	3.00
6.50	0.93	1.51
2.70	1.00	1.50
0.00	0.75	1.20

TABLE II. The parameters of the four Regge poles observed in the 23.14 MeV angular distribution.

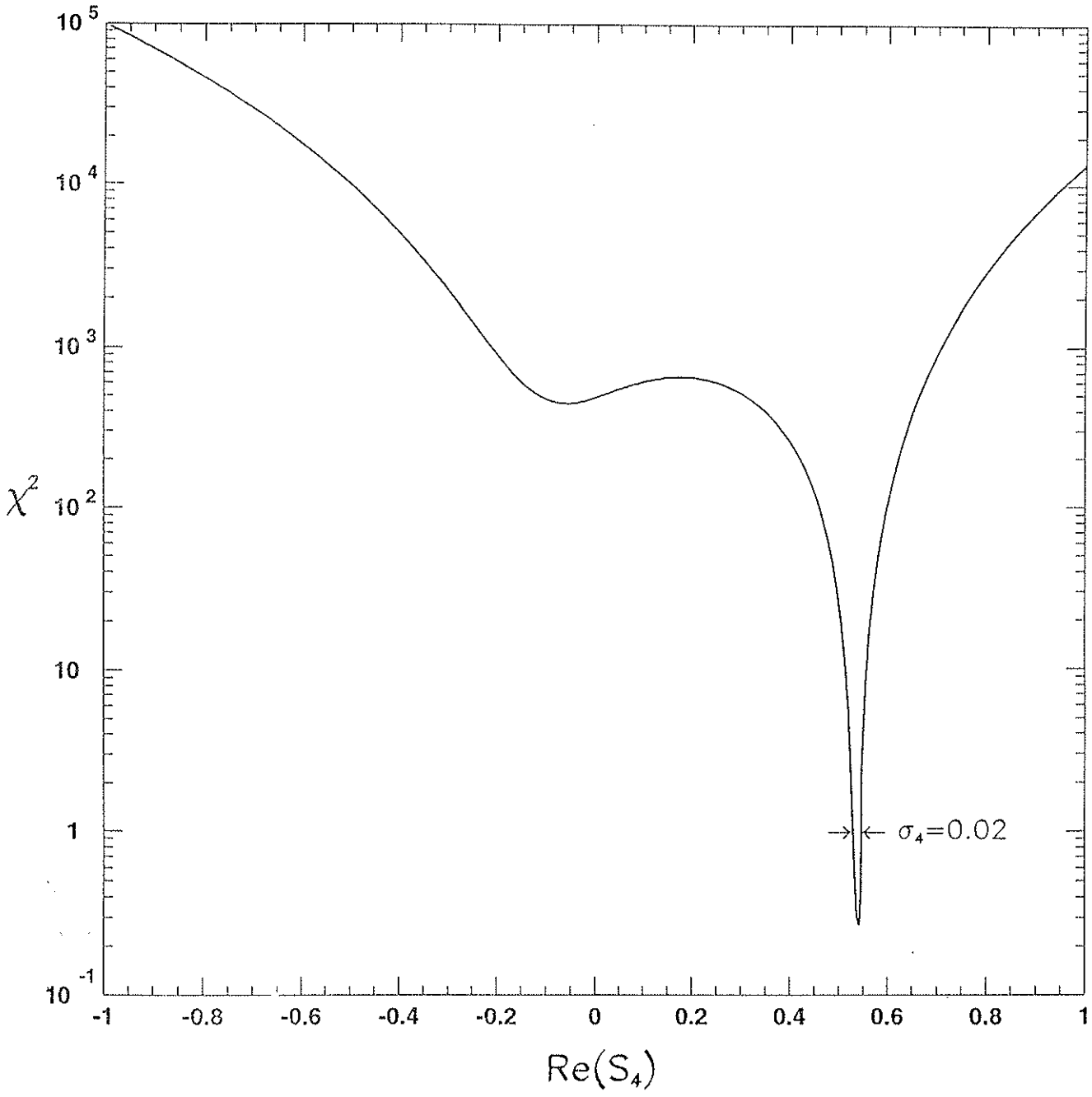
10^5
10^4
10^3
10^2
10
1
10^{-1}
χ^2
-1
-0.8
-0.6
-0.4
-0.2
0
0.2
0.4
0.6
0.8
1
σ_4=0.02
Re(S_4)

$^{12}C+^{16}O$

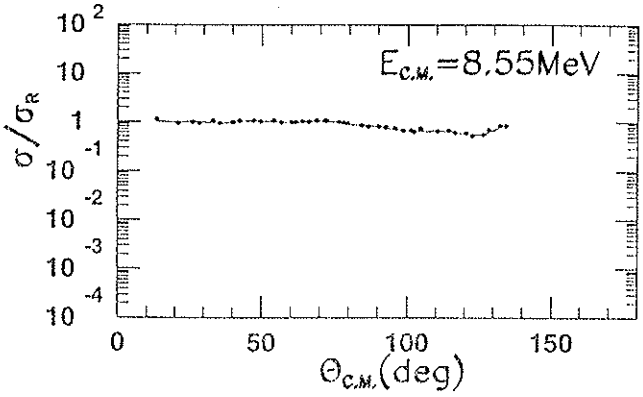
$E_{c.m.}$=8.55MeV
σ/σ_R
$\Theta_{c.m.}$(deg)

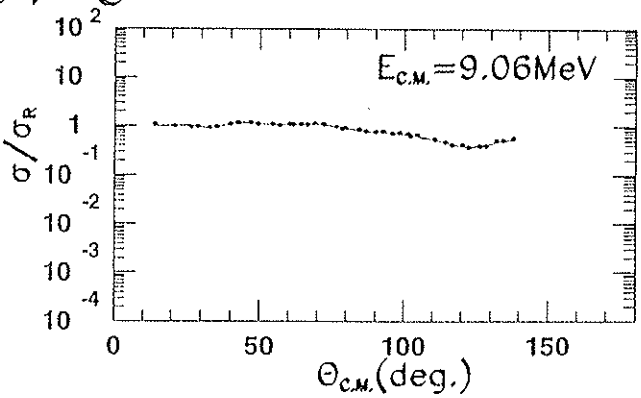
$E_{c.m.}$=9.06MeV
σ/σ_R
$\Theta_{c.m.}$(deg.)

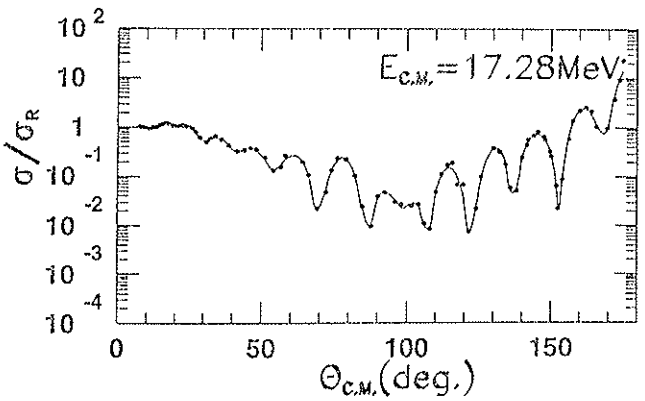
$E_{c.m.}$=17.28MeV
σ/σ_R
$\Theta_{c.m.}$(deg.)

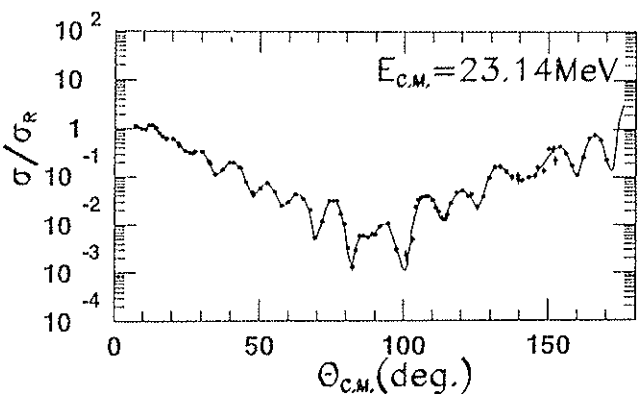
$E_{c.m.}$=23.14MeV
σ/σ_R
$\Theta_{c.m.}$(deg.)

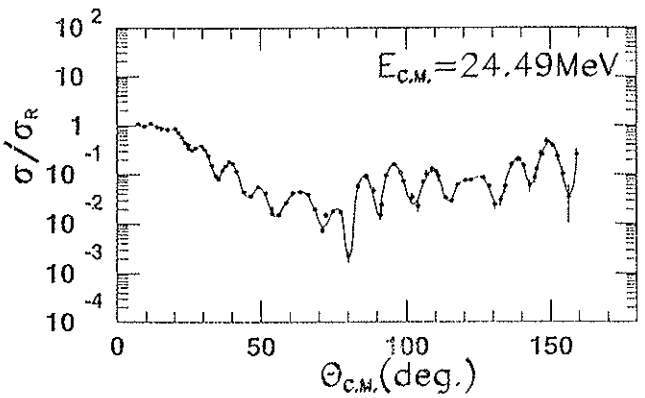
$E_{c.m.}$=24.49MeV
σ/σ_R
$\Theta_{c.m.}$(deg.)

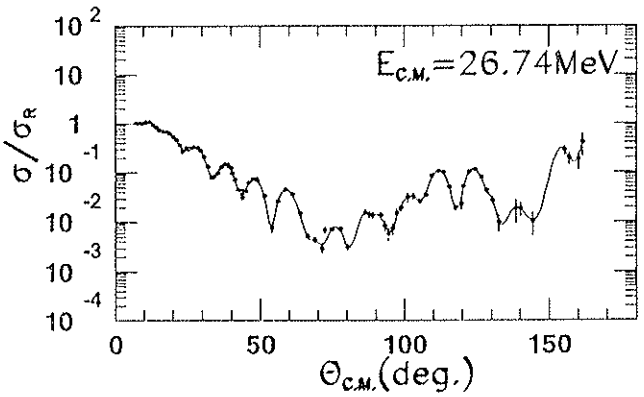
$E_{c.m.}$=26.74MeV
σ/σ_R
$\Theta_{c.m.}$(deg.)

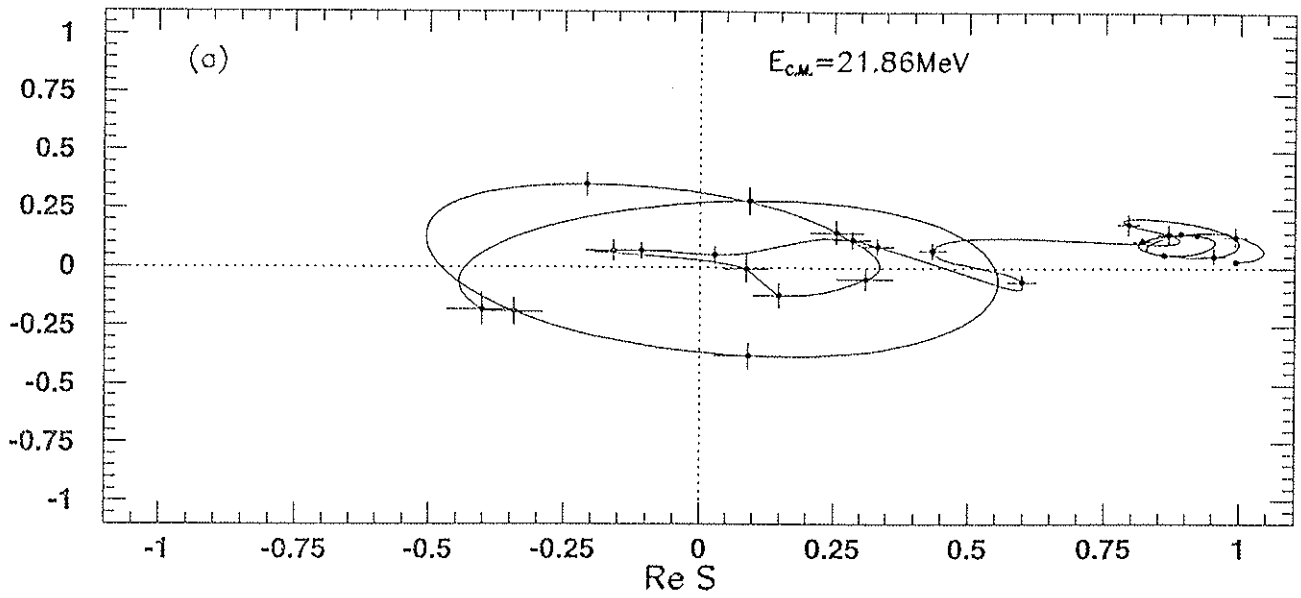
(a)
$E_{c.m.}$=21.86MeV
1
0.75
0.5
0.25
0
-0.25
-0.5
-0.75
-1
-1
-0.75
-0.5
-0.25
0
0.25
0.5
0.75
1
Re S

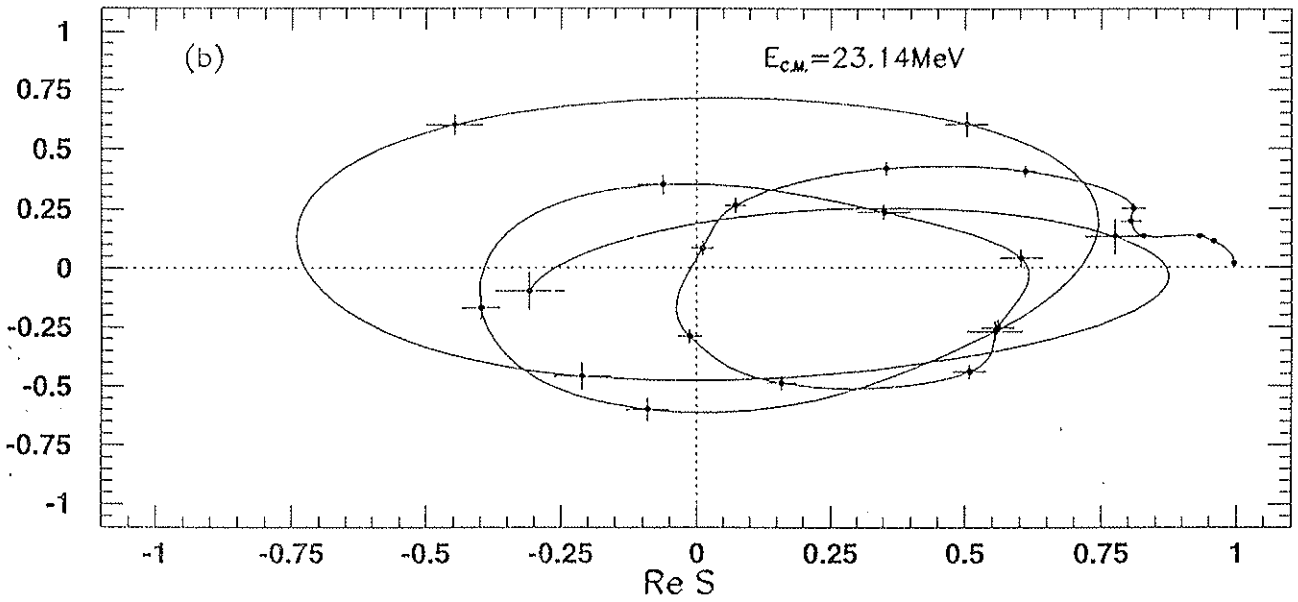
(b)
$E_{c.m.}$=23.14MeV
1
0.75
0.5
0.25
0
-0.25
-0.5
-0.75
-1
-1
-0.75
-0.5
-0.25
0
0.25
0.5
0.75
1
Re S

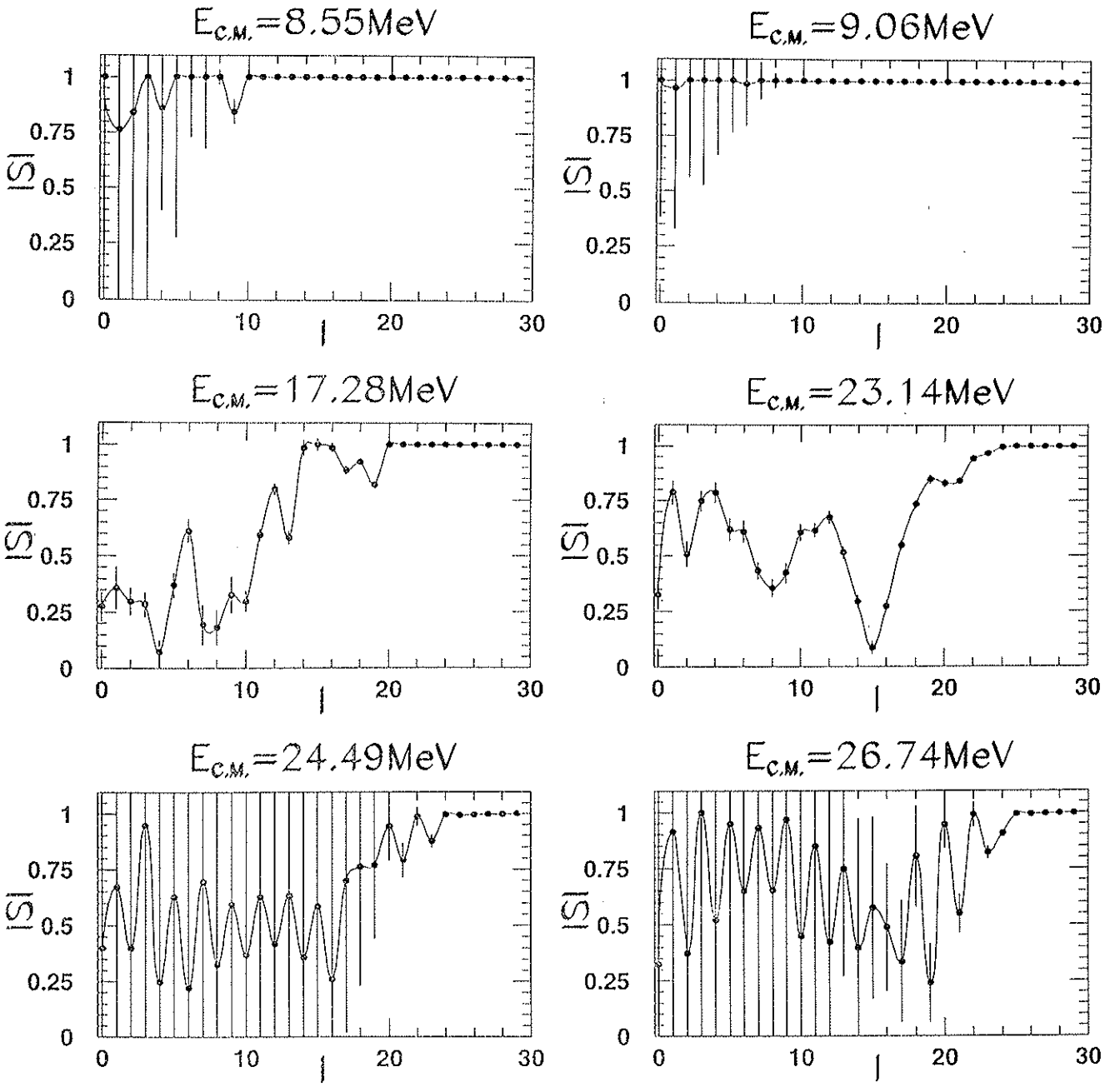
$E_{c.M.}$=8.55MeV
$E_{c.M.}$=9.06MeV
$E_{c.M.}$=17.28MeV
$E_{c.M.}$=23.14MeV
$E_{c.M.}$=24.49MeV
$E_{c.M.}$=26.74MeV
|S|
l
0
0.25
0.5
0.75
1
10
20
30

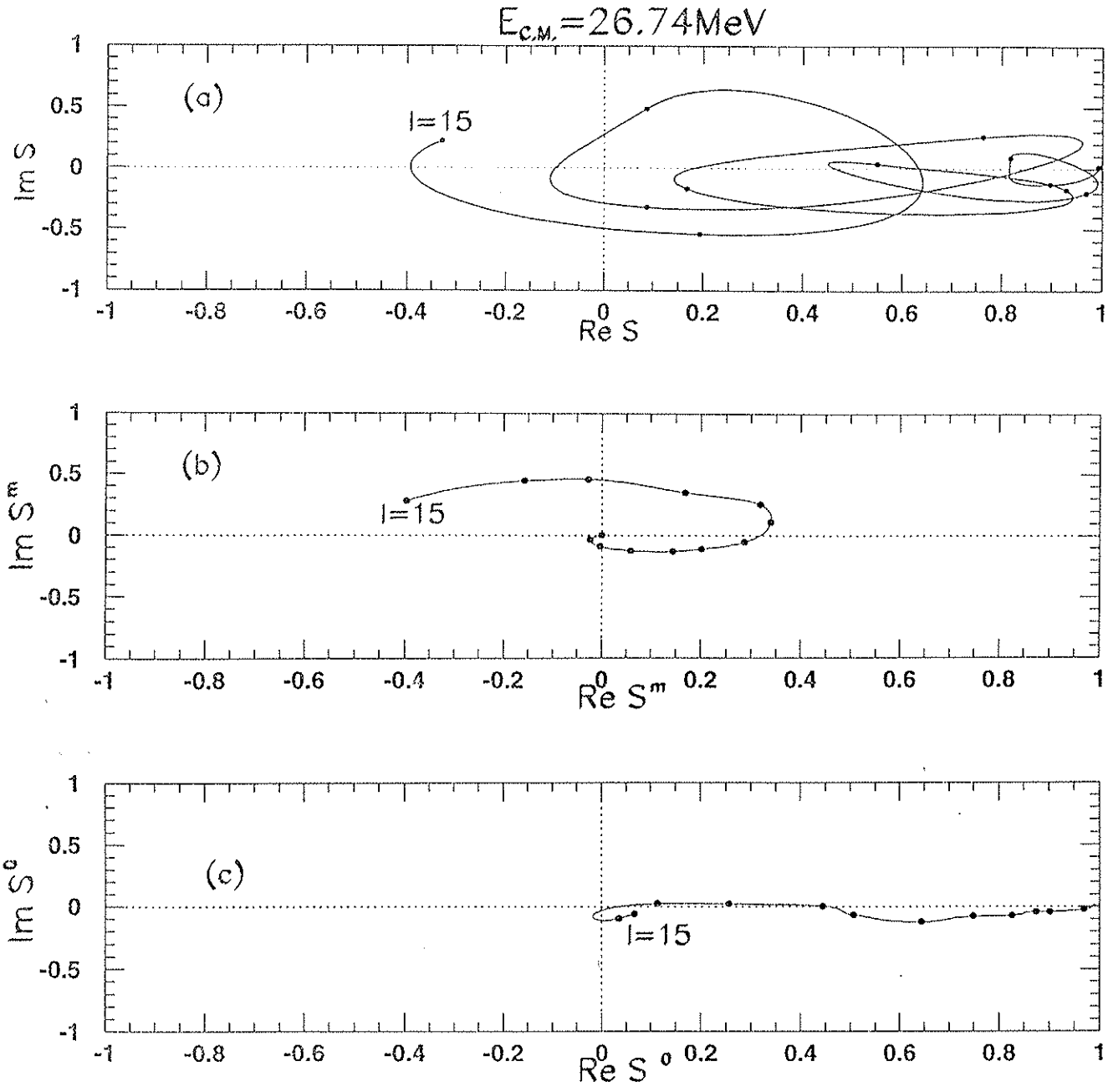
$E_{c.M.}$=26.74MeV
(a)
l=15
Im S
Re S
(b)
l=15
Im S^m
Re S^m
(c)
l=15
Im S^o
Re S^o

Anexo 2

Physics Letters B 304 (1993) 45–49
North-Holland

PHYSICS LETTERS B

Anomalous heavy ion scattering near the Coulomb barrier

A. Lépine-Szily, W. Sciani [1], Y.K. Watari, W. Mittig [2], R. Lichtenthaler F., M.M. Obuti [1], J.M. Oliveira Jr. [1] and A.C.C. Villari

Instituto de Física da Universidade de Sao Paulo, Caixa Postal 20516, 01498-970 Sao Paulo, SP, Brazil

Received 19 October 1992; revised manuscript received 12 February 1993

Striking oscillations were found in the elastic scattering of $^{12}C+^{24}Mg$ near the Coulomb barrier. These oscillations are not reproduced by the standard potentials at higher energies and provide the determination of the optical potential without continuous ambiguity. The dispersion relation between the real and imaginary parts of this optical potential is not satisfied at the strong absorption radius, but holds for their volume integrals.

In this letter we present for the $^{12}C+^{24}Mg$ system evidence that at energies near the Coulomb barrier the elastic scattering becomes sensitive to the interaction in the nuclear interior due to the closure of the reaction channels and the consequent lowering of the absorption in the nuclear interior and surface.

This evidence should be confronted with our knowledge of heavy ion optical potentials in other energy domains. Heavier systems ($A_P+A_T>50$) are usually well described by strongly absorbing optical potentials at any incident energy. They are subject to continuous ambiguities and the real potential thus is uniquely determined in a limited region only around the strong absorption radius.

For light heavy ion systems ($A_P+A_T<50$) at relatively low incident energies ($1.5V_{CB}\leq E_{CM}<3V_{CB}$, where V_{CB} is the Coulomb barrier) the optical potentials that reproduce the data are strongly energy dependent and surface transparent (STP) with a shallow real potential well. They fit the elastic scattering excitation functions of light heavy ion systems over a relatively large energy range [1–4]. Many of these systems exhibit the anomalous large angle scattering (ALAS) with a strongly oscillating back angle rise in the elastic scattering angular distributions. These features can also be fitted by explicitly coupling the α-transfer channels to the elastic channel [5–7] and the use of a normal and strongly absorbing optical potential.

The surface transparent shallow potentials fail to describe the elastic scattering at higher energies ($3V_{CB}<E_{CM}$ up to several hundred MeV). In the high energy region strongly attractive optical potentials or folding potentials work remarkably well over a very large energy range for these light heavy ion systems [8,9].

There is little information about optical model potentials around the Coulomb barrier for light heavy ion systems, mainly due to the lack of systematic measurements of the complete angular distributions for energies at and under the Coulomb barrier. For the $^{16}O+^{28}Si$ elastic scattering angular distributions, the calculations of Kobos and Satchler [10] using a folded real potential with attractive corrections produced much better fits to the data at higher energies ($E_{CM}>21$ MeV), than to the data around the Coulomb barrier.

We have measured complete elastic scattering angular distributions for the system $^{12}C+^{24}Mg$ at energies close to the Coulomb barrier, namely at energies E_{LAB} (^{12}C) = 19, 21 and 23 MeV, with the ^{12}C beam accelerated by the Pelletron Accelerator of the University of Sao Paulo. The data were measured with three counter telescopes formed by gas proportional counters and followed by silicon surface barrier detectors. The backward angles were measured by de-

Supported by CNPq/CAPES.

[1] Mailing address: GANIL, BP. 5027, F-14021 Caen Cedex, France.

tecting the recoil nucleus at forward angles. The target was isotopically enriched ^{24}Mg (99.8%) on a carbon backing, with a small amount of Bi used for normalization purposes.

We also make use in this discussion of our angular distributions measured at somewhat higher energies: 37.9 MeV [7] and 40 MeV [11]. The experimental data (fig. 1a) clearly exhibit an oscillatory behaviour even at the lowest energy (E_{LAB} = 19 MeV) that approximately corresponds to the height of the Coulomb barrier.

The data were analysed using the heavy ion direct reaction program PTOLEMY [12] and optical potentials with Woods–Saxon form factors. The data at the higher energies (37.9 MeV and 40 MeV) can be fitted by the optical potential I (see table 1), which displays the usual STP behaviour. If this potential I, which works well around 40 MeV, is extrapolated to the low energy region (E_{LAB} = 19, 21 and 23 MeV), the calculations show no oscillations, in contradiction with the experimental data (see dashed lines in fig. 1a). Neither the coupling of the inelastic scattering to the first 2^+ excited state of ^{24}Mg, nor of the α-transfer to the ^{16}O + ^{20}Ne channel could produce the observed oscillations in the elastic angular distributions. The coupling of the inelastic scattering was calculated with PTOLEMY and the α-transfer was taken into account by polarization potential [5] calculations.

Due to the difficulty in fitting the low energy angular distributions with optical model potentials with similar depths and geometries, we performed a systematic parameter search adopting the following strategy:

(i) The real depth (V_0) and the real radius (r_0) parameters were kept fixed in the search and allowing a free variation of the imaginary parameters (W_0, r_i, a_i) and of the real diffuseness parameter (a), in order to obtain a best fit.

(ii) The V_0 and r_0 values were varied on a grid,

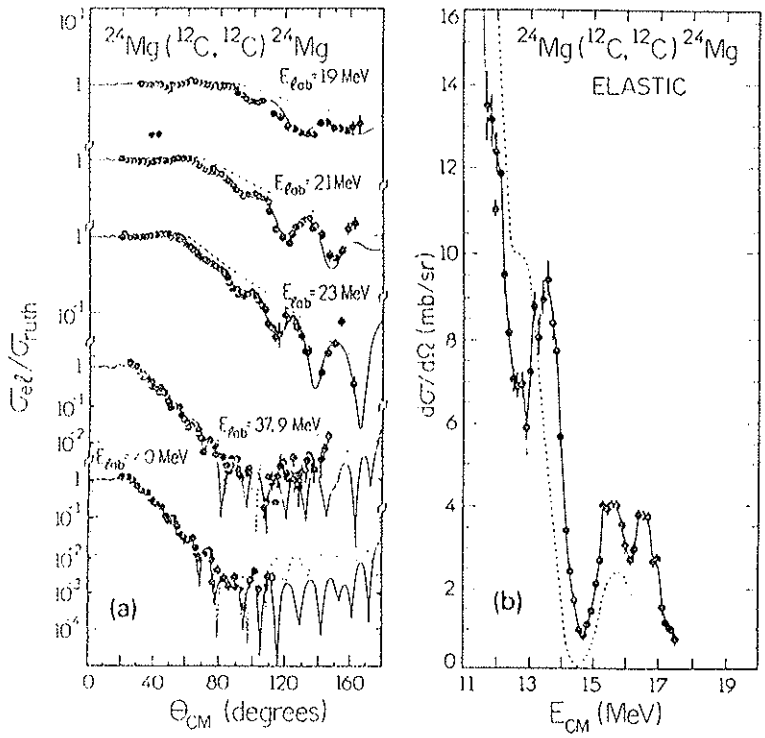

Fig. 1. (a) The experimental elastic angular distributions of ^{12}C + ^{24}Mg, measured in this work. The dashed lines are optical model calculations with STP potential I. The continuous lines are calculations with potential II. (b) The 180° excitation function measured by Mermaz et al. [14]. The dashed line is a calculation with potential II.

Table 1
The optical potential parameters used in the calculations with respective χ^2 values. The Coulomb radius used was $1.2\,A_1^{1/3}$. The Woods-Saxon form factors have the usual form

$$V(r) = V_0\left[1+\exp\left(\frac{r-r_0(A_1^{1/3}+A_2^{1/3})}{a}\right)\right]^{-1}.$$

Potential	E_{LAB} (MeV)	V_0 (MeV)	r_0 (fm)	a (fm)	W_0 (MeV)	r_i (fm)	a_i (fm)	χ^2
I	37.9 40.0	$7.15+0.5\,E_{CM}$	1.348	0.376	$0.9+0.15\,E_{CM}$	1.336	0.078	
II	19	38.652	1.290	0.40	0.429	1.77	0.681	9.9
	21	37.393	1.290	0.40	0.623	1.77	0.613	9.1
	23	36.422	1.290	0.40	0.783	1.77	0.443	10.8
	19–23	$48.716-0.536\,E_{LAB}$	1.290	0.40	$-1.281+0.090\,E_{LAB}$	1.77	$1.722-0.0548\,E_{LAB}$	
	37.9	34.98	1.29	0.4	2.1	1.77	0.48	
	40.0	34.98	1.29	0.4	1.959	1.77	0.41886	

from 10 to 44 MeV, with 1 MeV steps in V_0 and from 1.0 to 1.6 fm with 0.02 fm steps in r_0.

(iii) The back angle experimental errors were artificially reduced in these searches so as to enhance the importance of the back angle oscillations.

The results of this systematic search are presented in a three-dimensional plot (fig. 2), where the axes are V_0, r_0 and $1/\chi^2$, where χ^2 has the usual definition and measures the quality of the fit. The best fit parameters, producing oscillating cross-sections with good phase and period, correspond to low χ^2 values and peaks on the $1/\chi^2$ surface. The three surfaces, corresponding to the three incident energies, present ridges for correlated (V_0, r_0) values, corresponding to best fit potential families. They are superimposed on plane regions, which correspond to completely smooth angular distributions, without oscillations, with nearly constant χ^2 values.

The existence of only one peak in the $1/\chi^2$ plane at the same $r_0 = 1.29$ and approximately the same V_0 for the three energies (dotted peaks in fig. 2) allows us to determine a unique optical potential in the studied parameter range, and within the reported constraints (r_0 independent of energy, conventional Woods–Saxon shape). We call potential II (table 1) the parameters corresponding to this peak. The solid line through the low energy angular distributions in fig. 1a is the fit obtained with potential II. It is interesting to note that the absence of ridges below $V_0 = 30$ MeV on the $1/\chi^2$ surface for 21 MeV allowed us to conclude that these low energy data cannot be reproduced by potentials with $V_0 < 30$ MeV.

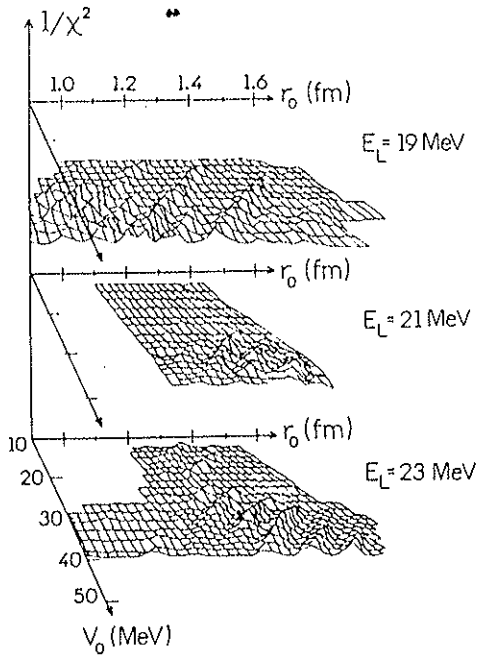

Fig. 2. Three-dimensional plots of the optical model parameters V_0, r_0 versus $1/\chi^2$, where χ measures the quality of the fit.

Among the Woods–Saxon shaped optical potentials, with energy independent radii, this is the first or shallowest real potential, unique for $V_0 \leq 45$ MeV. Probably there is a discrete ambiguity for larger V_0,

but this was not investigated in this work. It was found that real potentials of the same ridge cross at well defined points between 5.5 and 6.5 fm. Different ridges correspond to different crossing-points.

The deep valleys existing between the ridges (see fig. 2) indicate clearly that potentials between the best fit ridges do not reproduce the oscillations. The period and phase of the oscillations are determined by the strength of the real potential in the internal region around 6.2 fm and *not* around the strong absorption radius.

The imaginary potentials corresponding to these ridges are very poorly determined in the external region, although they were found to cross approximately around 5.5–6.5 fm. They are weakly absorbing even in the internal region, and they have a very large range, extending to radii much larger than the usual potential. The inelastic coupling may be important, due to the fact that both participants are deformed, and the largely extending absorption can be partly due to this coupling that is not included in the calculations.

The imaginary radius and real geometry of potential II are constant and the V_0, W_0 and a_i parameters have linear energy dependences. Contrary to the energy dependent shallow STP, the real potential depth V_0 decreases with energy and thus becomes shallower for higher energies. The large imaginary diffuseness also decreases with energy, reducing the absorptive range as the energy increases. We can also fit the angular distributions at 37.9 and 40 MeV with the same geometry of potential II, but the energy dependent parameters do not follow the linear dependence verified around 20 MeV. Their best fit parameters are in table 1 and the best fits are presented in fig. 1a, as continuous lines (these fits are as good as those obtained by STP potential I).

The dispersion relation [13–15] between the real and the imaginary parts of the optical potential is satisfied for heavier systems at the strong absorption radius. In our case it is satisfied neither at $R_{SA}=8.5$ fm, nor at 6.2 fm. In contrast the potential volume integrals J_V and J_W do satisfy the dispersion relation, thus confirming our sensitivity to the whole nuclear interior. The results of data and calculations are shown on fig. 3. Normally, the dispersion relation should be satisfied at any radial distance. However, due to ambiguities in the heavy ion potentials, it was shown in

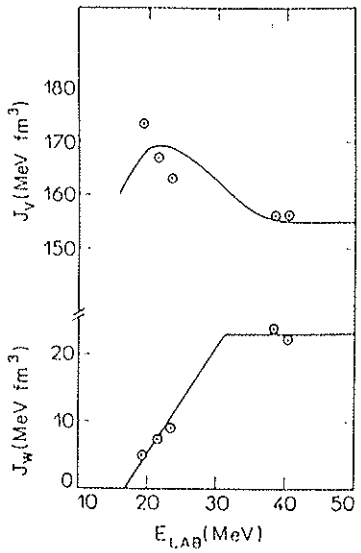

Fig. 3. The imaginary and real potential volume integrals of potential II are indicated by circles and the solid lines are dispersion relation calculations [12,13].

ref. [14] that the comparison between the experimental threshold anomaly and the dispersion relation calculations should be performed around the strong absorption radius, because the potentials are well determined in this radial region. In the present case, the imaginary part is poorly determined at the "strong" absorption radius, and is only weakly absorbing, even in the nuclear interior. Thus, the strong absorption radius has lost the physical meaning it has at higher energies and for heavier systems. This is also confirmed by our "notch-test" calculations, which showed that we are sensitive to the real potential between 1.5 and 8 fm. Moreover, it has already been verified [15] for nucleon–nucleus and α–nucleus scattering, where the scattering is sensitive to the potential over a wide radial region, that the dispersion relation should be taken between the volume integrals. At much higher energies ($E/A \geq 6$ MeV), the $^{12}C+^{12}C$ scattering exhibits similar features [16].

The excitation function at 180° was calculated using this energy dependent optical potential II and it is compared to the experimental data of Mermaz [17] (see dashed line in fig. 1b). The peak at $E_{CM}=13.5$ MeV is shifted in the calculation, but the deep valley at $E_{CM}=14.5$ MeV and the peak around 15.5

are remarkably well reproduced, as well as the general trend.

In order to get a better understanding of the influence of the nuclear interior we calculated the optical model wave-functions for various potentials. It turned out that:

(i) the standard potential produces wave-functions that are strongly absorbed in the nuclear interior ($r < 5$ fm);

(ii) the potentials we found to reproduce the oscillations, give rise to standing waves in the pocket of the effective interaction ($r < 5$ fm), producing constructive interference between the reflected waves in the internal and external barriers;

(iii) the potentials between the ridges of fig. 2 do not produce the same constructive interference and the outgoing wave-functions are strongly attenuated.

Thus, we observed striking oscillations in the elastic angular distributions of $^{12}C+^{24}Mg$ near the Coulomb barrier. These are not reproduced by the standard optical model parameters, which fit very well the oscillations at higher energies. We can conclude from the present analysis that these oscillations of $^{12}C+^{24}Mg$ at energies near the Coulomb barrier are sensitive to the nuclear interior, eliminating the continuous ambiguity observed for strongly absorbing optical potentials. Using conventional Woods–Saxon form factors and energy independent radii, we determined the shallowest real potential family, with real depth decreasing with energy and deeper than the STP used at higher energies. The imaginary potential has a very large range, showing absorption at large distances, but very weak absorption in the nuclear interior. This unique potential family also reproduces the 180° excitation function remarkably well. The real and imaginary parts of this potential were found not to satisfy the dispersion relation at the strong absorption radius, however, it was found to hold for the volume integrals of the potential.

We are pleased to acknowledge fruitful discussions with M.E. Brandan, L.C. Gomes, N. Alamanos and G.R. Satchler.

References

[1] R.H. Siemssen, H.T. Fortune, R. Malmin, A. Richter, Y.W. Tippie and P.P. Singh, Phys. Rev. lett. 25 (1970) 536.
[2] H.T. Fortune, A. Richter, R.H. Siemssen and J.L. Yntema, Phys. Rev. C 20 (1979) 648.
[3] W. Mittig, P. Charles, S.M. Lee, I. Badawy, B. Berthier, B. Fernandez and J. Gastebois, Nucl. Phys. A 233 (1974) 48.
[4] V. Shkolnik, D. Dehnhard and M.A. Franey, Phys. Rev. C 28 (1983) 717.
[5] R. Lichtenthäler F., A. Lépine-Szily, A.C.C. Villari and O. Portezan F., Phys. Rev. C 39 (1989) 884.
[6] A. Lépine-Szily, R. Lichtenthäler F., M.M. Obuti, J.M. de Oliveira Jr., O. Portezan F., W. Sciani and A.C.C. Villari, Phys. Rev. C 40 (1989) 681.
[7] A. Lépine-Szily, M.M. Obuti, R. Lichtenthäler F., J.M. Oliveira Jr. and A.C.C. Villari, Phys. Lett. B 243 (1990) 23.
[8] M.E. Brandan, Phys. Rev. Lett. 60 (1988) 784.
[9] P. Roussel, N. Alamanos, F. Auger, J. Barette, B. Berthier, B. Fernandez, L. Papineau, H. Doubre and W. Mittig, Phys. Rev. Lett. 54 (1985) 1779.
[10] A.M. Kobos and G.R. Satchler, Nucl. Phys. A 427 (1984) 589.
[11] R. Lichtenthäler F., A. Lépine-Szily, A.C.C. Villari, W. Mittig, V.J.G. Porto and C.V. Acquadro, Phys. Rev. C 26 (1982) 2487.
[12] M.H. MacFarlane and S.C. Pieper, report ANL 76-11, unpublished.
[13] G.R. Satchler, Phys. Rep. 199 (1991) 147.
[14] M.A. Nagarajan, C. Mahaux and G.R. Satchler, Phys. Rev. Lett. 54 (1985) 1136.
[15] C. Mahaux and H. Ngô, Nucl. Phys. A 378 (1982) 205.
[16] M.E. Brandan, M. Rodriguez-Villafuerte and A. Ayala, Phys. Rev. C 41 (1990) 1520.
[17] M.C. Mermaz, A. Greiner, B.T. Kim, M.J. Levine, E. Müller, M. Ruscev, M. Petrascu, M. Petrovici and V. Simion, Phys. Rev. C 24 (1981) 1512.

ANEXO 3

Measurements of excitation functions of the $^{12}C+^{24}Mg$ system near the Coulomb barrier

P. Fachini[1], R. Lichtenthäler[1], A. C. C. Villari[1,2], W. Sciani[1], J. M. Oliveira Jr[1,3], G. F. Lima[1], V. Chisté[1], A. C. G. Martins [1], J. M. Casandjian[2], A. Lépine-Szily[1], L. C. Gomes[1]

[1] *Departamento de Física Nuclear*
Instituto de Física da Universidade de São Paulo
Caixa Postal 66318, CEP 05389 - 970
São Paulo, Brasil

[2] *Grand accélérateur National d'Ions lourds, Boîte Postale 5027, 14021 Caen Cedex, France*

[3] *Departamento de Ciências e Matemática*
Universidade de Sorocaba
Caixa Postal 578, CEP 18060-000
Sorocaba, SP, Brasil

Measurements of the elastic scattering excitation functions of $^{12}C+^{24}Mg$ were performed at $\Theta_{cm} = 90$ deg and $\Theta_{cm} = 140$ deg in the energy range 10.2 MeV $\leq E_{cm} \leq$ 17.3 MeV with energy steps of 33 keV and 50 keV respectively. The comparision of our excitation functions with the one measured by Mermaz at 180 deg indicates the presence of correlated structures. With the assignment of spins to these structures, the presence of a molecular rotational band following the grazing trajectory can be suggested. The auto-correlation analysis of the 90 deg excitation function detected the presence of fluctuations with widths $\Gamma = 110$ keV and the fluctuation cross-section was estimated.

I. INTRODUCTION

The excitation functions of n–α systems show strong structures in the elastic, inelastic and α–transfer reactions, when measured with good energy resolution. In several systems of the s–d shell [1–3] at energies of about two to three times the Coulomb barrier, these structures have been characterized by intermediate widths between 500 keV and 2 MeV, with fine structures superimposed on it, with width in the range 50 keV $\leq \Gamma_{cm} \leq$300 keV. This behaviour, associated with oscillating angular distributions and large values for the cross-sections observed at backward angles, configured the so-called "Anomalous Large Angle Scattering" (ALAS) [4]. These features are frequently also present in forward and intermediate angle excitation functions as well [5,6]. Many interpretations have been proposed to explain these phenomena in a consistent manner, among which we mention the search for isolated resonances of molecular character [6,7], observed in lighter systems as the $^{12}C+^{12}C$ scattering [8,9], and models based on modifications of the optical potential of the interacting system [5,10,11], that could be originated by the coupling to different channels [12,13]. No clear distinction could be made between the different models on the basis of the available experimental data and in particular the small difference in width between the fine and intermediate structures indicates the difficulty of separating resonant from non–resonant structures. More recently, an optical model analysis of the elastic scattering angular distributions of $^{12}C+^{24}Mg$ [14] at energies near the Coulomb barrier, resulted in surprisingly low values of the ratio W/V between the imaginary and real potential depths, allowing the formation of resonant-like states in the pocket of the real effective potential.

This fact was our motivation to perform measurements of the elastic scattering excitation functions of $^{12}C+^{24}Mg$ near the Coulomb barrier, with good energy resolution ($\Delta E_{cm} \approx 33$ keV). Measurements of excitation functions of spin zero particles at $\Theta_{c.m} = 90$ deg are suitable for the observation of statistical fluctuations due to the fact that only even partial waves waves participate of the collision process at this angle. In addition, the comparision with measurements at other angles, can provide a criterium for the determination of the parities of isolated resonances.

II. THE DATA

The measurements were performed using the ^{12}C beam produced by the Pelletron Accelerator of the University of São Paulo, bombarding an isotopically enriched (99.92%) ^{24}Mg target of 4.6μg/cm^2, evaporated on a carbon backing of 30μg/cm^2. The emerging ^{12}C and ^{24}Mg nuclei were detected in kinematic coincidence, using two surface barrier silicon detectors. The geometry of the detection system was chosen in order to maximize the efficiency for the elastic

scattering. A Monte Carlo simulation was performed to determine the efficiency of the kinematic coincidence, taking into account the geometry of the detection system, the beam characteristics such as the dimensions of the spot on the target and its divergence, and the effects due to the angular straggling of the scattered particles in the target.

The total kinetic energy of each event, independent of the scattering angle, could be obtained from the energies of both particles measured simultaneously, allowing a perfect separation between the elastic peak and the first excited state of the ^{24}Mg(E_{exc} = 1.37 MeV) using a detection solid angle of 5 msr. The excitation functions measured at $\Theta_{cm} = 90 \pm 2$ deg and $\Theta_{cm} = 140.0 \pm 2.5$ deg are presented in FIG. 1.

III. THE ANALYSIS

An auto-correlation analysis was performed for both excitation functions. Inserted in FIG. 1 we present the auto-correlation function obtained by the expression:

$$C(\varepsilon, \Delta) = \left(\frac{\sigma(E)}{\langle\sigma(E)\rangle_\Delta} - 1\right)\left(\frac{\sigma(E+\varepsilon)}{\langle\sigma(E+\varepsilon)\rangle_\Delta} - 1\right) \tag{1}$$

using $\Delta = 1$ MeV for $\Theta_{cm} = 90$ deg and $\Delta = 1.3$ MeV for $\Theta_{cm} = 140$ deg. The values of Δ used in this analysis were extracted from the Pappalardo functions $C(0, \Delta)$ which should have exhibited plateaus around these values. However no clear plateau was observed indicating that the difference in width between the narrow and broad structures is not sufficient to permit the complete separation of the two in the auto-correlation function. The coherence widths obtained by fitting the experimental auto-correlation function with the expression (see solid curve on FIG. 1):

$$C(\varepsilon) = C(0)\frac{\Gamma^2}{\Gamma^2 + \varepsilon^2} \tag{2}$$

are respectively $\Gamma = 110(50)$ keV for $\Theta_{cm} = 90$ deg and $\Gamma = 360(200)$ keV for $\Theta_{cm} = 140$ deg. The errors were estimated performing auto-correlation analysis varying the Δ of 30%, around the values $\Delta = 1$ MeV and $\Delta = 1.3$ MeV. An estimation of the coherence widths for the two excitation functions was made using the peak counting method [16] and resulted similar to those, obtained by the auto-correlation analysis. The coherence width of $\Gamma = 110$ keV, observed at $\Theta_{cm} = 90$ deg is characteristic of fluctuations due to the formation of compound nucleus ^{36}Ar. Thus we calculated the fluctuating cross-section $\langle\sigma_{fluc}\rangle = 0.048(14)$ mb given by:

$$\langle\sigma_{fluc}\rangle = \langle\sigma_{mean}\rangle(1 - y_d) \tag{3}$$

where y_d is defined by:

$$C(0) = \frac{1 - y_d^2}{N_{eff}} \tag{4}$$

with $N_{eff} = 1$ for elastic scattering. This value corresponds to $\approx 0.3\%$ of the mean elastic cross section and could be regarded as the average contribution of the compound elastic process to the elastic scattering. The same analysis for the $\Theta_{cm} = 140$ deg auto-correlation function results in fluctuating cross-sections of the same order. However it is not clear whether the larger width obtained at this angle can be considered as characteristic of the compound nucleus. The different coherence widths obtained at 90 deg and 140 deg we attribute to the fact that probably there is a fine structure superimposed on an intermediate one whose widths are not sufficiently different to be separated in the auto-correlation analysis. The relative intensities of those structures can change with the angle causing the auto-correlation function to be more sensitive to one or other width. In fact it is expected [15] the largest Ericson fluctuations to occur at angles where few orbital angular momenta contribute as is the case for $\Theta_{c.m.} = 90$ deg where only even partial waves are present.

As a next step, we calculated the variations of the experimental cross-section around its mean value through the function $(\sigma/\langle\sigma\rangle_\Delta - 1)$. We used $\Delta = 2$ MeV. This function is interesting since it emphasizes the structures around the average cross-section presented in the excitation functions. In FIG. 2 we plot this function for $\Theta_{cm} = 90$ deg and $\Theta_{cm} = 140$ deg, together with the excitation function measured by Mermaz [3] at $\Theta_{cm} = 180$ deg. For this comparison the data of Mermaz have been shifted by 300 keV upwards in energy, what can be justified by the use of different targets and energy calibrations. The vertical lines are guides to highlight the 6 observed correlated structures. The fact that we have measurements at $\Theta_{cm} = 90$ deg where only even partial waves contribute and at $\Theta_{cm} = 140$ deg and $\Theta_{cm} = 180$ deg where all partial waves contribute, provides us with an experimental criterium for the determination of the parities of these "resonances". Besides, the supposition that the spins of these resonances should follow a

trajectory around the grazing angular momentum for this system, allows us to assign angular momentum values for these structures (see FIG. 2). The values of spins assigned are consistent with a Regge pole analysis of measured angular distributions for this system [17] at several energies in this range. The apparent absence of the structures at 14.42 MeV at $\Theta_{cm} = 180\,\mathrm{deg}$ can be due to the fact that the measurements at $\Theta_{cm} = 180\,\mathrm{deg}$ were performed with energy resolution and steps of 150 keV. In FIG. 2 (upper right) we plotted E_{cm} for the correlated structures as a function of $\ell(\ell+1)$, where ℓ are the assigned spins and we observe that it apparently follows a linear relation, as would be expected for a rotational-like spectrum. A fit of the data using the following equation:

$$E_{cm} = V_{cb} + \frac{\hbar^2}{2I}\ell(\ell+1), \tag{5}$$

results in a value for the moment of inertia of 3.37×10^5 MeV.fm^2 and a value for the Coulomb barrier of 10.56 MeV, which can be compared with the value of $V_{cb} = 12.34$ MeV obtained using the optical potential of ref. [14]. The moment of inertia calculated by the expression $I = \frac{2}{5}(M_1R_1^2 + M_2R_2^2) + \mu(R_1 + R_2)^2$ where μ is the reduced mass of the system results 5.04×10^5 MeV.fm^2 using $r_o = 1.3\,fm$. If one neglects the first term, which corresponds to consider a rotation in the sliding mode, one obtains $I = 3.37 \times 10^5$ MeV.fm^2, in very good agreement with our result. We also considered the possibility of the band starting at $l = 3$ instead of $l = 5$. However this assignment was discarded as it resulted in a too small moment of inertia.

IV. CONCLUSIONS

We measured excitations functions of the elastic scattering ^{12}C+ ^{24}Mg at $\Theta_{cm} = 90\,\mathrm{deg}$ and $\Theta_{cm} = 140\,\mathrm{deg}$ in the energy range 10.2 MeV $\leq E_{cm} \leq$ 17.3 MeV with energy steps of 33 keV and 50 keV and resolution of 33 keV. We exhibited correlated structures in the $\Theta_{cm} = 90\,\mathrm{deg}$,$\Theta_{cm} = 140\,\mathrm{deg}$ and $\Theta_{cm} = 180\,\mathrm{deg}$ excitation functions. The spin values assigned to these structures following the grazing angular momentum trajectory and consistent with the parity selection at $\Theta_{cm} = 90\,\mathrm{deg}$, resulted in an angular momentum band whose moment of inertia is in agreement with a rotating dinuclear system in the sliding mode. The auto-correlation analysis detected the presence of fluctuations at 90 deg whose coherence width are similar to those expected due to the compound nucleus formation. The average fluctuation cross-section associated to these structures is of 0.048(14) mB what corresponds to $\approx 0.3\%$ of the elastic cross-section.

---

* Present address: GANIL, B. P. 5027, 14021-Caen, Cedex, France.

[1] J. Barrete, M. J. LeVine, P. Braun-Munzinger, G. M. Berkowitz, M. Gai, J. W. Harris, C. M. Jachcinski, C. D. Uhlhorn, Phys. Rev. C 60, 1759 (1979).
[2] P. Braun-Munzinger and J. Barrete, Phys. Reports 87, n°5, (1982).
[3] M. C. Mermaz, A. Greiner, B. T. Kim, M. J. LeVine, E. Müller, M. Ruscev, M. Petrascu, M. Petrovici, V. Simion, Phys. Rev. C 24, 1512 (1981).
[4] P. Braun-Munzinger, G. M. Berkowitz, T. M. Cormier, J. W. Harris, and C. M. Jachcinski, Phys. Rev. Lett. 38, 944 (1977).
[5] , D. Dehnhard, V. Shkolnik, M. A. Franey, Phys. Rev. Letters 40, 1549 (1978).
[6] S. J. Sanders, H. Ernst, W. Henning, C. Jachcinski, D. G. Kovar, J. P. Schiffer, J. Barrete, Phys. Rev. C31, 1775 (1985).
[7] N. Cindro, Ann. Phys. Fr. 13, 289 (1988).
[8] D. A. Bromley, J. A. Kuehner, E. Almqvist, Phys. Rev. Lett. 4, 365 (1960).
[9] E. Almqvist, D. A. Bromley, J. A. Kuehner, Phys. Rev. Lett. 4, 515 (1960).
[10] S. Y. Lee, Nucl. Phys. A311, 518 (1978).
[11] S. Kahana, B. T. Kim, M. C. Mermaz, Phys. Rev. C20, 2124 (1979).
[12] R. Lichtenthäler, A. Lépine-Szily, A. C. C. Villari, O. Portezan Filho, Phys. Rev. C39, 884 (1989).
[13] A. Lépine-Szily, R. Lichtenthäler, M. M. Obuti, J. M. Oliveira Jr, O. Portezan Filho, W. Sciani, A. C. C. Villari, Phys. Rev. C40, 681 (1989)
[14] A. Lépine-Szily, W. Sciani, Y. Watari, W. Mittig, R. Lichtenthäler, M. M. Obuti, J. M. Oliveira Jr, A. C.-C. Villari, Phys. Lett. B304, 45 (1993)
[15] T. Ericson, Annals of Physics 23, 390 (1963)
[16] D. M. Brink, R. O. Stephen, Phys. Lett. B5, 77 (1963).

[17] W. Sciani, private communication

FIG. 1. Excitation Functions measured at $\Theta_{cm} = 90\,\mathrm{deg}$ and $\Theta_{cm} = 140\,\mathrm{deg}$. Inserted is shown the result of the auto-correlation analysis (dots) and the fit with a Lorentzian (solid line)

FIG. 2. The quantity $(\sigma/\langle\sigma\rangle_\Delta - 1)$ for $\Delta = 2$ MeV at $\Theta_{cm} = 90\,\mathrm{deg}$ and $\Theta_{cm} = 140\,\mathrm{deg}$ (a) and (b) and the excitation function measured by Mermaz at $\Theta_{cm} = 180\,\mathrm{deg}$. In the right upper side is plotted $E_{cm} \times \ell(\ell + 1)$ corresponding to the structures observed.

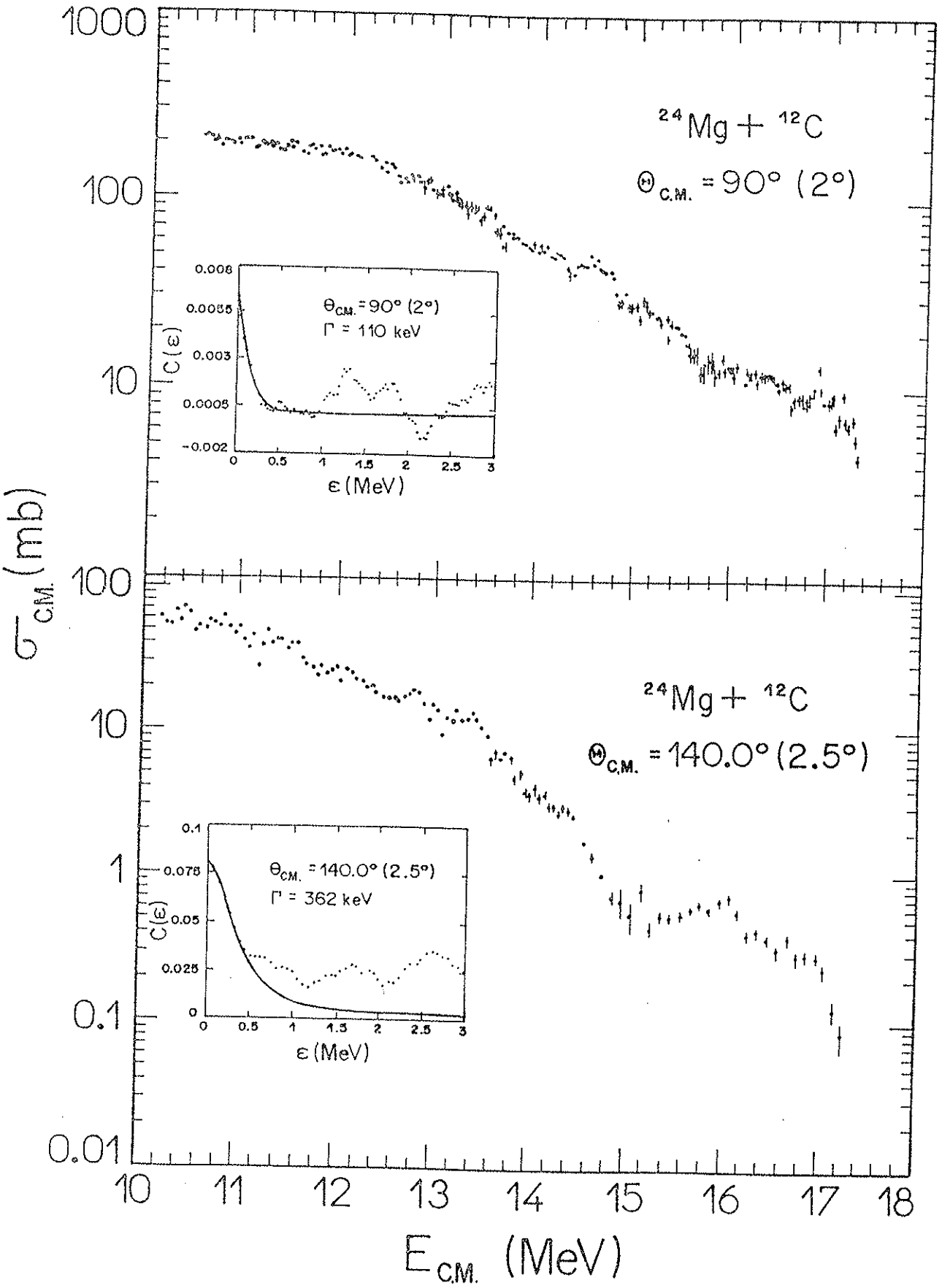
$^{24}Mg + {}^{12}C$
$\Theta_{C.M.} = 90°$ (2°)
$\Theta_{CM.} = 90°$ (2°)
Γ = 110 keV
C(ε)
ε (MeV)
$^{24}Mg + {}^{12}C$
$\Theta_{C.M.} = 140.0°$ (2.5°)
$\Theta_{CM.} = 140.0°$ (2.5°)
Γ = 362 keV
C(ε)
ε (MeV)
$\sigma_{C.M.}$ (mb)
$E_{C.M.}$ (MeV)

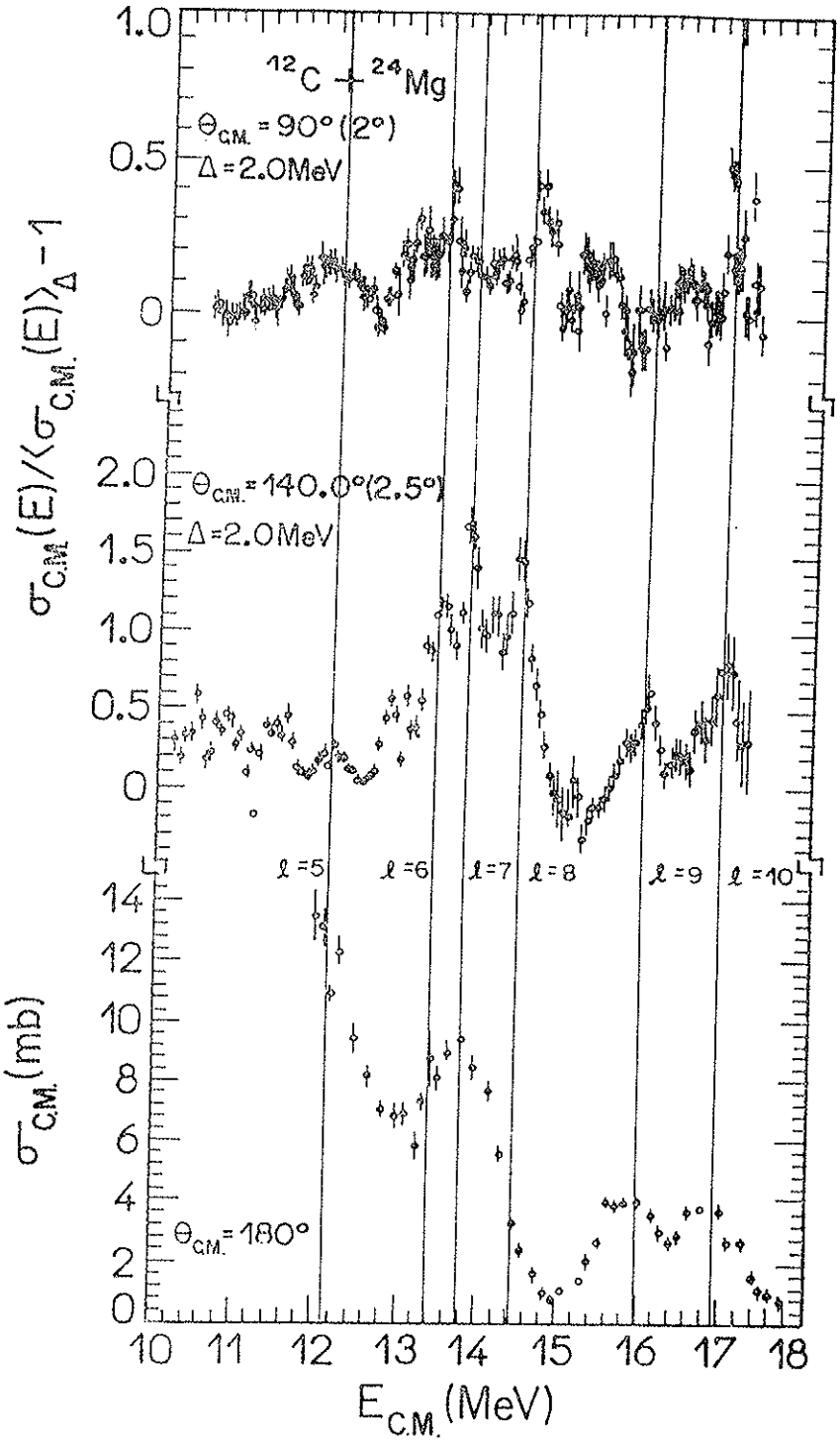
$^{12}C + ^{24}Mg$
$\theta_{C.M.} = 90°(2°)$
$\Delta = 2.0$MeV
$\theta_{C.M.} = 140.0°(2.5°)$
$\Delta = 2.0$MeV
$\theta_{C.M.} = 180°$
$\ell = 5$
$\ell = 6$
$\ell = 7$
$\ell = 8$
$\ell = 9$
$\ell = 10$
$\sigma_{C.M.}(E)/\langle\sigma_{C.M.}(E)\rangle_\Delta - 1$
$\sigma_{C.M.}$(mb)
$E_{C.M.}$(MeV)

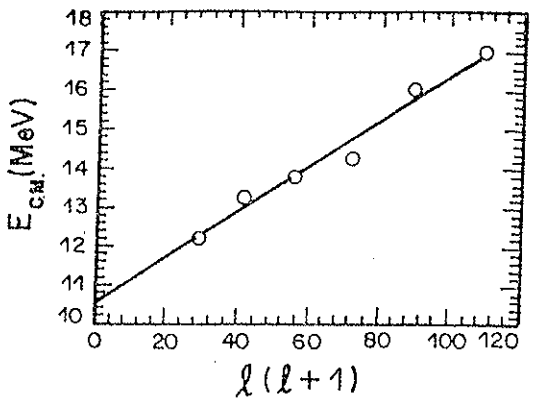
$E_{C.M.}$(MeV)
$\ell(\ell+1)$

ANEXO 4

Physics Letters B 269 (1991) 49–53
North-Holland

PHYSICS LETTERS B

An algebraic optical potential for heavy ion collisions

R. Lichtenthaler Filho, A.C.C. Villari, L.C. Gomes
Departamento de Física Nuclear, Instituto de Física da Universidade de São Paulo, C.P. 20516, 01498 São Paulo SP, Brazil

and

P. Carrilho Soares
Instituto de Física, Universidade Federal do Rio de Janeiro, C.P. 68528, 21945 Rio de Janeiro RJ, Brazil

Received 22 May 1991, revised manuscript received 5 August 1991

Using an inversion procedure for the SO(3, 1) algebraic potential the best shape for reproducing the S-matrix elements of a Woods–Saxon potential is determined. The algebraic optical potential thus found is applied to the elastic scattering of $^{12}C+^{26}Mg$ at $E_{LAB}=24.8$, 27.7, 31.2, 34.8, 37.8 and 40.0 MeV.

Alhassid and Iachello [1] proposed the use of the Woods–Saxon shape for the algebraic potential V_l in the analysis of heavy ion scattering data within the SO(3, 1) AST. They assumed

$$V_l = \frac{V_0 + iW_0}{1+\exp\{(l-l_0)/\Delta\}} \tag{1}$$

and

$$S_l = \frac{\Gamma(l+1+i\eta+iV_l)}{\Gamma(l+1-i\eta-iV_l)}, \tag{2}$$

where η is the Sommerfeld parameter given by

$$\eta = \frac{Z_1 Z_2 e^2 \mu}{\hbar^2 k}, \tag{3}$$

and V_0, W_0, l_0 and Δ are parameters to be adjusted in the analysis. In the present paper we consider an alternative shape for V_l which seems to us more adequate for the analysis of low energy heavy ion elastic scattering.

Two inversion problems, both starting with given S_l matrix elements, may be considered: one concerning $V(r)$, the potential in r-space and the other concerning V_l, the algebraic potential. The first problem has been discussed, in the semi-classical limit, in order to obtain $V(r)$ from given V_l by Amado and Sparrow [2] in SO(3, 2) and Hussein et al. [3] in SO(3, 1) symmetry. In this paper we present a numerical procedure to solve directly the second problem, i.e., the problem of finding V_l from given S_l matrix elements, in the SO(3, 1) symmetry.

We use this procedure to obtain the V_l that corresponds to a Woods–Saxon shape in r-space. With practical applications in mind we found a two-parameter family of shapes that best fits the exact V_l obtained.

Let us consider a given S_l and look for a V_l that satisfies eq. (2). Writing

$$V_l = V_l^{(0)} + \omega_l \tag{4}$$

where $V_l^{(0)}$ is ansatz and ω_l the correction to be found, we have from eq. (2), by expanding to first order in ω_l

$$\omega_l = \frac{-i\log(S_l/S_l^{(0)})}{\psi(l+1+i\eta+iV_l^{(0)})+\psi(l+1-i\eta-iV_l^{(0)})}, \tag{5}$$

where ψ is the digamma function and $S_l^{(0)}$ is the matrix element calculated using $V_l^{(0)}$. Starting from

$$V_l^{(0)} = \frac{-i\log S_l}{\psi(l+1+i\eta)+\psi(l+1-i\eta)}, \tag{6}$$

where

$\bar{S}_l = S_l \exp(-2i\sigma_l)$,

σ_l being the Coulomb phase shifts, the iteration of eqs. (4) and (5) quickly gives the desired value of V_l that satisfies eq. (2).

A few comments on the above procedure are necessary: (i) we observed that for $|S_l| \ll 1$ the procedure always converged very quickly; (ii) the procedure can easily be extended to the many-channel problem (matrix S_l) by first going to the representation in which S_l is diagonal, applying the inversion procedure to the diagonal representation of S_l and finally going back to the original representation by applying to V_l the inverse of the transformation that

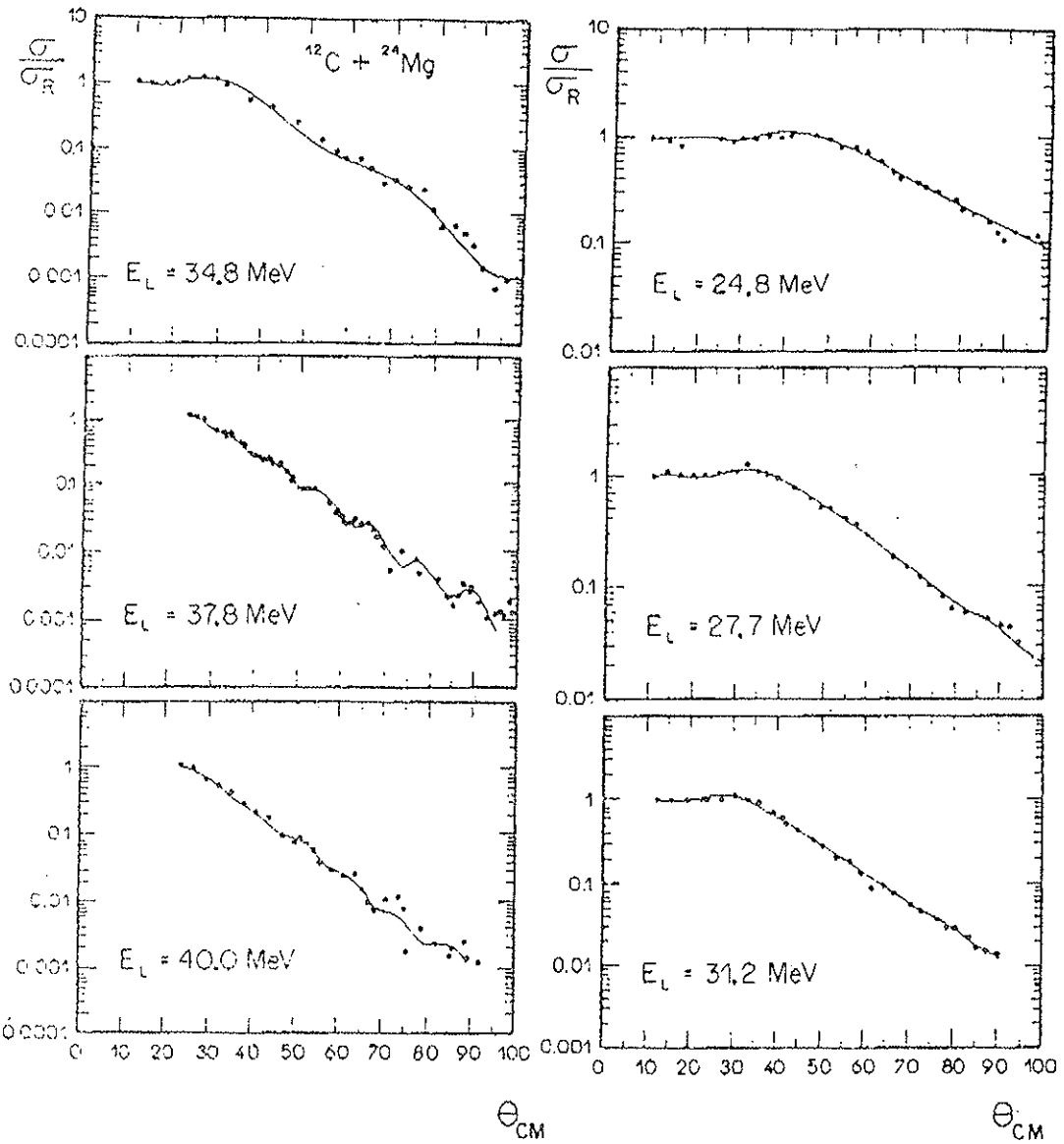

Fig. 1. (a) Circles represent the values of V_l/I_c obtained by inversion from the optical model W–S. S-matrix for three different values of diffuseness. The solid lines are the algebraic potentials calculated using (12) for the parameters indicated in the figure. The dashed curve is the form of eq. (1). (b) Similar results as (a) but varying the radius parameter.

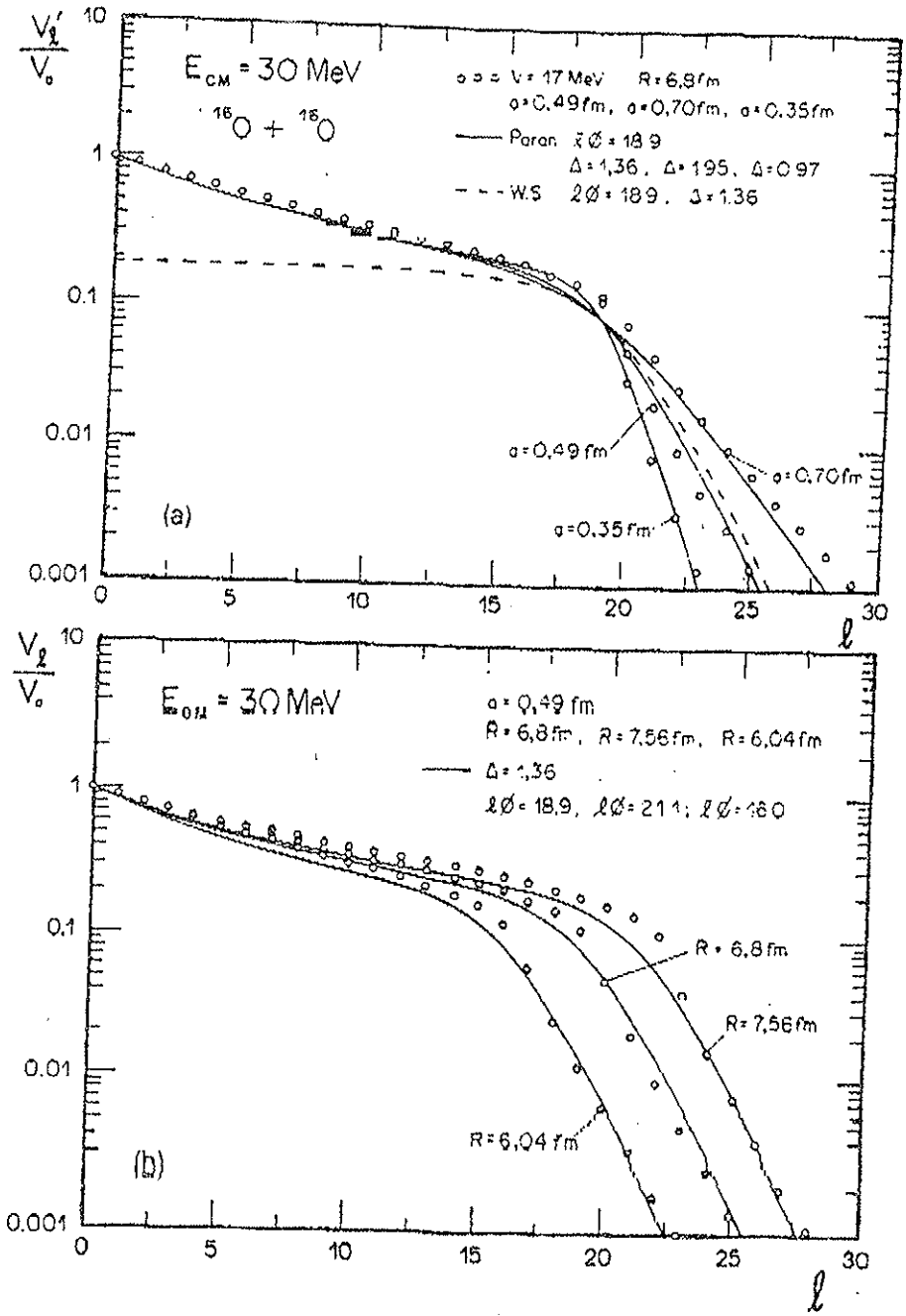

Fig. 2. Result of the analysis of the $^{12}C + ^{24}Mg$ elastic angular distributions using expression (12) for the energies E_{LAB} = 24.8, 27.7, 31.2, 34.6, 37.8 and 40 MeV. The dots are experimental data of ref. [4] and the solid curves are our best fits.

diagonalized S_ℓ; (iii) the presence of the log term in eq. (6) makes the relation between S_ℓ and V_ℓ multivalued, that is, for a given S_ℓ we obtain many discrete values of V_ℓ that solve eq. (2), depending on which of the branches of $\log \hat{S}_\ell$ in eq. (6) one starts the procedure. We would like to emphasize the privilege afforded the algebraic potential in the SO(3, 1) symmetry to possess such a simple solution for the

inversion of the scattering problem.

In our case, the multivaluedness encountered requires further restrictions on our solution. We impose that

(i) $V_l \to 0$ for $l \to \infty$

(ii) $|\mathrm{Im}(\log S_{l+1}) - \mathrm{Im}(\log S_l)| < 2\pi$. (7)

With these restrictions V_l is uniquely determined. We calculated S_l for the W–S potential in r-space:

$$V(r) = \frac{V_0}{1+\exp[(r-R)/a]}, \tag{8}$$

with the following values for the parameters:

$V_0 = 17$ MeV, $a = 0.49$ fm, $R = 6.8$ fm,

$Z_1 = Z_2 = 8$.

Our choice corresponds to the real part of an optical potential for $^{16}O + ^{16}O$ at $E_{CM} = 30$ MeV [4]. From the S_l obtained, we calculated V_l as explained above. We observed that as far as the dependence on η is concerned, the following ansatz:

$$\frac{V_l}{V_0} = f_l(Rk_c, ak_c), \tag{9}$$

is valid if η does not vary by more than 50% from the initial value used. The parameter k_c is given by

$$k_c = \sqrt{\frac{2\mu}{\hbar^2}(E - E_B)}, \tag{10}$$

where E_B is the Coulomb barrier, μ the reduced mass of the system and E the energy in the center of mass system. We notice that $\hbar k_c$ is the semiclassical value of the relative momentum of the system at the Coulomb barrier. Eq. (9) says that actually the shape of V_l depends only on the two dimensionless parameters

$$l_0 = k_c R \quad \text{and} \quad \Delta = k_c a. \tag{11}$$

In fig. 1 the circles exhibit a semi-log plot of $f_l(l_0, \Delta)$ as a function of l for different values of R and a. The solid curves exhibit the analytical expression

$$f_l = (1 + 2l/l_0)^{-\Delta} \times \{1 + \exp[(l - l_0)/\Delta]\}^{-1} \tag{12}$$

with the corresponding values of l_0 and Δ given by eq. (11). The dashed curve in fig. 1a is the W–S shape of ref. [1]. We noticed that the major disagreement between eqs. (12) and (1) is for values of l below the grazing l_c value. Fig. 2 is the result of our analysis using the expression given by eq. (12) on the $^{12}C + ^{26}Mg$ elastic scattering data for six different values of the energy as indicated.

Table 1 gives the values of the parameters found for the different values of E_{LAB}. Column 5 and 6 show the values of R and a respectively, obtained using eq. (11) with k_c calculated from eq. (10) for $E_B = 14$ MeV. We observe that R and a obtained in this way stay approximately constant as expected near the values obtained by the usual W–S optical model analysis [5]. We have used only the forward angles in the analysis because as explained by Lépine-Szily et al. [6], the backward angle behaviour of the angular distributions is dominated by the coupling with α-transfer channels.

We would like to mention that a similar search for V_l has been carried on by Amos et al. [7] using both the SO(3, 2) and SO(3, 1) symmetries. Our conclusions disagree with these authors in the following point as far as the SO(3, 1) symmetry is concerned. For a given set of S_l elements, one finds infinitely many solutions for V_l where the sign of Re V_l is not uniquely fixed, although we observed that the condition

$$|\mathrm{Re}\, V_l| \leqslant c(l)$$

given in ref. [1] is always fulfilled. However, in all the solutions we have investigated Im $V_l \geqslant 0$, for $|S_l|$

Table 1
The result of the analysis of the data shown in fig. 2. The first column shows the beam energy in the lab frame of reference, column 2 shows the values of k_c given by eq. (10); columns 3 and 4 show the best values of l_0 and Δ. Columns 5 and 6 show the values of R and a obtained from eq. (11).

E_{LAB} (MeV)	k_c (fm^{-1})	l_0	Δ	R (fm)	a (fm)
24.8	0.985	6.87	0.66	6.97	0.67
27.7	1.31	8.73	0.97	6.67	0.74
31.2	1.61	11.53	1.01	7.16	0.63
34.8	1.87	11.99	1.41	6.41	0.75
37.6	2.09	13.93	1.56	6.64	0.66
40.0	2.20	14.14	1.56	6.46	0.71

$\leqslant 1$ which is in agreement with ref. [1] but in disagreement with the statement Im $V_l(k) < 0$ of Amos et al. [7].

References

[1] Y. Alhassid and F. Iachello, Nucl. Phys. A 501 (1989) 585.
[2] R.D. Amado and D.A. Sparrow, Phys. Rev. C 34 (1986) 1937.
[3] M.S. Hussein, M.P. Pato and F. Iachello, Phys. Rev. C 38 (1988) 1072.
[4] T. Tamura and H.H. Wolter, Phys. Rev. C 6 (1972) 1976.
[5] R. Lichtenthäler Filho, A. Lépine-Szily, A.C.C. Villari, W. Mittig, V.J.G. Porto and J.C. Acquadro, Phys. Rev. C 26 (1982) 2487.
[6] A. Lépine-Szily, M.M. Obuti, R. Lichtenthäler Filho, J.M. Oliveira Jr. and A.C.C. Villari, Phys. Lett. B 243 (1990) 23.
[7] K. Amos, L. Berge, H. Fiedeldey, I. Morrison and L.J. Allen, Phys. Rev. Lett. 64 (1990) 625.

PHYSICAL REVIEW C VOLUME 50, NUMBER 6 DECEMBER 1994

Second order effects in the algebraic potential for heavy-ion systems near the Coulomb barrier

R. Lichtenthäler, D. Pereira, L. C. Chamon, and L. C. Gomes
Instituto de Física da Universidade de São Paulo, Laboratório Pelletron, C. P. 20516, CEP 01452-990, São Paulo, S. P., Brazil

A. Ventura
Ente Nuove Tecnologie, Energia e Ambiente, Viale Ercolani 8, I-40138, Bologna, Italy

L. Zuffi
Dipartimento Di Fisica dell'Università di Milano, Italy, and Istituto Nazionale di Fisica Nucleare, Sezione di Milano, Via Celoria 16, I-20133 Milano, Italy

(Received 26 July 1994)

The energy dependence of the algebraic potential for heavy-ion elastic scattering near to the Coulomb barrier is investigated. The inclusion of an additional term in the complex algebraic potential to take into account the reflection due to the imaginary well is proposed. With this new term 12 elastic scattering angular distributions of the $^{16}O+^{63}Cu$ system ranging from $E = 39$ to 64 MeV in the laboratory system were analyzed. The real and imaginary strengths of the algebraic potential exhibit a dependence with energy similar to the dispersive behavior associated with the threshold anomaly.

PACS number(s): 25.70.Bc, 24.10.−i

I. INTRODUCTION

The algebraic scattering theory (AST) proposed by Alhassid and Iachello [1] is a useful method for analyzing heavy-ion scattering data. One of the most practical versions of AST is based on SO(3,1) symmetry. In this case the S matrix can be written as a ratio of two Euler gamma functions:

$$S_\ell = \frac{\Gamma(\ell + 1 + iv)}{\Gamma(\ell + 1 - iv)}, \tag{1}$$

where v, called the algebraic potential, is equal to the Sommerfeld parameter $\eta = \mu Z_1 Z_2 e^2/\hbar^2 k$ for the case of a pure Coulomb interaction. In this case the symmetry is exact. In order to take into account the strong interaction, the algebraic potential must be generalized to be dependent on the angular momentum ℓ:

$$v(\ell) = \eta + v_s(\ell). \tag{2}$$

Absorption can be taken into account by making the algebraic potential complex provided $\mathrm{Im}(v) \geq 0$ to guarantee unitary bound for the S matrix. A few models have been proposed for the ℓ dependence of the real and imaginary parts of the algebraic potential [1,2]. Also theoretical investigations based on semiclassical methods have given some insight into the shape of the algebraic potential for high values of ℓ [3,4]. In general, these models are based on a Woods-Saxon shape in ℓ space similar to the Woods-Saxon well commonly used in the usual optical model calculations. By means of an inversion procedure developed by two of us [2] we were able to investigate the behavior of $v(\ell)$ that exactly reproduces the S matrix obtained from realistic optical model calculations. This study shows that second order contributions of the imaginary part to the real potential are very important and should be included in the algebraic potential in order to give a more precise description of the scattering between heavy ions.

II. EXPERIMENTAL DETAILS

The elastic scattering cross sections for the $^{16}O+^{63}Cu$ system have been measured using the ^{16}O beam from the 8UD Pelletron Accelerator. The detecting system was a set of nine surface barrier detectors spaced 5° apart. The solid angle between each detector and the target was 10^{-4} sr with an angular aperture $\Delta\theta = 0.5°$. The typical thickness of the enriched (99.9%) Cu target was 30 $\mu g/cm^2$ evaporated onto a 5 $\mu g/cm^2$ carbon foil, for the low energy measurements 39 MeV $\leq E_{lab} \leq$ 46 MeV and self-supporting targets with thickness between 60 and 80 $\mu g/cm^2$ for the high energy measurements 47 MeV $\leq E_{lab} \leq$ 64 MeV. In both cases, a thin layer of gold was evaporated onto the targets for data normalization, and we have used a surface barrier detector as a monitor, to be sure of no target deteriorations during the measurements. The energy resolution was 200 keV, which allows a good separation between the elastic peak and the inelastic group corresponding to the excitation of the first five low lying states of the ^{63}Cu nucleus. Figure 1 exhibits as dots the experimental data for the measured 12 angular distributions in the ranges 39 MeV $\leq E_{lab} \leq$ 64 MeV and $40° \leq \theta_{c.m.} \leq 175°$.

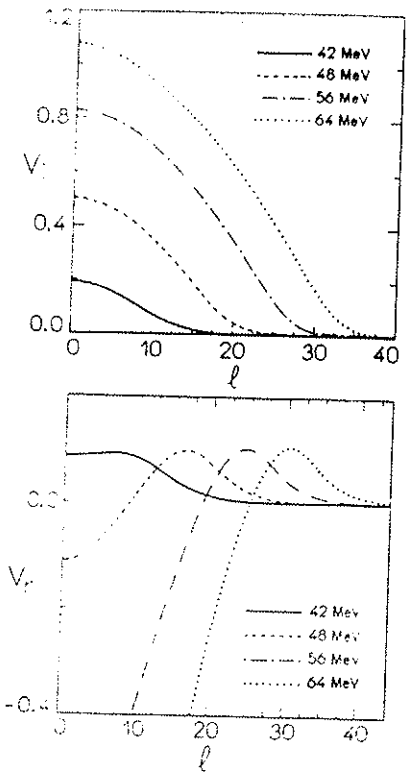

FIG. 1. In the upper part we exhibit the imaginary part of the algebraic potential obtained by inversion of optical model S matrix at the energies 42, 48, 56, and 64 MeV. In the bottom the same for the real part of the algebraic potential.

III. RELATION BETWEEN OPTICAL MODEL AND ALGEBRAIC POTENTIAL

One of the most interesting aspects of the SO(3,1) S matrix [Eq. (1)] is the simplicity of the inverse problem $S(\ell)$ to $v(\ell)$. It can be easily solved by expanding the S matrix in a Taylor series [2] around v^0 and taking the first term of the expansion, and we have

$$v(\ell) = v^0 + \frac{-i\ln(S/S^0)}{\psi(\ell+1+i\eta+iv^0)+\psi(\ell+1-i\eta-iv^0)},$$

where ψ is the digamma function. For high partial waves ($\ell \geq 2\ell_g$) we have $v^0 \approx 0$ and

$$S^0 = \frac{\Gamma(\ell+1+i\eta)}{\Gamma(\ell+1-i\eta)}.$$

For large values of the Sommerfeld parameter we can use the asymptotic form for the digamma function $\psi \to \ln$ and one obtains

$$v(\ell) = \frac{\delta_r + i\delta_i}{\ln[(\ell+1)^2+\eta^2]^{1/2}}. \qquad (3)$$

Equation (3) shows that the real and imaginary parts of the algebraic potential are related to the phase shift $\delta_r + i\delta_i$ in a straightforward way. In many situations involving heavy-ion scattering, Eq. (3) is sufficiently accurate but, for exact numerical results, Eq. (2) has to be solved iteratively. We applied Eq. (2) to determine the algebraic potential corresponding to a Woods-Saxon optical potential in the Schrödinger equation that reproduces the elastic scattering angular distributions of the $^{16}O+^{63}Cu$ system for laboratory energies from 39 to 64 MeV. The parameters of this optical potential were assumed to be constant in the whole energy range. In Fig. 1 we present the real and imaginary parts of the algebraic potential obtained by inversion at the energies 42, 46, 56, and 64 MeV. We observe that in spite of the fact that the optical potential is constant with energy, the same does not happen in the algebraic one. As the imaginary part increases, the real potential bends down to negative values in the region $\ell \leq \ell_g$. This is an indication that there is a repulsive term in the potential which causes the nuclear deflection function $2d\delta_r/d\ell$ to be positive in this region. The decreasing of the real algebraic potential with energy for low values of ℓ confirms the presence of a repulsive potential. For higher values of the angular momentum $\ell \geq \ell_g$ the algebraic potential becomes positive, again decreasing exponentially with ℓ as expected for an attractive nuclear potential [3]. This repulsive term has a simple optical interpretation. It corresponds to a reflection in the imaginary well that manifests with a real phase shift and therefore a real algebraic potential. In order to parametrize this term we suggest the following form:

$$v_s(\ell) = v_s^0(\ell) + \alpha(v_s^0(\ell))^2 \quad \text{for} \quad |v_s^0| < 1,$$

with

$$v_s^0(\ell) = v_r f_r(\ell) + iv_i f_i(\ell),$$

where v_r and v_i are the strengths and $f_r(\ell)$ and $f_i(\ell)$ the Woods-Saxon form factors of the real and imaginary algebraic potentials, respectively. With these considerations we have

$$v_s(\ell) = v_r f_r(\ell) - \alpha v_i^2 f_i(\ell)^2 + iv_i f_i[1+2\alpha v_r f_r(\ell)].$$

In our analysis we simplified somewhat the above equation. First we arbitrarily assumed $\alpha = 1$, to reduce the number of parameters involved. We neglected the positive term that modulates $v_i f_i(\ell)$ on the assumption that its effects are to a large extent taken under consideration in the choice of the parameters for $\mathrm{Im}(v_s)$. The second term we took explicitly into account as, being negative, it cannot be simulated by any reasonable variation of the parameters for $\mathrm{Re}(v_s)$. Therefore we set

$$v_s(\ell) = v_r f_r(\ell) - v_i^2 f_i^2(\ell) + iv_i f_i(\ell). \qquad (4)$$

Equation (4) has six parameters which are the two strengths, the two grazing angular momenta, and the two diffuseness for the real and imaginary parts. With these parameters one reproduces very well the shapes of Fig. 1. It is interesting to note that even if the real strength v_r is zero, we still have a contribution to the real part of the algebraic potential that comes from the second term in Eq. (4). We have also observed this fact in optical model

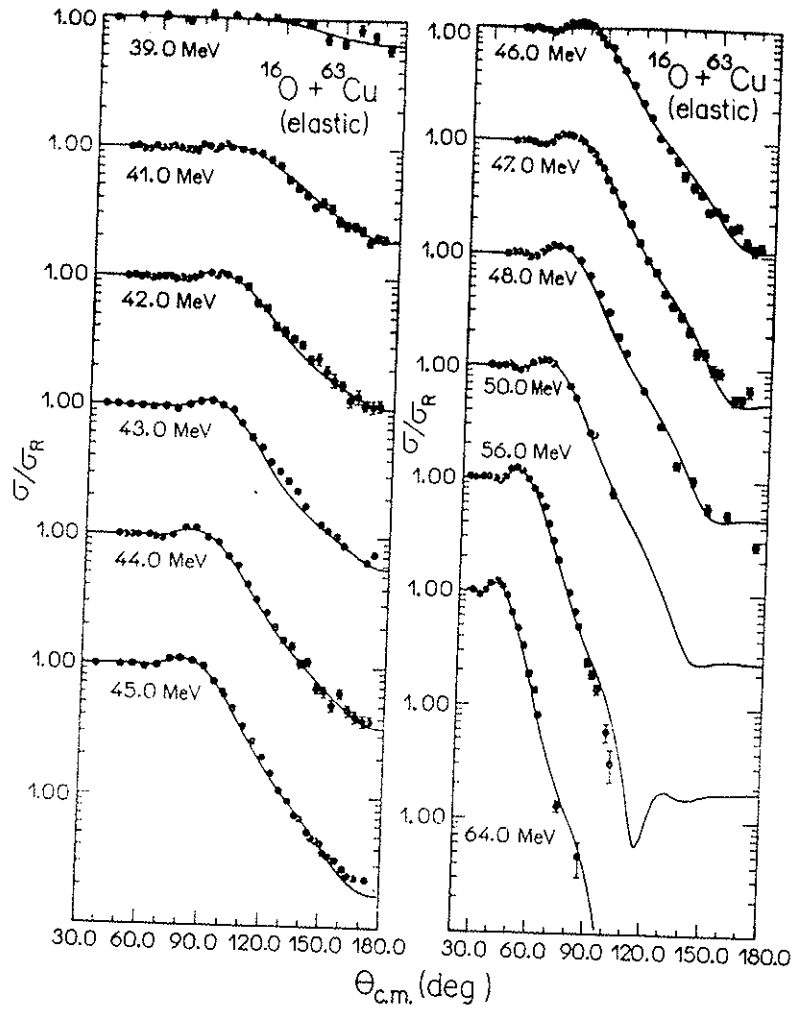

FIG. 2. The elastic angular distributions for the 12 energies measured. The solid curve is the result of our calculations.

calculations when even with a zero real potential there still remains a negative real phase shift which comes from the reflection in the imaginary well.

IV. ANALYSIS AND RESULTS

Using Eq. (4) we analyzed the 12 elastic angular distributions at energies ranging from $E_{\rm lab} = 39$ up to 64 MeV, the Coulomb barrier being at $E_{\rm lab} = 40$ MeV. The six parameters have been freely varied to reproduce the experimental data. In Fig. 2 we show our results. The reduced chi square of the fits is about unity or even lower at some energies. In Fig. 3 we plot the strengths of the real and imaginary potentials obtained as a function of the energy. The solid curve in Fig. 3 is only a guide to the eyes. An interesting phenomenon occurs at the energies around 43 MeV where the strength of the real potential presents a maximum. This behavior is necessary to reproduce the principal maximum of the diffraction of the data at forward angles. If we do not increase the real potential at these energies, the calculated angular distributions become flat in this region, in disagreement with the experimental data which still present maxima for 42,

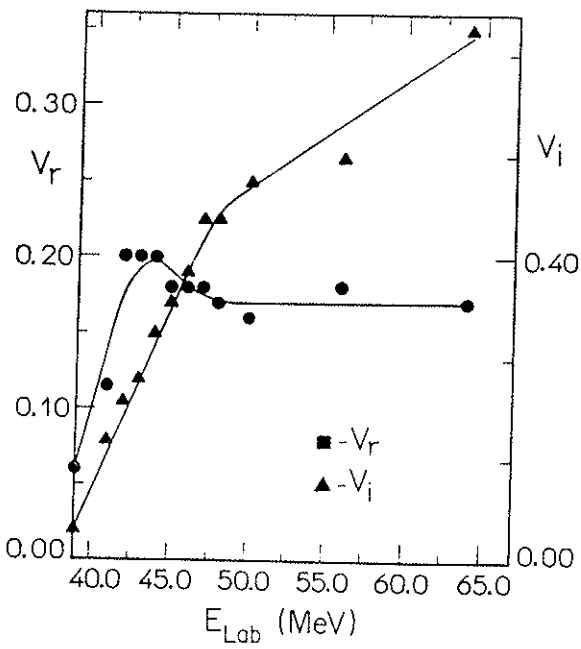

FIG. 3. The values of the strengths v_r and v_i of the real and imaginary parts of the algebraic potential as a function of the energy.

43, and 44 MeV. For lower energies the real potential goes to zero since we are below the Coulomb barrier. Above 46 MeV the real potential seems to become constant. The imaginary strength increases with energy although apparently in a less pronounced way for higher energies. This is expected due to the opening of reaction channels mainly coming from the inelastic excitations. As can be seen in Fig. 3, the real strength v_r of $v_s(\ell)$ exhibits in the neighborhood of the Coulomb barrier a variation with energy similar to the one associated with the threshold anomaly observed in the optical potential analysis using the Schrödinger equation [5]. We believe that this anomalous behavior is observed in the algebraic potential because second order effects were taken into consideration, leaving the real strength v_r in Eq. (4) directly related to the real strength of the optical potentials used in the Schrödinger equation. This point is at the moment subject to further investigation.

The form factor grazing angular momenta, used in the algebraic potential, follow approximately the relation $\ell_g = kR$ where $k = \sqrt{2\mu(E - E_b)}/\hbar$ and E_b is the Coulomb barrier. If we adjust R and E_b to reproduce the values of the imaginary grazing angular momentum, we obtain $E_b = 32.2$ MeV and $R = 7.6$ fm, which agree with the values obtained from fusion measurements and optical model calculations for this system [6].

V. CONCLUSIONS

We analyzed the elastic scattering angular distributions for the $^{16}O+^{63}Cu$ system at several energies from the neighborhood of the Coulomb barrier $E_{lab} = 39$ up to 64 MeV in the context of the algebraic scattering theory. An inversion procedure allowed us to investigate the relation between the optical model S matrix and the algebraic potential and revealed that second order effects like reflection in the imaginary well are very important to give a realistic description of the scattering between heavy ions. We propose a simple way to parametrize this effect which seems to work very successfully for this system. The fits obtained are of very good quality and allow us to observe the behavior of the algebraic potential at energies near the Coulomb barrier.

[1] Y. Alhassid and F. Iachello, Nucl. Phys. **A501**, 585 (1989).
[2] R. Lichtenthaler Filho, A. C. C. Villari, L. C. Gomes, and P. Carrilho Soares, Phys. Lett. B **269**, 49 (1991).
[3] M. S. Hussein, M. P. Pato, and F. Iachello, Phys. Rev. C **38**, 1072 (1988).
[4] K. Amos, L. Berge, L. J. Allen, and H. Fiedeldey, Phys. Rev. C **47**, 2827 (1993).
[5] G. R. Satchler, Phys. Rep. **199**, 147 (1991).
[6] L. C. Chamon, D. Pereira, E. S. Rossi, C. P. Silva, G. R. Razeto, A. M. Borges, L. C. Gomes, and O. Sala, Phys. Lett. B **275**, 29 (1992).

AN EXO 6

Analytic extension of the nuclear algebraic potential

R. Lichtenthäler
Departamento de Física Nuclear, Laboratório do Pelletron,
Universidade de São Paulo, Caixa Postal 20516, 01452-990 São Paulo, São Paulo, Brazil

L. C. Gomes
Grupo de Física Nuclear Teórica e Fenomenologia de Partículas Elementares
Instituto de Física Universidade de São Paulo, Caixa Postal 20516, 01498-970 São Paulo, São Paulo, Brazil
(Received 27 May 1994)

An analytic extension of the nuclear algebraic potential in the complex energy and angular momentum planes is discussed and an approximation for the algebraic potential in agreement with the known analytic properties of the S matrix is proposed. The invariance of the energy spectrum of the Coulomb part of the interaction is established. The results are applied to the Regge pole analysis of the $^{12}C + ^{24}Mg$ elastic collision at $E_{lab} = 23.0$ MeV.

PACS number(s): 24.10.−i, 11.55.Jy, 12.40.Nn

The algebraic scattering theory (AST) of Alhassid and Iachello [1] built upon the dynamical symmetry SO(3,1) has been applied, with success, in analyses of heavy ion scattering [2–6]. In this theory the S matrix has the form of a ratio of two gamma functions with arguments as in the case of pure Coulomb scattering but modified by adding nuclear algebraic potentials $v_\ell(E)$, which are complex and both energy and ℓ dependent. Of particular interest to us is the application of the AST to analyze the scattering data from collisions of heavy ions at energies near to the Coulomb barrier. Such studies have been made previously by Lepine-Szily *et al.* [2,3]. In a previous paper [6], using a numerical procedure that calculates exactly the algebraic potential for a given S matrix, we were able to propose a three-parameter shape for $v_\ell(E)$ that qualitatively reproduces the S matrix of a regular Woods-Saxon (WS) potential in the Schrödinger equation. Such a shape was able to fit both the diffractive behavior of the elastic channel as well as, by its derivative, the coupling among channels [7]. The interest in low energy heavy ion collisions stems from the importance in the scattering processes not only of diffractive phenomena but also of effects that reflect in resonances and Regge poles attributes in the scattering matrix. In the complex energy plane, resonances of the (now) S function are described by pairs of poles and zeros with the poles placed in the lower half plane [8]. In contrast, Regge poles [9,10], intimately connected to resonances, correspond to poles and zeros associated also in pairs, but with the poles located in the first quadrant of the complex angular momentum plane. In this paper we investigate the consequences of these analytic structures of the S matrix on the algebraic potential proposed in Ref. [1].

One important feature of the algebraic potential is to leave unmodified the original Coulomb energy spectrum, irrespective of the number of Regge poles or resonances added to it. This invariant property shows that the original poles of the symmetry do not disturb the poles introduced by the algebraic potential.

The WS shape commonly used for $v_\ell(E)$ is not in agreement with the known analytic properties of the S matrix. The WS shape has poles in the ℓ plane, and these simple poles in the algebraic potential produce essential singularities in the S matrix that are spurious to its analytic representation. In this paper we propose a new shape for the algebraic potential which is an integral function of ℓ in the right side of the complex plane. Such a shape eliminates the singularities of the S matrix introduced by the WS shape. It also has the correct asymptotic behavior for large values of ℓ to guarantee the

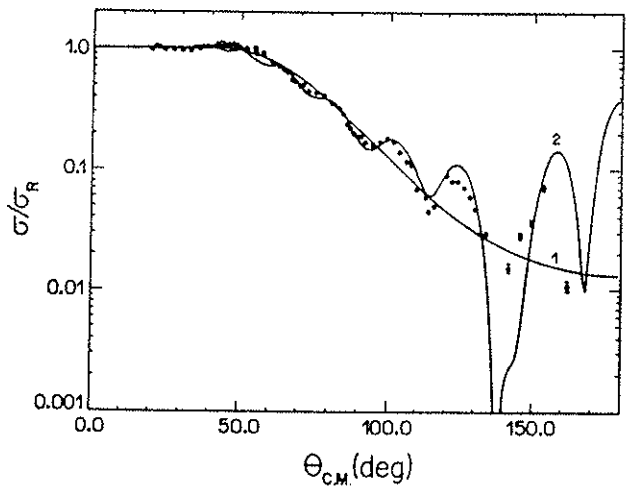

FIG. 1. The analysis of the elastic angular distribution of $^{12}C+^{24}Mg$ at $E_{lab} = 23.0$ MeV. Curve 1 is the result of the analysis with only the background potential whose shape is given by Eq. (8). The parameters used were $\lambda_0 = 7.0$, $\alpha = 0.5$, $V = 2.0$, and $W = 2.0$. Curve 2 represents the result of adding a pole to the background potential as given by Eq. (7). The fitting of the data was obtained with the pole at $\lambda_p = 9.75$, partial width $D = 0.10$, total width $\Gamma = 0.15$, and mixing phase $\phi = 0.3$ rad.

0556-2813/94/50(6)/3163(4)/$06.00

applicability of the Regge-Watson transform [9]. We use this shape as the background potential in the Regge pole analysis of the elastic angular distribution of the $^{12}C + ^{24}Mg$ system at $E_{lab} = 23.0$ MeV.

Let us consider the collision of two spinless ions in the AST framework. The algebraic potential $v_\ell(E)$ is related to the nuclear S matrix S_ℓ by the well-known equation [1]

$$\frac{\Gamma(\ell+1+i\eta+iv_\ell)}{\Gamma(\ell+1-i\eta-iv_\ell)}\cdot\frac{\Gamma(\ell+1-i\eta)}{\Gamma(\ell+1+i\eta)} = S_\ell. \tag{1}$$

This form for the S matrix was also obtained, from a totally different approach, by Müller and Schilcher [11] for the case of a superposition of Yukawa potentials in the Schrödinger equation. This remarkable result shows that although this form for S_ℓ does not exhibit the exact SO(3,1) symmetry, it does constitute a natural basis for the analysis of the strong interaction contribution in heavy ion collisions and so is the starting point of our analysis.

Extending the S matrix into the complex angular momentum plane by using the extension $\ell \to \lambda - 1/2$ where λ is the complex angular momentum variable, we define (twice the phase shift)

$$z = -i\ln[S(\lambda)], \tag{2}$$

and with Eq. (1) now specifying the S function, on differentiating with respect to z, we find

$$\frac{\partial v(\lambda,z)}{\partial z} = \frac{1}{\psi(\lambda+1/2+i\eta+iv(\lambda,z))+\psi(\lambda+1/2-i\eta-iv(\lambda,z))}, \tag{3}$$

where $\psi(z)$ is the digamma function defined in Ref. [12]. In the above equation λ and η are considered to be two fixed parameters and we are concerned mainly with the z dependence of v. For this reason we will omit from now on the argument λ in v. Actually, we define $v(z)$ as the solution of Eq. (3) with the initial condition $v(0) = 0$. We will now consider some global properties of the algebraic potential.

First we observe that $v \equiv 0$ for

$$\lambda + 1/2 \pm i\eta = -\nu, \tag{4}$$

where ν is a non-negative integer. This results from the fact that $\psi(\lambda + 1/2 \pm i\eta) = \infty$ and thus, for $z = 0$, we have both $v(0) = 0$ and $f(0) = 0$. Since Eq. (3) is of first order in z, the solution for $v(0) = 0$ and $dv(0)/dz = 0$ is $v \equiv 0$. The consequence of this fact is that the bound states of the Coulomb part of the interaction determined by Eq. (4) are invariant with respect to the nuclear interaction; i.e., v preserves the original singularities of the Coulomb S matrix.

Expanding $v(z)$ in the neighborhood of z_0, we obtain from Eq. (3)

$$v(z) = v^0 + \frac{z-z_0}{\psi(\lambda+1/2+i\eta+iv^0)+\psi(\lambda+1/2-i\eta-iv^0)}(1+\epsilon), \tag{5}$$

with $v^0 = v(z_0)$ and ϵ, the relative error of the linear term given by

$$\epsilon \approx \frac{(z-z_0)/(2i)}{[\psi(\lambda+1/2+i\eta+iv^0)+\psi(\lambda+1/2-i\eta-iv^0)]^3}[\psi'(\lambda+1/2+i\eta+iv^0)-\psi'(\lambda+1/2-i\eta-iv^0)].$$

The presence of trigamma function $\psi'(z) = d\psi(z)/dz$ in the numerator of the above equation makes ϵ small for applications to heavy ion collisions near the Coulomb barrier. We mention that Eq. (5) was the starting point for obtaining the iterative numerical procedure of Ref. [6].

Let us introduce

$$z^{(n+1)} = 2\pi + z^{(n)},$$

where n is an index to indicate on which sheet of $\ln(S)$ z is being considered. Defining $v^{(n)} \equiv v(z^{(n)})$ and $w^n \equiv v^{(n+1)} - v^{(n)}$ we have

$$w^{(n)} = \frac{2\pi}{\psi(\lambda+1/2+i\eta+iv^{(n)}(z))+\psi(\lambda+1/2-i\eta-iv^{(n)}(z))},$$

within the approximation involved in deriving Eq. (5).

From these considerations we see that the logarithmic nature of z leads to an enumerate family $\{v^{(n)}\}$ of ambiguous algebraic potentials, all corresponding to the same S. In particular, whenever v varies with energy (angular momentum) from the neighborhood of one member of the family to another with larger (smaller) index we may assume the occurrence of resonance (Regge pole) in the S matrix.

Now, the branch points of z occur whenever $S = 0$

or $S = \infty$, with the poles corresponding to resonances in the complex E plane and to Regge poles in the complex λ plane. Thus, the singularities of v are similar to the logarithmic ones, with the branch points associated with resonances or Regge poles according to whether we consider the energy or the angular momentum complex planes, respectively.

The above results are easily applied to Regge pole analysis of elastic differential cross sections. We suppose that the S matrix representation in the complex λ plane takes the form [13,14]

$$S(\lambda) = S^0(\lambda)\left(1 + \frac{iD\,\exp(2i\phi)}{\lambda - \lambda_p - i\Gamma/2}\right), \tag{6}$$

where $S^0(\lambda)$ is the background S matrix and the factor in brackets represents a pole and its associated zero. The phase ϕ is the so-called mixing phase.

From Eq. (5) we obtain

$$v(\lambda) = v^0(\lambda) + \frac{-i\,\ln(1 + \frac{iD\,\exp(2i\phi)}{\lambda - \lambda_p - i\Gamma/2})}{\chi}, \tag{7}$$

where

$$\chi = \psi(\lambda + 1/2 + i\eta + iv^0(\lambda)) + \psi(\lambda + 1/2 - i\eta - iv^0(\lambda))$$

is obtained from Eq. (5). Equation (7) can be extended naturally to include any number of Regge poles. The background potential $v^0(\lambda)$ deserves some consideration. The traditional WS shape [1] contains poles for $\lambda = \lambda_0 + i(2n+1)\pi\Delta$ where n is an integer. These poles, in the argument of the gamma functions in Eq. (1), produce essential singularities in the finite complex λ plane which, besides being spurious to the analytic representation of $S(\lambda)$, make problematic the determination of the true poles of the S matrix. We propose the following shape based on three factors:

$$v^0(\lambda) = (V + iW)f(\lambda),$$

with

$$f(\lambda) = \frac{\Gamma(\frac{\lambda_0}{\Delta} + 1, \frac{\lambda}{\Delta})}{\Gamma(\frac{\lambda_0}{\Delta} + 1)}\left(1 + \frac{\Delta}{\lambda_0^2}\lambda\right)^{\frac{-\lambda_0}{\Delta}}[\psi(\lambda + 1/2 + i\eta) + \psi(\lambda + 1/2 - i\eta)]^{-1}, \tag{8}$$

where $\gamma(n, z)$ is the incomplete gamma function [12]. The first factor in $f(\lambda)$ corresponds to the traditional WS shape but, being written in terms of the incomplete gamma function, it does not introduce spurious singularities in the S matrix. The second factor corrects the asymptotic behavior of the first and makes the form factor $f(\lambda)$ similar to the one proposed in Ref. [6]. The third factor guarantees the vanishing of $v^0(\lambda)$ for the condition given by Eq. (4). The parameters λ_0 and Δ have the physical meaning of grazing angular momentum and diffuseness, respectively.

Figure 1 exhibits an analysis of the elastic angular distribution for the ^{12}C+^{24}Mg system at $E_{\rm lab} = 23.0$ MeV [15]. Curve 1 is the result of the analysis using only the background potential. We observe that it describes well the overall pattern of the elastic cross section but has no oscillating behavior at backward angles. Curve 2 represents the result of adding a pole to the previous background potential as given by Eq. (7). The absence of oscillations in the backward angles from the background potential makes the determination of the pole parameters quite reliable. We would like to emphasize that the analysis proposed here differs in a substantial aspect from previous ones in that the number and the positions of the poles present in the AST S matrix are easily controlled. This is not the case in the Schrödinger approach with space-dependent potentials where the presence of poles in the S matrix is difficult to control [16]. Our approach can be applied to other data and the variation of the pole position with energy will furnish the necessary information for the determination of possible shape resonances of the system.

This work was partially supported by the CNPq.

[1] Y. Alhassid and F. Iachello, Nucl. Phys. **A501**, 585 (1989).
[2] A. Lépine-Szily, M. M. Obuti, R. Lichtenthäler Filho, J. M. Oliveira, Jr., and A. C. C. Villari, Phys. Lett. B **243**, 23 (1990).
[3] A. Lépine-Szily, J. M. Oliveira, Jr., P. Fachinni, R. Lichtenthäler Filho, M. M. Obuti, W. Sciani, M. K. Steinmayer, and A. C. C. Villari, Nucl. Phys. **A539**, 487 (1992).
[4] M. S. Hussein, M. P. Pato, and F. Iachello, Phys. Rev. C **38**, 1072 (1988).
[5] K. Amos, L. Berge, L. J. Allen, and H. Fiedeldey, Phys. Rev. C **47**, 2827 (1993).
[6] R. Lichtenthäler Filho, A. C. C. Villari, L. C. Gomes, and P. Carrilho Soares, Phys. Lett. B **269**, 49 (1991).
[7] R. Lichtenthäler Filho, A. Ventura, and L. Zuffi, Phys. Rev. C **46**, 707 (1992).
[8] H. M. Nussenzveig, *Causality and Dispersion Relations* (Academic Press, New York, 1972).
[9] T. Regge, Nuovo Cimento **14**, 951 (1959).
[10] R. Newton, *The Complex j-plane* (Benjamin, New York, 1964).

[11] H. J. Müller and K. Schilcher, J. Math. Phys. **9**, 255 (1968).
[12] *Handbook of Mathematical Tables*, edited by M. Abramowitz and I. A. Segun (Dover Publications, New York, 1964).
[13] K. W. McVoy, Phys. Rev. C **3**, 1104 (1971).
[14] C. K. Gelbke, T. Awes, U. E. P. Berg, J. Barrette, and M. J. LeVine, Phys. Rev. Lett. **41**, 1778 (1978).
[15] A. Lépine-Szily, W. Sciani, Y. K. Watari, W. Mittig, R. Lichtenthäler Filho, M. M. Obuti, J. M. Oliveira, and A. C. C. Villari, Phys. Lett. B **304**, 45 (1993).
[16] T. Takemasa and T. Tamura, Phys. Rev. C **18**, 1282 (1978).

ANEXO 7

Spin formalism in the algebraic scattering theory for heavy ions

R. Lichtenthäler Filho
Departamento de Fisica Nuclear, Instituto de Fisica da Universidade de São Paulo, Caixa Postal 20516, 01498 São Paulo, São Paulo, Brazil

A. Ventura
Ente Nuove Tecnologie, Energia e Ambiente, Viale Ercolani 8, I-40138 Bologna, Italy

L. Zuffi
Dipartimento di Fisica dell' Universitá di Milano, Milano, Italy
and Istituto Nazionale di Fisica Nucleare, Sezione di Milano, Via Celoria 16, I-20133 Milano, Italy

(Received 12 December 1991)

We develop a simple method of treating spin effects in the frame of algebraic scattering theory and apply it to the system $^{16}O+^{65}Cu$ at $E_{c.m.}=44.77$ MeV.

PACS number(s): 24.10.−i, 25.70.Bc

The algebraic scattering theory (AST) has been developed by Alhassid and Iachello [1] and has proved to be a very useful technique for the analysis of heavy-ion scattering data when a large number of channels are open [2,3]. The version of AST used in the present work is based on the assumption that the Hamiltonian for heavy-ion scattering exhibits an approximate SO(3,1) symmetry. In this case the S matrix can be written in closed form as a ratio of two Euler gamma functions:

$$S_l=\frac{\Gamma(l+1+iV)}{\Gamma(l+1-iV)} , \tag{1}$$

V is called the algebraic potential and is equal to the Sommerfeld parameter, $\eta(k)=\mu Z_1 Z_2 e^2/\hbar^2 k$, for pure Coulomb scattering when the SO(3,1) symmetry is exact. If there is strong interaction, the algebraic potential can be generalized to a function of wave number k and angular momentum l:

$$V(k,l)=\eta(k)+V^N(k,l) , \tag{2}$$

where $V^N(k,l)$ is the nuclear potential. The adoption of Eqs. (1) and (2) is justified by the dominance of Coulomb interaction in heavy-ion processes.

When reaction channels are explicitly taken into account in the interaction of two spinless particles, Eq. (1) assumes a matrix form:

$$\mathbf{S}=\frac{\Gamma(\mathbf{L}+1+i\mathbf{V})}{\Gamma(\mathbf{L}+1-i\mathbf{V})} , \tag{3}$$

where $\mathbf{V}$ is the algebraic potential matrix, which contains the dynamics of the scattering in the different channels, and $\mathbf{L}$ is a diagonal matrix, whose nonzero elements are all equal to the orbital angular momentum L. In the spinless case, $\mathbf{L}$ is thus a multiple of the identity matrix 1 and commutes with $\mathbf{V}$, so that the problem can be solved by means of a simple algorithm: (i) diagonalize $\mathbf{V}$; (ii) write the $\mathbf{S}$ matrix in the representation where both $\mathbf{S}$ and $\mathbf{V}$ are diagonal,

$$S_{\alpha\alpha}=\frac{\Gamma(L+1+iV_{\alpha\alpha})}{\Gamma(L+1-iV_{\alpha\alpha})} ,$$

where $V_{\alpha\alpha}$ is the αth eigenvalue of $\mathbf{V}$; (iii) go back to the original representation by means of the transformation $\mathbf{S}=\mathbf{Z}\mathbf{S}_{\rm diag}\mathbf{Z}^{-1}$, where $\mathbf{Z}$ is the matrix whose columns are the eigenvectors of $\mathbf{V}$.

The introduction of spin makes the algebraic approach more difficult to treat, because, in general, $\mathbf{L}$ is not multiple of the identity matrix and does not commute with the algebraic potential matrix. In this paper we propose a simple method of solving the coupled-channel problem in AST, based on the assumption that we can replace $\mathbf{L}$ in the argument of the gamma function in formula (3) by the total angular momentum $\mathbf{J}$. This approximation, equivalent to replacing $L(L+1)$ with $J(J+1)$ in the centrifugal potential of the coupled Schrödinger equations, was first proposed by Tanimura [4] and analyzed in detail by Esbensen, Landowne, and Price [5]. The S matrix can now be written as

$$\mathbf{S}=\frac{\Gamma(\mathbf{J}+1+i\mathbf{V})}{\Gamma(\mathbf{J}+1-i\mathbf{V})} , \tag{4}$$

where $\mathbf{J}$ and $\mathbf{V}$ commute, so that we can use the same algorithm as in the spinless case. We do not make approximations in the potential matrix, which remains the same as in the exact treatment.

From now on, for the sake of simplicity, we suppose that only the target nucleus has a spin different from zero and that the projectile cannot be excited during the collision: The matrix elements are thus labeled as $V^J_{\alpha',L';\alpha,L}$ and $S^J_{\alpha',L',\alpha,L}$ where L (L') are the possible values of the initial (final) orbital angular momentum and α (α') the other quantities characterizing the initial (final) state, such as masses, charges, and quantum numbers of the intrinsic states. It is important to note that, in the spinless case, $\mathbf{V}$ is an $n\times n$ matrix, where n is the number of states of the target taken explicitly into account; when we have a spin different from zero, the dimension of the algebraic potential matrix for a given J and parity is determined by summing the numbers of possible angular momentum substates for each state of the target nucleus explicitly taken into account.

The scattering amplitudes can now be written in the form [6]

$$f_{\alpha',M_{\alpha'},\alpha M_\alpha}(\theta)=\frac{\sqrt{4\pi}}{2ik_\alpha}\sum_L\sum_{L'}\sum_J \hat{L}(LS_\alpha 0M_\alpha|JM_\alpha)(L'S_{\alpha'}m'M_{\alpha'}|JM_\alpha)(\hat{S}^J_{\alpha'L',\alpha L}-\delta_{\alpha\alpha'}\delta_{LL'}\delta_{S_\alpha S_{\alpha'}})e^{i(\sigma_{\alpha L}+\sigma_{\alpha'L'})}Y^{m'}_{L'}(\theta)\ . \quad (5)$$

Here the z axis has been chosen along the direction of the incident beam; $\hat{L}=\sqrt{2L+1}$, $m'=M_\alpha-M_{\alpha'}$, S_α is the spin of the target in state α, and

$$\hat{S}^J_{\alpha'L',\alpha L}=\frac{S^J_{\alpha'L',\alpha L}}{e^{i(\sigma_{\alpha L}+\sigma_{\alpha'L'})}}\ . \quad (6)$$

The unpolarized cross section for the $\alpha\rightarrow\alpha'$ reaction is given by

$$\frac{d\sigma_{\alpha\alpha'}(\theta)}{d\Omega}=\frac{k_{\alpha'}}{k_\alpha}\frac{1}{2S_\alpha+1}\sum_{M_\alpha}\sum_{M_{\alpha'}}|f_{\alpha'M_{\alpha'},\alpha M_\alpha}(\theta)+f_C(\theta)\delta_{M_{\alpha'}M_\alpha}|^2\ , \quad (7)$$

where $f_C(\theta)$ is the usual Coulomb amplitude [6].

One comment is necessary at this point: When we have spin in the entrance channel ($L\neq J$), the elastic S-matrix element $S^J_{\alpha L,\alpha L}$ of formula (4) does not match exactly the Coulomb S-matrix element, $S^C_{\alpha L,\alpha L}=\exp(2i\sigma_{\alpha L})$ at high J, when $V^N=0$, and formula (6) gives spurious terms in the partial wave summation. These spurious terms can be avoided if we rewrite expression (6) as

$$\hat{S}^J_{\alpha L,\alpha L}=\frac{S^J_{\alpha L,\alpha L}}{S^C_{\alpha J,\alpha J}}\ ,$$

where

$$S^C_{\alpha J,\alpha J}=\frac{\Gamma(J+1+i\eta_\alpha)}{\Gamma(J+1-i\eta_\alpha)}\ . \quad (8)$$

We have tested formulas (5), (7), and (8) for elastic scattering of ^{16}O on ^{65}Cu by assigning to the target spin either a fictitious value 0 or the true value $\frac{3}{2}$: The computed ratios $\sigma/\sigma_R(\theta)$ are practically the same in the complete angular range 0°–180° with differences only on the fourth significant digit.

As a preliminary calculation, we have applied our formalism to the analysis of cross sections for the system $^{16}O+^{65}Cu$ at $E_{c.m.}=44.77$ MeV, measured by Chamon and Pereira [7]. The experimental data consist of the differential elastic cross section and the cumulative excitation of the five lowest-lying levels of ^{65}Cu.

The elements $V_{\alpha L,\alpha'L'}$ of the potential matrix $\mathbf{V}$ have been calculated according to the general expression [6]

$$V_{\alpha L,\alpha'L'}=\frac{1}{\sqrt{4\pi}}\sum_\lambda(-1)^{J-S_\alpha}i^{L'-L-\lambda}\hat{L}\hat{L}'\hat{S}_{\alpha'}(LL'00|\lambda 0)W(L,L',S_\alpha,S_{\alpha'}|\lambda,J)V^\lambda_{\alpha\alpha'}(\bar{L})(S_{\alpha'}||V||S_\alpha)\ . \quad (9)$$

Here $\hat{L}=\sqrt{2L+1}$, λ is the multipolarity of the transition, S_α is the spin of the target in state α, W is a Racah coefficient, and the reduced matrix element is defined as in Ref. [6]; the expressions adopted for the transition form factors $V^\lambda_{\alpha\alpha'}(\bar{L})$ are the following: nuclear elastic [8],

$$V^0_{\alpha\alpha}(\bar{L})=\left[1+2\frac{\bar{L}}{L_0}\right]^{-\pi/2}\frac{V_R+iV_I}{1+e^{(\bar{L}-L_0)/\Delta}}\ ; \quad (10)$$

nuclear inelastic,

$$V^\lambda_{\alpha\beta}(\bar{L})=-\eta_{\text{nucl}}\frac{dV^\lambda_{\alpha\alpha}(\bar{L})}{d\bar{L}}\ , \quad (11)$$

where $V^\lambda_{\alpha\alpha}$ has the same structure as formula (10), but, in principle, different depths U_R and U_I and different critical momentum and diffuseness; Coulomb excitation [1],

$$V^{C\lambda}_{\alpha\beta}(\bar{L})=\eta_{\text{Coul}}\times\begin{cases}(\bar{L}/L_C)^{\lambda+1}\ , & \bar{L}<L_C\ ,\\ (L_C/\bar{L})^\lambda\ , & \bar{L}>L_C\ .\end{cases} \quad (12)$$

Here V_R, V_I, U_R, U_I, η_{nucl} and η_{Coul} are to be adjusted

TABLE I. AST parameters for elastic and inelastic scattering of $^{16}O+^{65}Cu$.

Final state	V_R	V_I	L_0	Δ	L_C	U_R	U_I	η_{nucl}	η_{Coul}
$^{65}Cu(\frac{3}{2})^-_1$	2.0	3.4	26.0	1.3	10.0				
$^{65}Cu(\frac{1}{2})^-_1$	2.0	3.4	24.7	2.2	10.0	7.0	5.0	0.14	−0.038
$^{65}Cu(\frac{5}{2})^-_1$	2.0	3.4	24.7	2.2	10.0	7.0	5.0	0.15	−0.040
$^{65}Cu(\frac{7}{2})^-_1$	2.0	3.4	24.7	2.2	10.0	7.0	5.0	0.13	−0.036
$^{65}Cu(\frac{5}{2})^-_2$	2.0	3.4	24.7	2.2	10.0	7.0	5.0	0.021	−0.006
$^{65}Cu(\frac{3}{2})^-_2$	2.0	3.4	24.7	2.2	10.0	7.0	5.0	0.035	−0.010

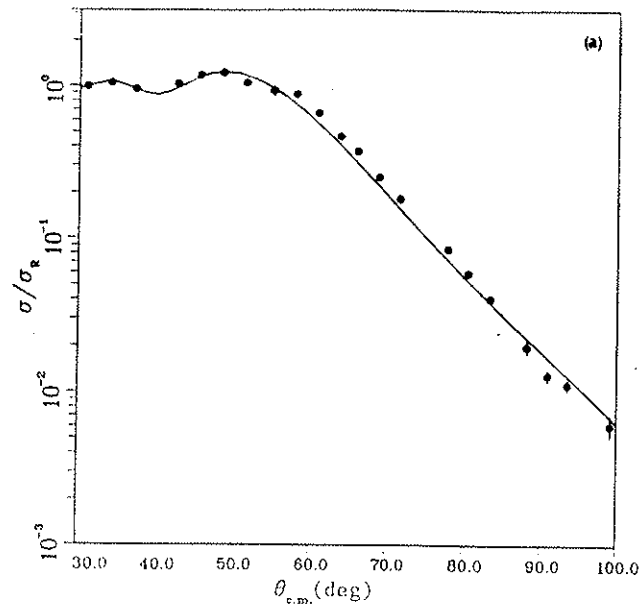

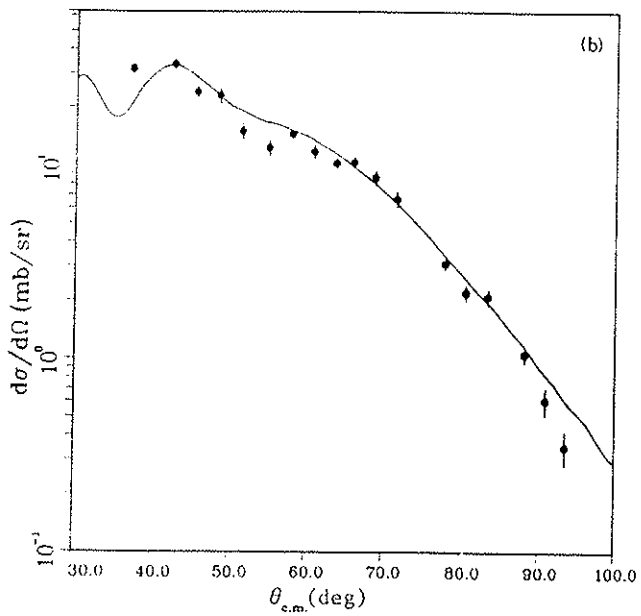

FIG. 1. (a) Elastic scattering cross section divided by Rutherford cross section for $^{16}O+^{65}Cu$ at $E_{c.m.}=44.77$ MeV. (b) Inelastic scattering to the five lowest-lying levels of ^{65}Cu. Here 300 partial waves have been included in the scattering amplitudes. The experimental data are taken from Ref. [7].

on the experimental data. The diagonal form factors are calculated at the proper value of the orbital angular momentum $\bar{L}=L$ and the off-diagonal factors at $\bar{L}=\frac{1}{2}(L+L')$, the arithmetic mean of the initial and final angular momenta. In the same way, the critical angular momentum and diffuseness in form factor (11) are the arithmetic mean of the corresponding values in formula (10) for the entrance and exit channels. Moreover, the algebraic potential does not contain spin-spin or spin-orbit interactions.

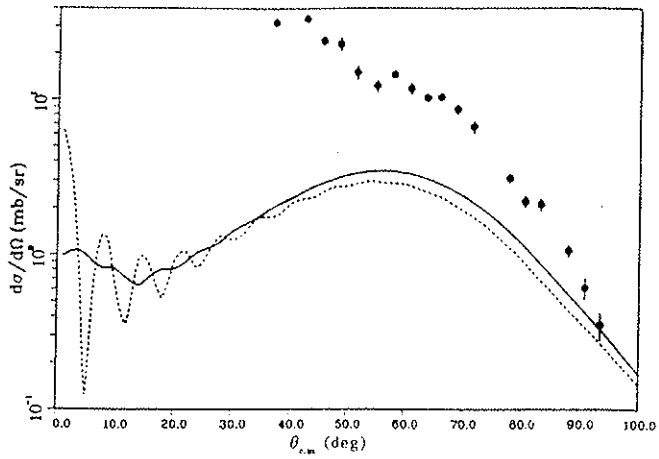

FIG. 2. Nuclear contribution to inelastic scattering to the five lowest-lying levels of ^{65}Cu. Solid curve, experimental spin value assigned to each level; dashed curve, spin 0 assigned to each level. The experimental data are the same as in Fig. 1(b).

In these preliminary calculations, we have coupled to the ground state of ^{65}Cu the five lowest excited states through $\lambda=2$ transitions. The parameters that define the diagonal matrix elements of the potential have been determined by a least-squares fit of the experimental angular distribution for elastic scattering [7]. The inelastic coupling strengths (η_{Coul} and η_{nucl}) have been derived from experimental $B(E2)$ values [9], with a normalization obtained by fitting the experimental cumulative excitation to the five lowest-lying states of ^{65}Cu [7].

The elastic and inelastic scattering cross sections for $^{16}O+^{65}Cu$ at $E_{c.m.}=44.77$ MeV, calculated with the parameters listed in Table I, are compared in Fig. 1 with the experimental data [7]. The spin effects are emphasized in Fig. 2, where we compare two calculations of pure nuclear excitation with the true spins and with spin zero in all channels. We observe that the effect of the spin is to wash out the oscillations in the angular distribution, as expected from general considerations. The differences in the magnitude of the cross sections are due to different values of the geometric part of formula (9) in the two cases.

The quality of these preliminary results encourages us to extend the AST analysis to other incident energies and reaction channels, by including also existing data of one-proton transfer [7], with the main goal of extracting coupled-channel effects on the fusion cross section. In the more extended analysis, the transition matrix elements for the various channels will be obtained by means of calculations based on the interacting boson and interacting boson-fermion models, so as to give a simultaneous algebraic description of excitation of intrinsic states and scattering.

We thank Dr. L. Chamon and Dr. D. Pereira for providing us with their experimental data.

[1] Y. Alhassid and F. Iachello, Nucl. Phys. **A501**, 585 (1989).
[2] A. Lépine-Szily, M. M. Obuti, R. Lichtenthäler Filho, J. M. Oliveira, Jr., and A. C. C. Villari, Phys. Lett. B **243**, 23 (1990).
[3] A. Lépine-Szily, J. M. Oliveira, Jr., P. Fachini, R. Lichtenthäler Filho, M. M. Obuti, W. Sciani, M. K. Steinmayer, and A. C. C. Villari, Nucl. Phys. **A539**, 687 (1992).
[4] O. Tanimura, Phys. Rev. C **35**, 1600 (1987).
[5] H. Esbensen, S. Landowne, and C. Price, Phys. Rev. C **36**, 1216 (1987); **36**, 2359 (1987).
[6] G. R. Satchler, *Direct Nuclear Reactions* (Clarendon, New York, 1983).
[7] L. Chamon, Ph.D. thesis, University of São Paulo, 1990.
[8] R. Lichtenthäler Filho, A. C. C. Villari, L. C. Gomes, and P. Carrilho Soares, Phys. Lett. B **269**, 49 (1991).
[9] D. E. J. Riedemann, Ph.D. thesis, University of Amsterdam, 1991, and references therein.

Anexo 8

The Algebraic Scattering Theory and its application to heavy-ions reactions

Rubens Lichtenthäler Filho*
Departamento de Física Nuclear, Universidade de São Paulo
C.P. 20516, CEP 01498 São Paulo SP, Brasil

Abstract

We present the most conspicuous aspects of the Algebraic Scattering Theory as well as recent developments and applications to heavy ion collisions near the Coulomb barrier.

1 The $SO(3,1)$ S-matrix

Algebraic Scattering Theory[1] has been proposed by Alhassid and Iachello as an alternative approach to the study of low energy heavy ion collisions. In the algebraic approach, the Schroedinger equation is replaced by recursion relations for the algebraic Jost functions $A_l(k)$ and $B_l(k)$ and one obtains the S-matrix for elastic scattering:

$$S_l(k) = exp(il\pi)B_l(k)/A_l(k) \tag{1}$$

For the SO(3,1) symmetry the recursion relations take the form:

$$-N(l,v)A_{l+1}(k) = (l+1-iv)A_l(k) \tag{2}$$

$$+N(l,v)B_{l+1}(k) = (l+1+iv)B_l(k) \tag{3}$$

where $N(l,v)$ is a normalization factor which drops out when we calculate the S-matrix. The function v, the algebraic potential, contains all the dynamic information about the scattering process. Solution of the recursion relations yields the SO(3,1) S-matrix as a ratio of two Euler Gamma functions

$$S_l = \frac{\Gamma(l+1+iv)}{\Gamma(l+1-iv)}. \tag{4}$$

*Supported by FAPESP

In the case of pure Coulomb scattering the algebraic potential is the Sommerfeld parameter:

$$v = \eta = \mu Z_1 Z_2 e^2/\hbar^2 k \tag{5}$$

and the $SO(3,1)$ symmetry is exact. In order to take into account the strong interaction, the algebraic potential must be generalized to be dependent on the angular momentum l:

$$v(l,k) = \eta(k) + v_s(l,k) \tag{6}$$

It is important to mention that the unitary bound for the S-matrix, $|S| \leq 1$, imposes that the imaginary part of the algebraic potential must be positive.

A few models have been proposed for the l dependence of the real and imaginary parts of the algebraic potential[1,2]. Also theoretical investigations based on semiclassical approaches give some insight about its shape for the large l region[3,4]. In the next section we will present an inversion procedure which will permits the investigation of the relation between the optical model and algebraic potential.

2 The Inverse Problem

One important feature of SO(3,1) S-matrix as defined in Eq. (4) is the simplicity of the inverse problem.

$$S_l(k) \longrightarrow v(l,k). \tag{7}$$

This problem is always solvable for any given set of S-matrix elements by expanding the SO(3,1) S-matrix in terms of $v(l,k)$ around a given v^0.

$$v(l,k) = v^0 + \frac{-ilog(S/S^0)}{\psi(l+1+i\eta+iv^0) + \psi(l+1-i\eta-iv^0)}, \tag{8}$$

where

$$S^0 = \frac{\Gamma(l+1+i\eta+iv^0)}{\Gamma(l+1-i\eta-iv^0)}, \tag{9}$$

and ψ is the Digamma function. For high partial waves ($l \geq 2l_{grazing}$) we have $v^0 \approx 0$ and a very simple formula for $v(l,k)$ can be obtained from Eq. (8) if we use the asymptotic form for the Digamma function $\Psi \rightarrow ln$:

$$v(l,k) = \frac{\delta_r(l,k) + i\delta_i(l,k)}{ln[(l+1)^2 + \eta^2(k)]^{1/2}}. \tag{10}$$

Eq. (10) shows that the real and imaginary parts of the algebraic potential are related to the phase shifts δ_r and δ_i respectively in a straightforward way. In many situations involving heavy ions Eq. (10) is sufficiently accurate, and in any case, high numerical precision is obtained iterating Eq. (8) to the desired accuracy.

We applied the inversion method to determine the algebraic potential corresponding to a realistic Woods- Saxon optical potential for the system $^{16}O +^{63} Cu$ in the

range of laboratory energies from 39MeV to 64MeV. The parameters of the optical potential were assumed constant over the whole energy range. In figure 1 we present the real and imaginary parts of the algebraic potential obtained by inversion at the energies 42MeV, 46MeV, 56MeV, and 64MeV. We can observe that in spite of the

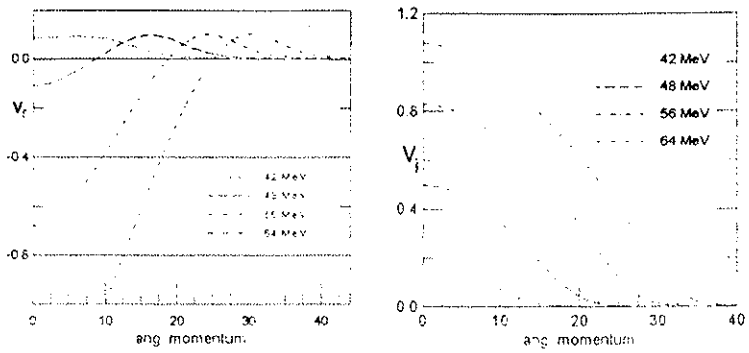

Figure 1: The real and imaginary parts of the algebraic potential.

fact that the optical potential is constant for all energies, this is not the case for the algebraic one. As the imaginary part increases, the real one bends down to negative values in the region $l \leq l_{grazing}$. This is an indication that there is a repulsive term in the potential which causes the deflection function $2d\delta_r/dl$ to be positive in this region. The decreasing of the real algebraic potential with energy also confirms the presence of a repulsive potential. For higher values of the angular momentum $l \geq l_g$, the algebraic potential becomes positive again with an exponential decrease with l as expected for an attractive nuclear potential[3]. This repulsion for small values of l has the simple optical interpretation as a reflection in the imaginary well which contributes with a real negative phase shift and therefore a real negative algebraic potential.

In order to describe this effect we suggest the following form for the algebraic potential:

$$v_s(l) = v_r f_r(l) - v_i^2 f_i^2(l) + i v_i f_i(l) \tag{11}$$

where v_r and v_i are the real and imaginary strengths and f_r and f_i the corresponding form factors taken as a Woods-Saxon[1] or modified Woods-Saxon[2] shapes. The first and third terms in the right hand side of Eq. (11) are the usual form factors that describe the refractive and absorptive scattering. The second term is supposed to take into account the contribution due to the reflection in the imaginary well. A justification to the use of the square of the imaginary form factor in the second term can be found in a paper by S.K.Kauffmann[5,6] where the author investigates the relation between the optical model parameters and the phase shifts for very heavy ion systems. In principle we could also include an additional term in Eq. (11) due to the second order scattering in the real and imaginary potentials which would give a positive imaginary contribution to the algebraic potential. However for the sake of

simplicity we prefer to keep Eq. (11) and argue that positive contributions to the imaginary potential can be taken into consideration by an adequate choice of the parameters. This is not the case for the second order term due to reflection in the imaginary well since it produces a negative contribution to the algebraic potential which cannot be simulated by reasonable variation of the parameters.

3 Analysis of the Elastic Scattering

Using Eq. (11) we analyzed the elastic angular distributions for the $^{16}O + ^{63}Cu$ at energies ranging from $E_{lab} = 39MeV$ up to $E_{lab} = 64MeV$ measured by Chamon and Pereira[7] For $f(l)$ we used the Wood-Saxon shape. The six parameters to be known are the strengths the grazing angular momentum and the diffuseness for the real and imaginary potentials. They have been freely varied to adjust the experimental data. In Fig. 2 we show our results. The reduced Chi-square of the fits are about unity or even lower at some energies.

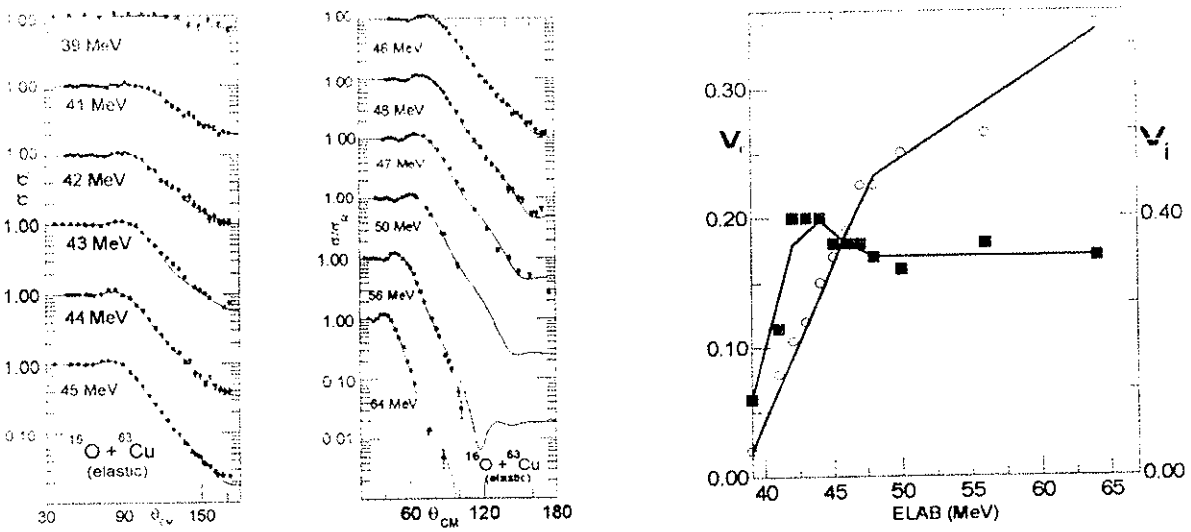

Figure 2: On the left the fits of the elastic scattering angular distributions of the $^{16}O + ^{63}Cu$ system. On the right the strengths of the real and imaginary algebraic potential.

The values of the grazing angular momentum obtained from the fits follow approximately the relation $l_g = kR$ where $k = \sqrt{2\mu(E - E_b)}/\hbar$ and E_b is the Coulomb barrier. By adjusting R and E_b to reproduce the imaginary grazing angular momentum one obtains $E_b = 40.4Mev$ and $R = 7.6fm$ which agrees very well with those obtained from optical model calculations and fusion measurements for this system[7].

In Fig. 2 we plot the strengths of the real and imaginary potential as a function of the energy. The solid curves are a guide to the eyes. An interesting phenomena occurs at the energies around 43 MeV where the strength of the real potential

presents a maximum. This behavior is necessary to reproduce the principal maximum of the diffraction pattern at forward angles. If we do not increase the real potential at these energies, the calculated angular distributions become flat in this region unlike the experimental data which present still a maximum for 42, 43 and 44 MeV. For lower energies the real potential goes to zero since we are below the Coulomb barrier. Above 46 MeV the real potential seems to become constant. The imaginary strength increases with energy although apparently in a less pronounced way for higher energies. This is expected to be due to the opening of reaction channels, mainly inelastic. As can be seen in Fig. 2, the real and imaginary strengths of $v_s(l)$ exhibit in the neighborhood of the Coulomb barrier a variation with energy similar to the one associated with the threshold anomaly[7].

4 Coupled Channels Formalism

When many reaction channels are explicitly taken into account the S-matrix assumes the form:

$$\mathbf{S} = \frac{\Gamma(\mathbf{L} + \mathbf{1} + \mathbf{iV})}{\Gamma(\mathbf{L} + \mathbf{1} - \mathbf{iV})} \tag{12}$$

where V is the algebraic potential matrix which contains the dynamics of the scattering in different channels. In the spinless case **L** is a multiple of the unity matrix and commutes with **V** what allows to solve the problem by means of a simple algorithm: (i) diagonalize **V** (ii)write the S-matrix in the representation where both S and V are diagonal

$$S_\alpha = \frac{\Gamma(l + 1 + iv_\alpha)}{\Gamma(l + 1 - iv_\alpha)} \tag{13}$$

where v_α are the α-eigenvalues of V. (iii) go back to the original representation by means of the transformation $\mathbf{S} = \mathbf{Z}\mathbf{S}_\alpha\mathbf{Z}^{-1}$ where **Z** is the matrix of the eigenvectors of **V**.

The introduction of spin makes the algebraic approach more difficult to treat because **L** is no longer a multiple of the unitary matrix and does not commute with **V**. A possible approximation[8] is to replace **L** by **J** in the argument of the gamma function:

$$\mathbf{S} = \frac{\mathbf{\Gamma(J + 1 + iV)}}{\mathbf{\Gamma(J + 1 + iV)}}. \tag{14}$$

As **J** and **V** commute, we can use the same algorithm as used above. We do not make approximations in the potential matrix **V** which remains the same as in the exact treatment. In fact for the spinless case the algebraic potential **V** is an $n \times n$ matrix where n is the number of channels considered in the calculation. However when we take into account the spin of the target S_i in the different channels, the dimension of the **V** matrix is enlarged to $N = \sum_{i=1}^{n}(2S_i + 1)$ for each J^π. The coupling matrix elements are determined by[9]:

$$V_{\alpha L,\alpha' L'} = (4\pi)^{-1/2}\sum_{\lambda}(-1)^{J-S_\alpha} i^{L'-L-\lambda}\hat{L}\hat{L}'\hat{S}_{\alpha'}(LL'00 \mid \lambda 0) \quad (15)$$
$$\times W(L,L',S_\alpha,S_{\alpha'} \mid \lambda,J)V^{\lambda}_{\alpha\alpha'}(l)(S_{\alpha'} \parallel V \parallel S_\alpha),$$

where α and α' are the channel masses and charges, L and L' are the possible values of the initial and final orbital angular momentum respectively. The inelastic coupling form factors $V^{\lambda}_{\alpha,\alpha'}(l)$ are composed of the nuclear (which is usually taken as the derivative of the elastic form factor) and the Coulomb excitation terms. for the latter we used the expression derived by Broglia and Winther[10]:

$$V_{coul}(l) = V_0 \frac{exp(-\xi(E,\Delta E,\eta,l))}{(1+\sqrt{1+(l/\eta)^2})^{\lambda}} \quad (16)$$

where ξ is given by:

$$\xi = C_\lambda \eta \Delta E/(4E)(1+\sqrt{1+(l/\eta)^2}); \quad (17)$$

the parameters C_λ and V_0 are adjustable. The reduced matrix elements $(S_{\alpha'} \parallel V \parallel S_\alpha)$ contain the nuclear structure information. They can be treated as free parameters or being determined from nuclear models such as *Rotational Model, Vibrational model, Interacting Boson Model(IBM),* or *Interacting Boson Fermion Model(IBMF).*

5 Nuclear Structure Calculations and Results

Inelastic scattering of ^{16}O by ^{63}Cu with the excitation of the low energy levels of the target ^{63}Cu can be described with good accuracy within the framework of the Interacting Boson-Fermion Model(IBMF)[11]. In the preliminary calculations of the present work, we have made the simplifying assumption that the low-lying states of the $^{64}_{30}Zn_{34}$ are generated by the excitation of two valence protons above the $Z = 28$ shell closure and six valence neutrons above the $N = 28$ closure without mixing with other configurations that are important at higher energies. This yields $N_p = 1$ proton boson and $N_n = 3$ neutron bosons interacting in the $U^{(b)}(5)$ Hamiltonian.

$$H_b = \epsilon \hat{n}_d + 10a_1 B^{(1)}.B^{(1)} + a_3 B^{(3)}.B^{(3)} \quad (18)$$

where $\hat{n_d} = \sqrt{(5)}(d^+ \times \tilde{d})^{(0)}$, $B^{(\lambda)}_\mu = (d^+ \times \tilde{d})^{(\lambda)}_\mu$, $(\mu = -\lambda, ..., +\lambda)$ are spherical tensors made of the usual d-boson creators and annihilators. Formula (18) with $\epsilon = 1.3MeV$, $a_1 = 0.01MeV$ and $a_3 = -0.205$ MeV reproduces the low-lying levels of ^{64}Zn with $n_d \leq 3$ which form the spectrum of an anharmonic vibrator. The spectrum of the ^{63}Cu is obtained from the ^{64}Zn by replacing the proton boson with an unpaired

proton whose valence space is limited to the first accessible orbital above the $Z = 28$ i.e. $2_{p_{3/2}}$, thus giving an $SU^{(f)}(4)$ symmetry to the fermion Hamiltonian

$$H_f = E_{3/2} a^+_{3/2} . \tilde{a}_{3/2}, \tag{19}$$

where E_j is the quasiparticle energy and a^+_{jm} creates a proton in the m substate of the j orbital. The modified annihilator is $\tilde{a}_{jm} = (-1)^{j-m} a_{j,-m}$.

the boson-fermion interaction is chosen of the form

$$H_{BF} = b_1 (B^{(1)} \times A^{(1)})^{(0)} + b_3 (B^{(3)} \times A^{(3)})^{(0)}, \tag{20}$$

where $A^{(\lambda)}_{\mu} = (a^+_{3/2} \times \tilde{a}_{3/2})^{(\lambda)}_{\mu}$, $(\lambda = 1, 3, \mu = -\lambda, ..., +\lambda)$.

The low energy levels of the ^{63}Cu considered in the coupled-channels calculations of the present work are obtained from the total Hamiltonian $H = H_f + H_B + H_{BF}$ with $b_1 = -0.07$ MeV and $b_3 = -2.65$ MeV. It may be shown that this choice of the boson-fermion interaction Eq.(20) is consistent with a Spin(5) Bose-Fermi symmetry[11] of the Hamiltonian.

In Fig. 3 we present the results of the analysis of the elastic and inelastic scattering angular distributions for the system $^{16}O + ^{63}Cu$.

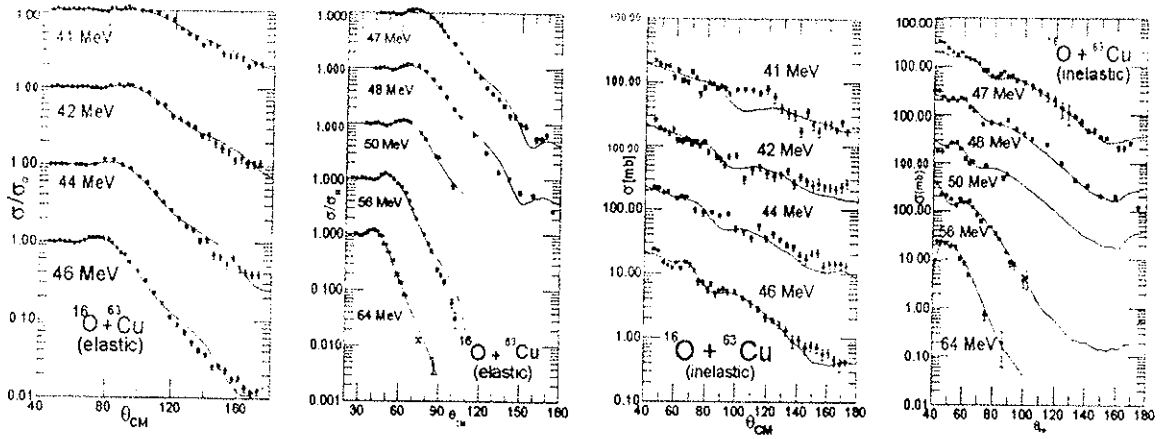

Figure 3: The fits of the elastic and inelastic angular distributions for the $^{16}O + ^{63}Cu$ system as indicated.

We considered the coupling with the five low lying states of the ^{63}Cu. The relative strengths of the reduced nuclear matrix elements used in this calculations have been determined in the context of the IBMF model as described above. It reduces the number of parameters to practically just an overall strength for the Coulomb excitation and a complex one for the nuclear excitation. The diagonal coupling elements were basically those determined from the analysis of the elastic angular distributions.

6 conclusions

We discuss some recent developments of the Algebraic Scattering Theory concerning the properties of the algebraic potential for the one channel elastic scattering. We also present a formalism which permits the inclusion of the spin in the algebraic description when many reaction channels are involved. The formalism is applied to the elastic and inelastic angular distributions for the $^{16}O +^{63} Cu$ system at energies in the neighborhood of the Coulomb barrier.

7 references

1. Y. Alhassid, F. Iachello, *Nucl. Phys.* **A501** (1989) 585.
2. R. Lichtenthäler Filho, A. C. C. Villari, L. C. Gomes and P. Carrilho Soares, *Phys. Lett.* **B269** (1991) 49.
3. M. S. Hussein, M. P. Pato and F. Iachello, *Phys. Rev.* **C38** (1988)1072.
4. K. Amos, L. Berge, L. J. Allen and H. Fiedeldey, *Phys. Rev.* **C47** (1993) 2827.
5. S.K.Kauffmann *Relation of Phase Shifts to Potential Parameters in the Elastic Scattering of Very Heavy Ions* (unpublished) (1976).
6. W. E. Frahn in *Treatise on Heavy Ion Sciences*, (D. A. Bromley Ed.,Plenum Press, N. Y. 1984), vol. 1, p 216.
7. D. Pereira, G. R. Razeto, O. Sala, L. C. Chamon, C. A. Rocha, J. C. Acquadro and C. Tenreiro, *Phys. Lett.* **B220** (1989) 347.
8. R. Lichtenthäler Filho, A. Ventura, L. Zuffi, *Phys.Rev.* **C46** (1992) 707.
9. G.R.Satchler, *Direct Nuclear Reactions*(Oxford University Press, New York, 1983),p161.
10. R. A. Broglia and A. Winther, *Heavy Ion Reactions*, Addison-Wesley,1990.
11. F.Iachello and P.Van Isacker, *The Interacting Boson-Fermion Model* (Cambridge University Press, 1991).